**Title**

Investigations on the Use of Al-Galinstan Amalgams and Al-Ga Amalgams to Make Hydrogen Fuel

**Author**

Schmierer, Joel Craig

**Publication Date**

2024

# Investigations on the Use of Al-Galinstan Amalgams and Al-Ga Amalgams to Make Hydrogen Fuel

By

JOEL CRAIG SCHMIERER
DISSERTATION

Submitted in partial satisfaction of the requirements for the degree of

DOCTOR OF PHILOSOPHY

in

Materials Science & Engineering

in the

OFFICE OF GRADUATE STUDIES

of the

UNIVERSITY OF CALIFORNIA

DAVIS

Approved:

Jerry Woodall, Chair

Susan Gentry

Subhash Risbud

Committee in Charge

2024

# Table of Contents

# Abstract

**Author Contact Information for Joel Craig Schmierer:**
**joelschmierer@gmail.com and Facebook**

**Major Professor: Jerry M. Woodall (jwoodall@ucdavis.edu)**

Hydrogen fuel can be harnessed to power countless technologies, including hydrogen fuel cell devices and hydrogen-powered cars, buses, boats, aircraft, etc. High-purity hydrogen can be easily, rapidly, and successfully produced from the direct reaction of water with "activated" Al. Al by itself does not significantly react with water, but activated Al is Al that is made to be water-reactive via dissolving it in liquid Ga or liquid "eGIS." eGIS is eutectic galinstan: 68.5wt%Ga, 21.5wt%In, and 10wt%Sn.

A fairly novel processing technique—amalgamation via a dental amalgamator—was used to fabricate activated Al. This is a single-step technique that is rapid, can be performed at room temperature, and increases the surface-area-to-volume ratio of the activated Al to facilitate faster hydrogen-generation rates, as compared to traditional fabrication technologies.

A very promising result was that the 10wt%eGIS-90wt%Al amalgam was shown to offer a full yield of high-purity hydrogen when it was reacted in water, regardless of variability in water pH and variability in chemical substance contaminants that were present in several tested types of waters—and even in relatively inexpensive and "dirty" tap water. The use of tap water, alkaline water, distilled water, and deionized water all resulted in the successful generation of approximately 100% yield of hydrogen. The 10wt%eGIS-90wt%Al amalgam reacted very rapidly in the 50°C deionized/distilled waters, reaching a 90% yield of hydrogen in as fast as 18 seconds, and reaching ~100% yield shortly thereafter. In 50°C waters, the hydrogen-generation rate of the 10wt%eGIS-90wt%Al amalgam in the deionized water was

essentially identical to that in the distilled water and was ~11 times faster than in the alkaline water and ~28 times faster than in the tap water.

Commercially relevant conditions of operational stability and shelf-life stability of the 10wt%eGIS-90wt%Al amalgam were investigated: annealing or aging at high temperature (400°C) for 1 week and at room temperature for 6 months. Remarkably, these conditions did not decrease the amalgam's hydrogen-generation rate or decrease its hydrogen-generation yield from ~100%.

Further analyses explored the roles of Ga and eGIS in Al-Ga/eGIS water-reactivity. Results were consistent with the hypothesis, based on the Al-Ga phase diagram, that Al-Ga amalgams that contain >20wt%Ga give ~100% hydrogen yields but Al-Ga amalgams that contain <20wt%Ga give vastly lower hydrogen yields. However, Al-eGIS amalgams that contain as little as 10wt%eGIS (if not less) were found to be highly water-reactive, rapidly producing ~100% yields of hydrogen. Evidence supported the hypothesis that the high degree of water-reactivity of many compositions of Al-eGIS amalgams, in contrast to some compositions of Al-Ga amalgams, is due to the ability of Ga to remain bonded with In and/or Sn in Al grain boundaries, rather than significantly diffusing into Al grains, thereby allowing Al to readily dissolve into the liquid eGIS-rich phase in the Al grain boundaries to facilitate significantly high amalgam water-reactivity. In a separate experiment, numerous different compositions of Al-In-Sn alloys, all Ga-free, displayed <1% yield of hydrogen in the tested water temperature range of ≤50°C. The results suggest that, at least for water bath temperatures of ≤50°C, the addition of Ga is needed for Al-galinstan alloys and amalgams to become activated (water-reactive).

# Acknowledgement

SEM data collection was carried out at the UC Davis Center for Nano and Micro Manufacturing (CNM2).

# Glossary

## *Key abbreviations*

| | |
|---|---|
| BSE | backscattered electron, as related to a backscattered electron image in SEM |
| $E^\circ$ | standard reduction potential |
| eGIS | eutectic galinstan (68.5wt%Ga, 21.5wt%In, and 10wt%Sn) |
| $\Delta G$ | nonstandard-state Gibbs free energy change of formation |
| $\Delta G^\circ$ | standard-state Gibbs free energy change of formation |
| GB | grain boundary |
| GIS | galinstan (Ga-In-Sn) of an unspecific or unknown ratio of Ga:In:Sn |
| $\Delta H^\circ$ | standard enthalpy of formation |
| IEP | isoelectric point |
| ppb | parts per billion (1000ppb = 1ppm) |
| ppm | parts per million (1ppm = 1mg/L) |
| RH | relative humidity |
| RT | room temperature |
| SE | secondary electron, as related to a secondary electron image in SEM |
| SEM | scanning electron microscope or microscopy |
| TDS | total dissolved solids (such as in ppm or mg/L) |
| wt% | weight percent |

## *Subscripts for phases*

| | |
|---|---|
| $_{(aq)}$ | aqueous solution |
| $_{(cr)}$ | crystalline solid |
| $_{(g)}$ | gas or vapor |
| $_{(l)}$ | liquid |
| $_{(s)}$ | solid |

## *Notes*

- Equations beginning with an alphabet letter are also located in Appendices.

- “Water-reaction rate” is defined in this work as *the measured time to 90% water-reaction yield* when amalgams or alloys are reacted with water.

- “$Al(OH)_3$” is often used in this work as shorthand for Al oxide/hydrate(s), as it is assumed (as discussed in Chapter 3) that $Al(OH)_3$ is the phase that is present in the largest wt% in the Al water-reaction product, which may contain multiple phases.

- The original source for the phase diagrams (for Al-Ga, Al-In, Al-Sn, and In-Sn) that are frequently referred to in this work is [1], but they may be more easily accessed and viewed via Appendix C of [2].

# Chapter 1: Introduction and Background Information/Concepts

## 1.1. Introduction

This dissertation explores the reaction of water and "activated" Al, which is Al that is made to be water-reactive via dissolving it in liquid Ga or liquid eGIS (eGIS is eutectic galinstan: 68.5wt%Ga, 21.5wt%In, and 10wt%Sn.), as a source of hydrogen energy. This source of hydrogen is a likely candidate to power certain niche technologies and, possibly, widespread technologies.

◦ *Niche applications:*

- ❖ autonomous undersea vehicles [3]
- ❖ primary and/or backup energy generators in remote public/private locations [4]
- ❖ safe, hands-on STEM science kits

◦ *Widespread applications:*

- ❖ hydrogen-powered vehicles (cars, buses, boats, aircraft, etc.)
- ❖ primary and/or backup energy generators in common, widespread public/private locations [4]
- ❖ hydrogen-enriched natural gas that is supplied to houses/buildings [4]

An economic benefit of the Ga/eGIS-activated Al water-reaction is that water and Al are inexpensive and abundant. From one perspective, Ga and eGIS may also be considered inexpensive as they are only used to activate Al and are nearly inert in ordinary water, so they can be nearly fully recovered after the Al water-reaction reaches completion with little effort (in Ga/eGIS-rich, Al-poor systems), allowing them to be reused many times. However, it was found that whenever Al-Ga/eGIS reacts with water, there is always a "small" amount of Ga/eGIS that appears to adhere and/or bond to the $Al(OH)_3$ reaction product [5]. This is detrimental to economic viability, because this Ga/eGIS is difficult to remove from the

$Al(OH)_3$ [5]; not only does this mean some Ga/eGIS is lost each time Al reacts with water, but also the $Al(OH)_3$ becomes contaminated with Ga/eGIS, so the $Al(OH)_3$ cannot be sold as a high-purity commercial product. However, significant progress has been made to this end; much work has focused on preventing Ga from combining with the $Al(OH)_3$ during the Al-water reaction and on removing already-combined Ga from the $Al(OH)_3$ [5].

Al-Ga/eGIS systems are generally easy to study, to design, and to engineer, as Al, Ga, and eGIS are relatively nontoxic, and because Al becomes activated by dissolving into Ga at ~RT (room temperature) and into eGIS at below RT. Any Al-Ga/eGIS alloy/amalgam composition can be quickly, easily, and successfully produced via using a furnace, hot plate, dental amalgamator, or any similar devices.

# 1.2. Background information/concepts

## 1.2.1. The reaction of Al with water

The main reaction of Al (dissolved in liquid Ga/eGIS) with water under common conditions of ~RT and 1atm is given below, where ΔG° and ΔH° are calculated from Table B1 (Appendix B) data.

Eq. 1.1 $2\ Al_{(l)} + 6\ H_2O_{(l)} \rightarrow 2\ Al(OH)_{3,\ (s,\ bayerite)} + 3\ H_{2,\ (g)}$ $\Delta G° = -898$ kJ $\Delta H° = -883$ kJ

This reaction is exothermic, as indicated by the negative ΔH° value. It is also irreversible under most ordinary conditions (such as those in this dissertation). When Al (dissolved in liquid Ga/eGIS) reacts with water, ~100% water-reaction yield of $H_2$ gas is observed, based on the 3:2 molar ratio of $H_2$ gas to Al in Eq. 1.1. The irreversibility of the reaction can be inferred since $H_2$ gas leaves the system once it is produced, as it is poorly soluble in water and leaves the water; also, the reaction in Eq. 1.1 has a large and negative ΔG° value, so there is a strong thermodynamic driving force for the forward reaction compared to that of the reverse reaction.

## 1.2.2. The amalgamation process

Amalgams are differentiated from alloys in that amalgams are made via a dental amalgamator whereas alloys are not. Amalgams are generally made from Al powder whereas alloys are not traditionally made from Al powder but from large ingots or pellets of Al. Traditionally, Al and Ga/eGIS are combined as alloys, rather than as amalgams, by stirring them together in a beaker on a hot plate (for Al-poor alloys) or in a crucible in a furnace at a high enough temperature to melt bulk Al (for Al-rich alloys). However, amalgamation is a fast, simple, and single-step process that can be performed at RT without the need for heating. In theory, amalgamation can be scaled to work with larger mixing/amalgamation machines than those used in proof-of-concept lab environments.

Amalgamation was very briefly used before in one prior work to make a 20wt%Ga-80wt%Al amalgam but was not further explained or studied in any detail for Al-Ga/eGIS systems [4]. In the amalgamation process, Al powder and liquid Ga/eGIS are simply shaken together at high speed to mix them. The shaking distributes the liquid Ga/eGIS to all Al powder particles. Then, the Ga/eGIS enters Al GBs (grain boundaries) (as seen in SEM images in later chapters in this dissertation). Figure 1.1 (Steps 1-3) below illustrates this amalgamation process.

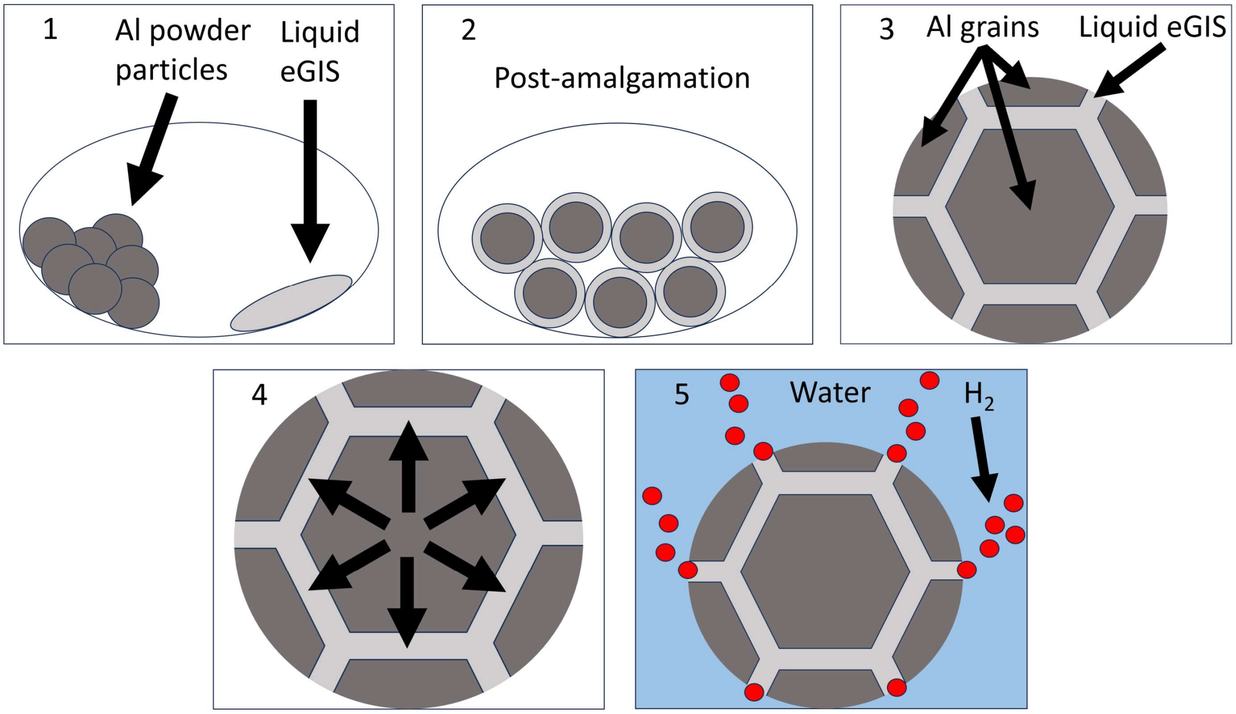

**Figure 1.1. Illustrations of the amalgamation process and of the mechanistic model for the reaction of a 10wt%eGIS-90wt%Al amalgam with water:**

◦ *Step 1:* Al powder and liquid eGIS are placed in a capsule.

◦ *Step 2:* Amalgamation (rapid shaking of the capsule) causes liquid eGIS to coat all of the Al powder particles.

◦ *Step 3:* Liquid eGIS thoroughly infiltrates Al GB networks.

◦ *Step 4:* Al grains slightly dissolve into liquid eGIS until a solubility limit is reached (A low amount is expected to dissolve at around RT, perhaps ~1wt%Al, to form ~99wt%eGIS-1wt%Al liquid.).

◦ *Step 5:* Dissolved Al rapidly reacts with water, rapidly depleting dissolved Al from liquid eGIS. This depletion causes Step 4 to reoccur.

◦ Steps 4 and 5 occur in alternating repetition until all Al in the Al particle is consumed.

### 1.2.3. Water-reactivity characteristics of Al-Ga/eGIS compositions

On easily observable timescales and under most common conditions, Ga appears to be non-water-reactive (p.432 of [7]), although it very slowly reacted in warm/hot, oxygenated water in pp.58-59 of [5] and in Chapter 3 of this dissertation. Solid-phase Al by itself is non-water-reactive [8]. When Al and Ga are combined, Al becomes highly water-reactive only if liquid Al forms (p.12 of [2], p.18 of [6]). According to the Al-Ga phase diagram [1], a Ga-rich/Al-poor liquid Al-Ga phase forms for all Al-Ga compositions that are both >20wt%Ga and >27°C (except if using Al-rich compositions at very unusually high temperatures).

As aforementioned, liquid Al is needed for Al-Ga water-reactivity. In one study (p.12 of [2]), several Al-Ga compositions were placed in water of 20°C, which is below the eutectic temperature, 27°C. This froze the liquid into solid phases, making them non-water-reactive. Upon raising temperature >27°C, the solid phases melted and became water-reactive. In studies, fully solid-phase 97wt%Al-3wt%Ga was found to be non-water-reactive in 22°C-50°C water (p.12 of [2]) and in 22°C-80°C water (p.18 of [6]).

Similar to Ga, on easily observable timescales and under most common conditions, eGIS appears to be non-water-reactive (p.12 of [2]), although it very slowly reacted in warm/hot, oxygenated water in Chapter 3 of this dissertation. When Al and eGIS are combined, Al generally becomes highly water-reactive. Evidence suggests that for Al in Al-eGIS, just as for Al in Al-Ga, to become water-reactive, solid Al must become liquid Al (such as by dissolving into liquid eGIS) (pp.12/15-16 of [2]).

A mechanistic model for the water-reactivity of partially-solid, partially-liquid bulk Al-Ga/eGIS alloys/amalgams was proposed (p.57 of [2]), and it is displayed in Figure 1.1 (Steps 3-5) for a 10wt%eGIS-90wt%Al amalgam. When a partially-solid, partially-liquid bulk Al-eGIS sample is made, as seen via SEM (pp.55-56 of [6]), essentially all Al grains become well-surrounded by, and in physical contact with $eGIS_{(l)}$ that is in Al GBs. This enables ~100% of Al grains in a sample to eventually dissolve over time into the $eGIS_{(l)}$ to become activated (water-reactive) by becoming liquid-phase Al (as Al grains are solid-phase and thus non-water-reactive) and so ~100% water-reaction yield in a sample can be achieved. Consequently, experimentally observing ~100% water-reaction yield means, by deductive reasoning, that all Al grains eventually became the water-reactive liquid Al phase. When an Al-eGIS sample is made, Al grains begin to physically contact $eGIS_{(l)}$ in Al GBs. The $eGIS_{(l)}$ may already be in Al GBs before Al grains first form from cooled liquid Al in a furnace-made Al-eGIS sample or may infiltrate Al GBs if $eGIS_{(l)}$ is placed in physical contact with an Al sample that contains GBs. The physical contact between Al grains and $eGIS_{(l)}$ causes the Al to dissolve from the Al grains and into $eGIS_{(l)}$ until a solubility limit is reached, resulting in solid Al grains surrounded by $Al_{(l)}$-$eGIS_{(l)}$ in Al GBs. Then, when an Al-eGIS sample is placed in water, reactions occur between water and $Al_{(l)}$ in $Al_{(l)}$-$eGIS_{(l)}$ on the water-contacting outer surfaces of the sample. When $Al_{(l)}$ reacts with water, water-reaction products may quickly and continuously form as they quickly and continuously move away from water-reaction interfaces into the water, rapidly depleting $eGIS_{(l)}$ of $Al_{(l)}$. To re-establish the equilibrium concentration of $Al_{(l)}$ in $Al_{(l)}$-$eGIS_{(l)}$, Al grains continuously dissolve as $Al_{(l)}$ into $eGIS_{(l)}$, and this $Al_{(l)}$ continuously migrates through $eGIS_{(l)}$ toward interfaces between $eGIS_{(l)}$ and water. These processes occur until all Al in the sample reacts with water, unless physical contact between Al and $eGIS_{(l)}$ is eliminated.

However, the aforementioned mechanistic model does not consider whether Ga may migrate from $eGIS_{(l)}$ (making it $GIS_{(l)}$ rather than $eGIS_{(l)}$) in Al GBs into Al grains, which may decrease Al water-reactivity. Such Ga migration may cause $eGIS_{(l)}$ (or $GIS_{(l)}$) in Al GBs to freeze (due to having low Ga wt%) and/or may prevent Al grains from dissolving into $eGIS_{(l)}$/$GIS_{(l)}$ in Al GBs. This Ga migration may occur due to time—that is, prolonged physical contact between liquid eGIS and Al grains—and/or elevated temperature.

This dissertation mainly investigates Al-eGIS amalgams that are 10wt%eGIS-90wt%Al. It is suspected Ga migration may occur for such a composition based on the Al-Ga phase diagram. In terms of only Al and Ga, this amalgam is ~8wt%Ga-92wt%Al. So, from the Al-Ga phase diagram, from about −100°C to 500°C, this composition is in the α-Al solid solution phase region comprising only a single, solid Al-Ga phase that is absent of any liquid phase. So, it is suspected that up to all Ga in the amalgam may migrate from liquid eGIS in Al GBs into Al grains to form the α-Al solid solution phase, which may partially/fully hinder amalgam water-reactivity. However, such phase diagrams only show phases at thermodynamic equilibrium, so they do not account for kinetic limitations—time and/or activation energy requirements needed for phases to form. So, if kinetic limitations are not overcome, Ga may largely remain in liquid eGIS in Al GBs and not significantly migrate into Al grains, thus not significantly negatively impacting amalgam water-reactivity. However, time—prolonged physical contact between liquid eGIS and Al grains—and/or elevated temperature may help overcome kinetic limitations and induce Ga migration.

Unfortunately, there is no quaternary Al-eGIS phase diagram in the literature for reference. Instead, Al-eGIS behavior is predicted from the binary alloy phase diagrams of Al-Ga, Al-In, Al-Sn, and In-Sn (These diagrams are accessible in [2], reproduced from [1]). From the Al-In and Al-Sn phase diagrams, there is essentially no solubility of In or Sn in α-Al at any temperature (There is a negligibly low maximum solubility of 0.13wt%Sn in α-Al at a high temperature of ~600°C.). So, neither In nor Sn should migrate from Al GBs, such as from $eGIS_{(l)}$ in Al GBs, into Al grains. Also, from the Al-In and Al-Sn phase diagrams, a nonzero amount of Al (that increases with increasing temperature) dissolves into $In_{(l)}$ and $Sn_{(l)}$, given $In_{(l)}$ and $Sn_{(l)}$ are already present.

If In and Sn remain in $eGIS_{(l)}$ in Al GBs and do not migrate into Al grains, this may improve the stability of the liquid Al phase (the liquid Al-eGIS/GIS phase) in a 10wt%eGIS-90wt%Al amalgam compared to the liquid Al phase (liquid Al-Ga) in, for example, a 10wt%Ga-90wt%Al amalgam. This is because in a 10wt%eGIS-90wt%Al amalgam, Ga is initially already bonded with In and Sn in liquid eGIS, and this bonding may prevent significant Ga migration from liquid eGIS in Al GBs into Al grains, even if there is prolonged physical contact between liquid eGIS in Al GBs and Al grains and/or elevated temperature. However, in a 10wt%Ga-90wt%Al amalgam, Ga is not bonded with In or Sn, so it may more readily migrate from Al GBs into Al grains due to prolonged physical contact between liquid Ga in Al GBs and Al grains and/or elevated temperature.

By definition, as they contain more Al, Al-rich Al-Ga and Al-rich Al-eGIS have high volumetric and mass energy densities (They produce much $H_2$ gas per volume and mass of Al-Ga or Al-eGIS.) compared to Al-poor Al-Ga and Al-poor Al-eGIS. Also, regardless of if it is in a bulk form or not, an Al-rich Al-Ga/eGIS amalgam is a powder with a fine particle size, so it has a large surface-area-to-volume ratio compared to those of bulk Al-Ga/eGIS alloys (made from large ingots or pellets of Al), allowing for increased water-reaction rate and increased rate of $H_2$ gas production. Further, according to the Al-Ga phase diagram, bulk Al-Ga/eGIS alloys/amalgams made in the S + L (solid + liquid) region and in the L region have much liquid phase surrounding solid-phase Al compared to bulk Al-Ga/eGIS alloys/amalgams made in the α-Al solid solution region. So, it takes more time for Al to diffuse through liquid Ga/eGIS to reach and react with water at the interface between water and liquid Ga/eGIS in bulk, non-Al-rich Al-Ga/eGIS alloys (p.55 of [2]) (and amalgams) than in bulk, Al-rich alloys/amalgams. To complete the clarification of why this is true, this is because the latter alloys/amalgams have very thin amounts of liquid Ga/eGIS in Al GBs that highly surround the Al grains, allowing for Al to quickly diffuse through liquid Ga/eGIS to reach and react with water at the interface between the water and the liquid Ga/eGIS. This results in the fast water-reactivity of (bulk or otherwise) Al-rich Al-eGIS amalgams. However, bulk, Al-rich Al-Ga amalgams were found in this dissertation (in Chapter 7) to be very poorly water-reactive, and Al-rich Al-Ga alloys were similarly found to be very poorly water-reactive (p.12 of [2], p.18 of [6]) compared to bulk, non-Al-rich Al-Ga/eGIS alloys/amalgams. So, this dissertation mainly investigates the 10wt%eGIS-90wt%Al amalgam, as it is Al-rich, is an amalgam rather than an alloy, and is highly water-reactive.

### 1.2.4. Proposed growth-and-exfoliation model of the cyclic formation of a semi-passivating $Al(OH)_3$ film on the liquid Al in an Al-eGIS amalgam powder particle that is underwater

Note that “$Al(OH)_3$” is often used in this work as shorthand for Al oxide/hydrate(s), as it is assumed (as discussed in Chapter 3) that $Al(OH)_3$ is the phase that is present in the largest wt% in the Al water-reaction product, which may contain multiple phases.

A scenario is proposed to explain why amalgam water-reaction rate varies with water type, where the independent variable in the trials is the type of water used. There are four steps to the process that is proposed in Figure 1.2 below.

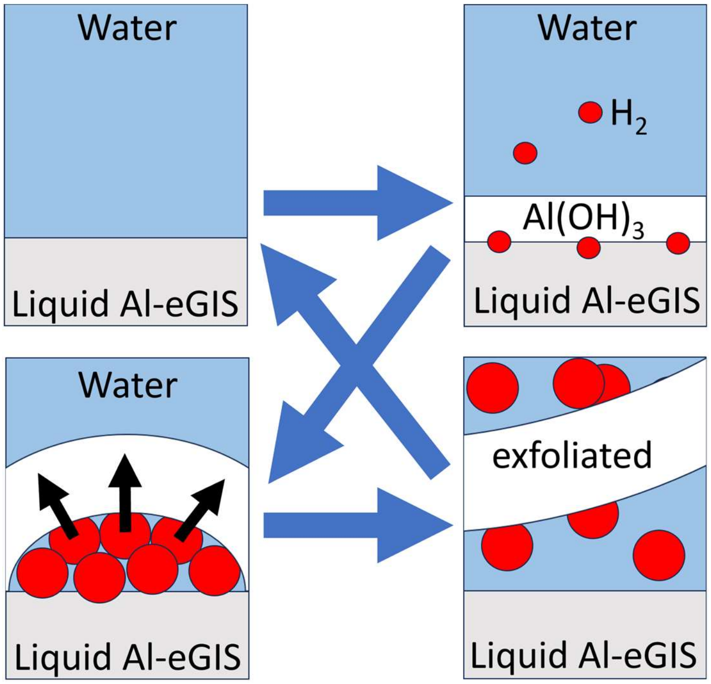

**Figure 1.2. Proposed model of Al water-reaction on water-contacting outer surfaces of an Al-eGIS amalgam powder particle.**

◦ *Step 1*: Liquid Al-eGIS and water are placed in contact, but no reactions have occurred yet.

◦ *Step 2*: Al begins to react with water, forming a thin $Al(OH)_3$ film on the liquid Al-eGIS and producing $H_2$ gas bubbles. Water may continuously diffuse through the film, reacting with Al to grow the film and to produce $H_2$ gas bubbles. Some $H_2$ gas bubbles begin to be trapped between the film and substrate. These bubbles exert pressure on the film, helping to physically delaminate it from the substrate.

◦ *Step 3*: $H_2$ gas bubbles continue to be produced and trapped between film and substrate until a critical pressure is reached for which the magnitude of the film's adhesive forces equals that of the de-adhesive forces exerted by $H_2$ gas bubbles.

◦ *Step 4*: The film delaminates.

◦ Steps 1-4 repeat until all Al in the amalgam reacts with water.

Reactions that occur at the interface between water and liquid Al (liquid Al dissolved in liquid eGIS/GIS) in an Al-eGIS amalgam, on outer surfaces of Al-eGIS particles contacting water, should be fully responsible for observed differences in amalgam water-reaction rate. Variation in amalgam water-reaction rate vs water type implies variation in degree of obstruction in the ability of liquid Al to interfacially react with water. The less that liquid Al is obstructed from reacting with water at the interface of liquid Al and water, the faster the water-reaction rate of the liquid Al would be, and thus the faster the amalgam water-reaction rate would be.

Multiple mechanisms influence the rate that liquid Al reacts with water at their interface:

- The presence of a cyclically-forming and semi-passivating film of $Al(OH)_3$
- The effect of water pH on the solubility of this $Al(OH)_3$ film
- Precipitation reactions—involving water contaminants—on/in this $Al(OH)_3$ film
- Adsorption of water contaminants on this $Al(OH)_3$ film
- Adhesion and bonding of this $Al(OH)_3$ film with Ga/eGIS oxide(s)/hydrate(s) films

In the literature, solid-phase, pure Al was cut underwater to react unpassivated Al with water [8]. A strongly passivating film was observed to quickly form, fully preventing any further reaction of water with Al. The authors present evidence for the rapid formation of hydrated Al (as $Al(OH)_3$ and/or $AlO(OH)$) and $Al_2O_3$ but do not quantify how much of each phase forms. The study shows that when Al is fully submerged underwater and its initial passivation film is removed, a new passivation film of Al oxide/hydrate(s) is formed rapidly and is strongly passivating, at least if the Al substrate is solid-phase. The results of the study suggest it is feasible that such a film of Al oxide/hydrate(s) that may be passivating to a degree may potentially also form, and may form rapidly, on the liquid Al in Al-Ga/eGIS samples, as Al is the same substrate material in both cases for the growth of the Al oxide/hydrate(s) film.

In another study [9], solid Al powder (that was surface-modified and placed in a high-vacuum environment) was reacted with water, and a model was presented to describe the interface between the

Al and its semi-passivating film. $[OH]^-$ ions and/or $H_2O$ molecules (p.4710 of [10], as cited in [9]) diffuse from surrounding water through the semi-passivating film on Al until they reach and react with Al, producing $H_2$ gas bubbles at the interface between Al and its film that become trapped between the two. The $H_2$ gas bubbles cannot quickly escape by diffusing away through the Al or the film, so they increasingly build up pressure until a critical gas pressure threshold is reached that allows the $H_2$ gas bubbles to rupture the film. This allows water to enter through the rupture and react with Al to grow another semi-passivating film. This cycle may repeat until all Al reacts with water.

Another study (p.79 of [5]) observes a large, bulk droplet of fully liquid Al-Ga that is fully submerged underwater. The Al-Ga reacts with water, and it is shown that $Al(OH)_3$ sheets form and agglomerate (The author states that this is likely due to hydrogen bonding among adjacent $Al(OH)_3$ particles.) on the surface of the Al-Ga alloy. It appears to be claimed that it was then observed that the evolution of $H_2$ gas bubbles, produced from the Al water-reaction at and/or just below the surface of the liquid alloy phase, in between the liquid alloy and the $Al(OH)_3$ sheets, delaminated the $Al(OH)_3$ sheets from the liquid alloy.

The evidence from these studies suggests a water-reaction mechanism, at the interface of liquid Al and water, via growth and exfoliation of semi-passivating $Al(OH)_3$ in which an $Al(OH)_3$ film grows on the surface of the liquid Al until it exfoliates, driven at least in part by the delaminating force exerted by $H_2$ gas bubbles, in a repeating process until all Al in a fully liquid Al-Ga alloy reacts with water. This model was previously proposed for fully liquid Al-Ga (p.79 of [5]).

Similar to this fully liquid Al-Ga, fully liquid Al-eGIS may have the same growth-and-exfoliation water-reaction mechanism, as both alloys are primarily composed of Ga, both contain only one phase, which is fully liquid in both cases, and Al is fully dissolved as a liquid in both cases. For a 10wt%eGIS-90wt%Al amalgam, its only water-reactive phase is its fully liquid Al-eGIS phase. So, it is hypothesized that a 10wt%eGIS-90wt%Al amalgam reacts with water via a growth-and-exfoliation model in which semi-passivating $Al(OH)_3$ cyclically forms on the liquid Al.

Growth-and-exfoliation cycles would occur many times over the course of complete water-reaction of a bulk Al-eGIS sample and should increase in rate with increased temperature. It may be possible to observe real-time bulk formation of $Al(OH)_3$ and its prolonged adherence on fully liquid Al-eGIS, followed by delamination due to $H_2$ gas bubble formation, similar to such observations with fully liquid Al-Ga (p.79 of [5]). Such observations may be possible by naked eye, camera (high-speed or otherwise), and/or microscope if a future experiment is performed in which in a large sample of fully liquid Al-eGIS is reacted in cold water to slow Al water-reaction rate.

Comparing Al-Ga/eGIS alloys/amalgams to the aforementioned studies ([8], [9]) that reacted solid-phase Al with water, it should take a significantly lower critical gas pressure for $H_2$ gas bubbles to physically delaminate the $Al(OH)_3$ film from liquid-phase Al than delaminating a film grown on solid-phase Al, as the liquid-solid interface of the liquid Al and solid-phase $Al(OH)_3$ would have disrupted bonding due to lack of a rigid, fixed crystal structure of the liquid. The bonding energy for delamination is unknown. It may require a small but nonzero force, so $Al(OH)_3$ may act as a semi-passivating film in each growth-and-exfoliation cycle for a short—but not negligible—time interval. Faster exfoliation of the $Al(OH)_3$ film from liquid Al than solid Al is consistent with the fast water-reaction rates of Al-eGIS/Ga alloys/amalgams containing a liquid phase as compared to the nonreactivity of such samples that do not contain a liquid phase.

One study determined that $H_2O$ and/or $[OH]^-$ likely diffuse from water and through an $Al_2O_3$ film toward its bonded, solid-phase Al substrate underneath if such a film is in contact with water (p.4710 of [10]). Additionally, diffusion in a film of Al hydrate is expected to be substantially faster than in the non-hydrated $Al_2O_3$ (p. 4706 of [10]). So, in an Al-eGIS amalgam, $H_2O$ and/or $[OH]^-$ may diffuse through the Al oxide/hydrate(s) film to react with Al. Diffusion through this film may readily occur as the film likely is well-hydrated, thin, and porous. It may also contain defects that assist migration of diffusive species, due to its rapid formation and also perhaps due to mechanical agitation from the nearby, vigorous production of $H_2$ gas bubbles.

While the $Al(OH)_3$ film grows and thickens, the diffusion path length within it increases, which may slow but not fully prevent water diffusion. Also, $H_2$ gas bubbles that are produced and entrapped at the Al-$Al(OH)_3$ interface may act as physical barriers that slow water diffusion toward Al. These factors slow amalgam water-reaction rate.

A factor controlling film exfoliation rate is local temperature. The initial water bath temperature for each experiment was 50°C. However, Al water-reaction is exothermic, releasing heat at Al water-reaction sites and increasing local temperatures of materials at/near water-reaction sites. Quantitative water bath temperature-increase measurements due to Al water-reaction were not recorded in this dissertation but were, when observed via thermometer, at least several °C. However, the temperature at the very small, highly local Al-water interface would be even higher than average water bath temperature measurements would indicate. Also, the temperature at Al-water interfaces would vary over the course of amalgam water-reaction, based on heat transfer rates among materials. The added exothermic heat may have several effects: increasing the rate of dissolution of Al from grains into liquid GIS, increasing the maximum wt% of dissolved Al that liquid GIS can hold, increasing the rate that dissolved Al diffuses through liquid GIS to reach the Al-water interface, increasing the rate that water diffuses through $Al(OH)_3$ to reach Al, and increasing reaction rates at the Al-water interface. These mechanisms all increase the production rate of $H_2$ gas bubbles at the Al-$Al(OH)_3$ interface, increasing the rate that $H_2$ gas pressure buildup contributes to $Al(OH)_3$ film exfoliation. Also, the added exothermic heat may increase the pressure that $H_2$ gas bubbles exert (due to the ideal gas law, $PV = nRT$) to delaminate the $Al(OH)_3$ film from the Al substrate, accelerating exfoliation rate and thus accelerating amalgam water-reaction rate.

For slower Al water-reactions, there is more time for heat that is produced from the Al water-reaction to diffuse away from amalgam water-reaction interfaces and away from water that is local to the amalgam, and toward colder water and colder materials farther away. So, Al water-reaction heat release would have increased all amalgam water-reaction rates but would have more weakly increased amalgam water-reaction rate of the already-slower tap/alkaline water-reactions than for the already-faster DI/distilled water-reactions. It is unclear how much this heat-diffusion-rate effect quantitatively affected measured amalgam water-reaction rates in the tested waters.

# Chapter 2: Experimental Procedures

## 2.1. Procedure for making the amalgams

Amalgams were made using 99.5%-purity, 30µm Al powder by Alpha Chemicals and either 4N-purity eGIS or 4N-purity Ga. eGIS composition was 68.50wt%Ga-21.50wt%In-10.00wt%Sn. These ingredients were added into a plastic capsule (brand: Tytin self-activating spherical dental amalgam capsules) and placed into a Silamat S5 dental amalgamator for amalgamation. They were amalgamated until further amalgamation time did not change amalgam water-reaction rate or yield.

All amalgamating was performed in a glovebox under 4N-purity $N_2$ gas, an inert gas, to significantly prevent the amalgam from reacting with moisture/$O_2$ gas present in ordinary air. Glovebox RH was consistently maintained at a measured 2%-10% via constantly flowing 4N-purity $N_2$ gas through the glovebox at a high enough rate to counteract leaks in the glovebox. RH was measured and monitored with thermo-hygrometers placed in the main glovebox chamber and in the glovebox antechamber.

## 2.2. Procedure for weighing the amalgams

Pressure fluctuations prevented accurate measurements of mass in the glovebox. So, after making an amalgam, a plastic spatula was used to transfer a portion of the amalgam from its initial plastic capsule into a new, identical plastic capsule: the reaction capsule. The reaction capsule was closed fully, removed from the glovebox, and weighed by mass. The difference in mass between the reaction capsule and its pre-weighed mass (the mass of the capsule when empty) accurately gave the mass of the amalgam in the capsule.

## 2.3. Procedures for reacting the amalgams and measuring amalgam water-reaction rate/yield

The following procedures were performed under ordinary air.

A 100-mL graduated cylinder (~2.9cm inner diameter) is completely filled with water, turned upside down, and submerged into a 2L crystallization dish that is ~70% full of water. The setup is on a hot plate to control water bath temperature. DI water was always used in this dissertation unless otherwise specified.

Once the water is at the desired temperature, the snap-on/snap-off cap of the reaction capsule is slightly opened, and the reaction capsule is immediately placed into the graduated cylinder by hand or tongs. It floats to the top of the graduated cylinder. The graduated cylinder is shaken by hand to jostle open the cap of the reaction capsule, exposing the amalgam to water. The amalgam reacts with water to produce $H_2$ gas, which partially fills the graduated cylinder and lowers the water level in the graduated cylinder over time. A video camera records the volume of $H_2$ gas over time, which corresponds to the water-reaction rate. The time to reach 90% water-reaction completion is determined from a linear interpolation of the measurements above and below 90% water-reaction yield. Once the water-reaction finishes and the water cools to RT, the water-reaction yield is recorded.

Water-reaction yield is determined by using the measured mass of the amalgam, the wt% of Al in the amalgam, and the 3:2 molar ratio of $H_2$ gas to Al that is found in all Al water-reaction equations (Eqs. B2.1-B2.5); it is assumed that the $H_2$ gas is ideal.

## 2.4. Variations in measured water-reaction rates

Water-reaction rate measurements in this work have small variations, but these are small enough to be insignificant in terms of the arguments presented in the analyses and conclusions in this work. In the data in this work that presented the largest degree of variation, the experimental uncertainty range of water-reaction rate measurements was at most ~15%. Variations are most likely due to small differences in how amalgams were made and how they reacted with water. During the amalgamation process, some Al-eGIS amalgams may have broken apart into less-agglomerated Al-eGIS particles, whereas other amalgams may have formed larger agglomerations of particles, essentially at random. The less-agglomerated ones should react faster with water, as they have increased surface-area-to-volume ratio. Also, when the amalgam particles react with water, the rate at which agglomerations of the particles in the amalgams break apart into smaller agglomerations can vary, essentially at random. An increased rate at which they break apart would increase surface-area-to-volume ratio of the amalgam, increasing water-reaction rate.

# Chapter 3: The Influences of Water Type on the Water-Reaction Rate and Yield of a 10wt%eGIS-90wt%Al Amalgam

## 3.1. Goal

Generally, for consistency across experiments, only DI water is used in experiments in this dissertation. However, this chapter investigates the influences of DI, distilled, alkaline, and tap waters on the water-reaction rate and yield of a 10wt%eGIS-90wt%Al amalgam.

## 3.2. Methods

The experimental setup and procedures described in Chapter 2 were employed.

A 10wt%eGIS-90wt%Al amalgam was made. Smaller samples from this parent sample were used for each amalgam water-reaction. Water pH was measured by using pH paper prior to amalgam water-reactions.

The tap water that was used was from an ordinary tap water faucet, located on the campus of the University of California, Davis in Davis, CA (lab room #1123 in Ghausi Hall). Measurements of some of its characteristics, including some of its contaminants, are available in the 2022 Drinking Water Quality Report for the University of California, Davis [11]. Note that not all substances in the tap water are required to be reported in the water quality report [12].

The DI water that was used was filtered from the aforementioned tap water with a Milli-Q water purification system. This system has several water-filtering mechanisms (Quantum TEX polishing cartridge, Millipak express 40 filter, and Q-gard T2 purification cartridge) that filter out a large variety of contaminants, including organics (including bacteria), ions, and loose particulates [13]. The system auto-measures the specific resistivity value of the DI water, but only while the DI water is still in the clean, closed-environment system of the purification system. The specific resistivity of the DI water used for these experiments was 18.2MΩ-cm at RT.

Total dissolved solids, TDS, may be estimated using Eq. 3.1 below.

Eq. 3.1 $\text{TDS} = k_e \times \text{EC}$

where TDS is in ppm, $k_e$ is a conversion factor between 0.55 and 0.8, and EC is specific conductance in microsiemens/cm at 25°C (p.285 of [14]).

Variation in the conductivity of each specific dissolved solid could lead to uncertainty in Eq. 3.1, but the equation serves as a rough approximation. Otherwise, there is incomplete compositional data and no gravimetric data available for the tested waters to obtain TDS.

Using the TDS and specific resistivity data for the tap water from Table 3.1 yields $k_e \approx 0.60$, which aligns with the asserted range of 0.55 to 0.8 in Eq. 3.1. Using $k_e = 0.60$ to calculate TDS for the DI water gives ~0.03ppm.

The distilled water that was used was Niagara Bottling’s Distilled Drinking Water. The producer’s water quality report provides the specific resistivity and TDS as >0.5MΩ-cm and <10ppm (p.10 of [15]). More accurate measurements were not provided due to the sensitivity of the analytical equipment used (p.13 of [15]). Using $k_e = 0.60$, the TDS is estimated as <1ppm.

The alkaline water that was used was BlueTriton Brands' "9.5-pH Ion-Charged Alkaline Water, Action," which lists ingredients as "purified water, less than 0.5% of magnesium sulfate, calcium chloride, potassium bicarbonate." In-depth data on this water appears to be unavailable. However, bluetriton.com states "multi-stage purification and filtration" are used for this water [16]. An independent party determined the TDS of this water was 80ppm [17]. From this value, specific resistivity for the alkaline water is estimated, using $k_e$ = 0.60, as ~0.0075 MΩ-cm.

## 3.3. Data

Table 3.1 and Figures 3.1-3.4 below show the water-reactivities of the 10wt%eGIS-90wt%Al amalgam with the tested waters.

**Table 3.1. Water-reactivities of 10wt%eGIS-90wt%Al amalgam in four types of water at 50°C.**

| Water type | Water pH | Specific resistivity of water (MΩ-cm) | TDS (ppm) | Water-reaction yield | Time to 90% water-reaction completion |
|---|---|---|---|---|---|
| DI water | ~5 | 18.2 | 0.03 (est.) | ~100% | 22s |
| Distilled water | ~5 | >0.5<br>(p.10 of [15]) | <1 (est.); <10<br>(p.10 of [15]) | ~100% | 25s |
| Tap water | ~8 | 0.00188<br>(p.7 of [11]) | 320<br>(p.7 of [11]) | ~99% | 607s |
| Alkaline water | ~9-10 | 0.0075 (est.) | 80 [17] | ~99% | 245s |

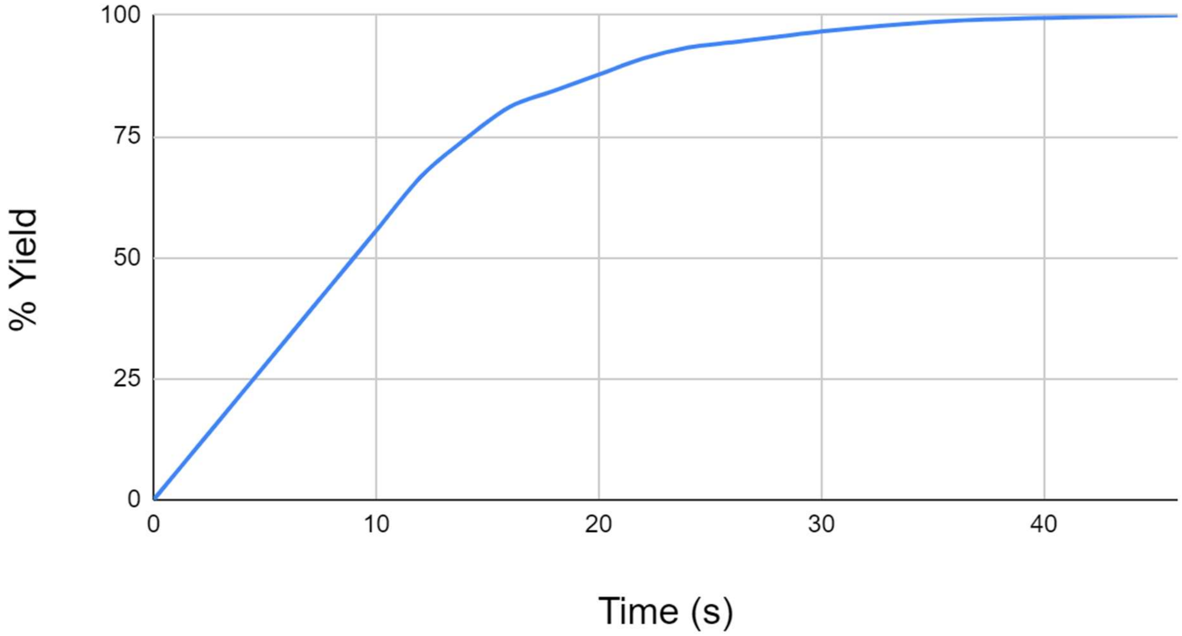

**Figure 3.1. Water-reaction rate curve for 10wt%eGIS-90wt%Al amalgam in 50°C DI water.**

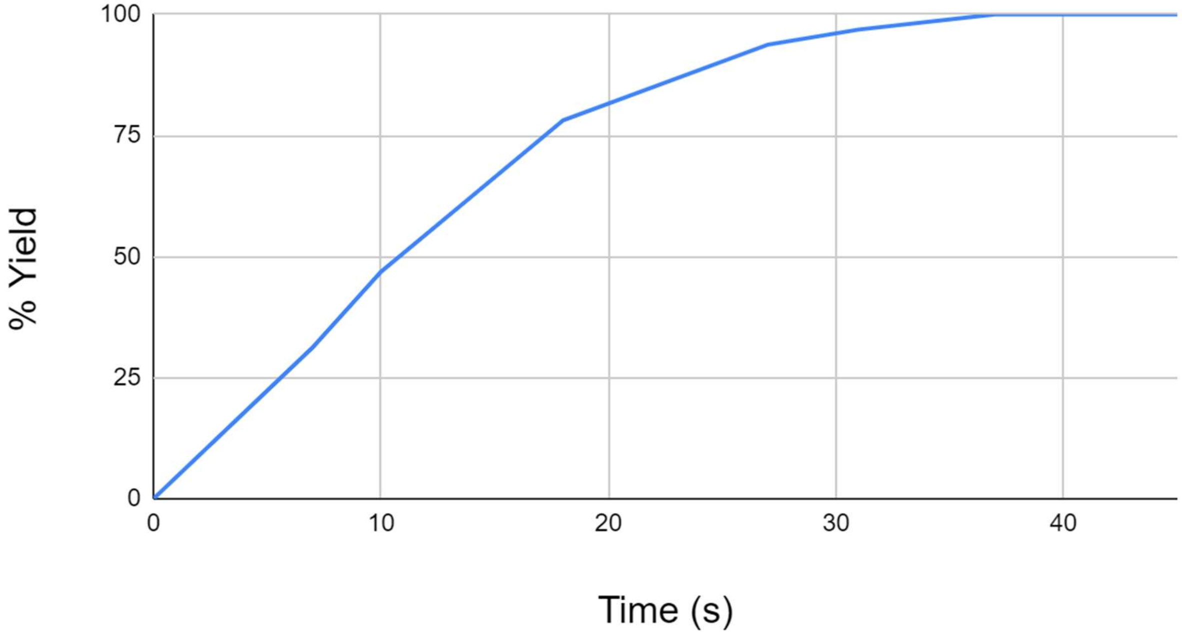

**Figure 3.2. Water-reaction rate curve for 10wt%eGIS-90wt%Al amalgam in 50°C distilled water.**

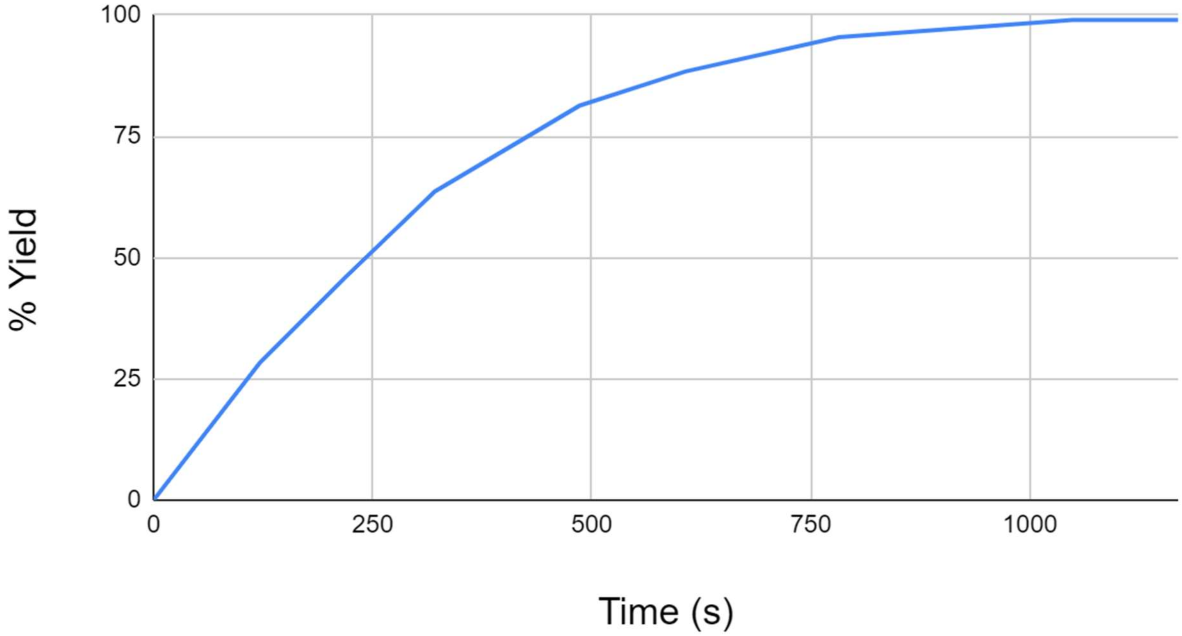

**Figure 3.3. Water-reaction rate curve for 10wt%eGIS-90wt%Al amalgam in 50°C tap water.**

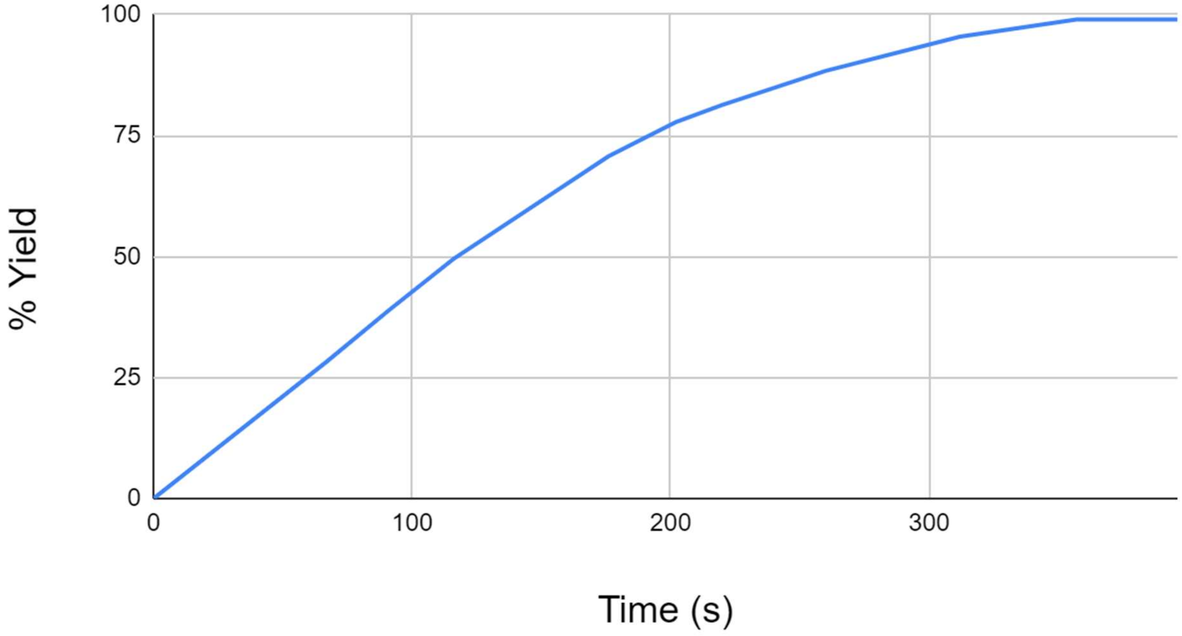

**Figure 3.4. Water-reaction rate curve for 10wt%eGIS-90wt%Al amalgam in 50°C alkaline water.**

## 3.4. Analyses of the waters that were used

Pure water contains no chemical substances other than $H_2O$ and its self-ionization products, such as $H^+_{(aq)}$, $[H_3O]^+_{(aq)}$, and $[OH]^-_{(aq)}$. However, all types of water used in this chapter's experiments include varying types and concentrations of chemical substance contaminants. These contaminants were not directly measured but are reported in section 3.2. Methods.

The pH of the DI and distilled waters was expected to be 7, but this did not match this dissertation's measurements of the water samples. Gases in the air, such as $CO_2$, can diffuse from air into water and affect the water pH. For instance, dissolved $CO_2$ can form carbonic acid, $H_2CO_3$, which acidifies water via deprotonation, as shown in Eq. 3.2 below.

Eq. 3.2 $$CO_{2,\,(aq)} + H_2O_{(l)} \rightleftharpoons H_2CO_{3,\,(aq)} \rightleftharpoons HCO_3^{-}{}_{(aq)} + H^+_{(aq)} \rightleftharpoons CO_3^{2-}{}_{(aq)} + 2\,H^+_{(aq)}$$ [19]

It is expected the DI and distilled waters were measured as ~pH 5, rather than pH 7, due to the effect of $CO_2$. The DI water was measured in the Milli-Q system to have a specific resistivity (18.2MΩ-cm) identical to that of pure water at RT (18.2MΩ-cm [18]), so it would have been pH 7 in the Milli-Q system. The pH could have decreased from pH 7 to ~pH 5 after it was dispensed from this system and into the open-air environment of the experimental setup. The acidification process would have occurred in all waters used, even if the water pH was initially measured in a controlled environment that prevented acidification, since the amalgam water-reactions were performed in "ordinary air" containing $CO_2$. However, quantitative values corresponding to decreases in pH value that occurred for the tap and alkaline waters due to the acidification process are undetermined, partly as the tap water used is cited as having an average pH of ~8.37 (p.8 of [11]), and the alkaline water is shown in its name title as having a pH of 9.5, and both of these pH values already align with their experimentally obtained pH paper measurements in Table 3.1.

Besides the contaminants from $CO_2$ acidification (Eq. 3.2), the DI water is expected to have very low levels of other contaminants. The Milli-Q unit uses a multi-step purification system that filters out a large variety of contaminants, including organics (including bacteria), ions, and loose particulates. Secondly, before it was dispensed from the closed-environment system of the Milli-Q system, the specific resistivity of the DI water was 18.2MΩ-cm, identical to that of pure water at RT (18.2MΩ-cm [18]). Also, amalgam water-reaction rates in the DI and distilled waters were closely identical, which is consistent with the expectation that these waters are of very similar contaminant composition and are of similarly-high purity.

Similarly, the distilled water is expected to have very low levels of other contaminants. Distillation is a process that significantly purifies water. The distilled water has a measured TDS of <10ppm (p.10 of [15]) (and an estimated TDS of <1ppm). Further, its water-quality report shows the distilled water has concentrations of >100 tested chemical substances that are all lower than the Minimum Reporting Level (MRL) of the analytical method (pp.10-13 of [15]).

The alkaline water has added ingredients (magnesium sulfate, calcium chloride, and potassium bicarbonate), but likely has low levels of other contaminants. This is because it underwent “multi-stage purification and filtration” [16]. The added ingredients would be present in the alkaline water as dissolved, conductive ions that raise the pH and likely account for its measured TDS value (80ppm).

The tap water has significantly higher concentrations of contaminants than the other three waters. The specific conductivity and TDS, of the DI water vs of the tap water, are dissimilar by 4 orders of magnitude. Also, the water-quality report displays concentrations of numerous contaminants that were measured to be present in ranges of ppb and ppm (pp.7-10 of [11]). Further, the tap water very likely contains more contaminants than those listed in its water-quality report, as not all types of contaminants are required to be included [12].

The contaminants determined to be present in the waters used in this chapter's experiments are not the only ones that can slow water-reaction rate of liquid Al-Ga/eGIS. For example, in one study (pp.44-52 of [6]), the concentration of either propylene glycol or sucrose that was added to water was varied, and a fully liquid Al-Ga alloy was reacted in these waters. In all cases, increasing the concentration of either propylene glycol or sucrose decreased the alloy water-reaction rate. Water-reactivity fully ceased once the amount of propylene glycol in water was increased to 50%. The causes of the water-reactivity losses were largely unclear (p.45 and p.50 of [6]). However, from the present study's analysis, perhaps adsorption of dissolved sucrose and propylene glycol molecules on the Al-Ga and/or on Al/Ga oxide(s)/hydrate(s) film(s) on the Al-Ga, such as via hydrogen bonding and/or electrostatic attraction, played a role by acting as a physical barrier between water and Al reaction sites. As sucrose is a water-soluble sugar and propylene glycol is a water-soluble alcohol, the present study proposes that there may be other untested water-soluble organic compounds that influence Al-Ga/eGIS water-reactivity.

In addition to unidentified water-soluble contaminants, it is possible unidentified water-insoluble contaminants, perhaps via surface adsorption, may also affect Al-Ga/eGIS water-reactivity. Such unidentified contaminants may be present in the tap water, as its contaminant-type data is non-exhaustive and as it was the least purified or filtered of the tested waters. Also, chemicals have been found to leach into water from plastics [20], such as the materials used in water bottles and used for housing the water in water purification systems. However, it is expected that contaminants due to leaching from plastics have minimal impact on Al-Ga/eGIS water-reactivity, as the DI and distilled waters are expected to have very closely identical contaminant composition profiles and have been shown to have very similar amalgam water-reaction rates, despite one being sourced from a common, store-purchased plastic bottle and one being dispensed from the Milli-Q water purification system.

## 3.5. Effect of water type on the water-reaction yield of a 10wt%eGIS-90wt%Al amalgam

From Table 3.1, water-reaction yield was ~100% regardless of tested water type. No chemical substance contaminants in any of the tested waters affected water-reaction yield and/or were present in low enough concentration to not affect water-reaction yield, at least under the experimental conditions. The result of ~100% yield in terms of amount of gas captured aligns with the expected 3:2 molar ratio of $H_2$:Al. This suggests the captured gas from the amalgam water-reactions is high-purity $H_2$ gas, regardless of which water was used, or else yield would very likely be noticeably different than ~100% yield. The consecutive results of ~100% yield suggest ~0wt% of Al in the amalgams reacted with any chemical substance contaminants in any of the tested waters at the expense of reacting with water to generate $H_2$ gas.

It is a promising result for Al-eGIS amalgam technology that the amalgam appears to offer a full yield of high-purity $H_2$ gas via water-reaction, regardless of the waters' variability in pH (~5, 8, and 9-10) and variability in types of chemical substance contaminants that they contained—and even in relatively inexpensive and "dirty" tap water.

## 3.6. Comparison of the water-reaction rates of a 10wt%eGIS-90wt%Al amalgam vs water type

The amalgam water-reaction rate in the DI water was fastest, about 1.1 times faster than in the distilled water, 11 times faster than in the alkaline water, and 28 times faster than in the tap water. Amalgam water-reaction rate is likely influenced by a combination of water pH and of other effects due to the types and quantities of chemical substance contaminants in the waters. These will be discussed later in this chapter.

## 3.7. Impact of water pH on the water-reaction rate of a 10wt%eGIS-90wt%Al amalgam

The 10wt%eGIS-90wt%Al amalgam reacted, respectively, about 2.5 times faster in the alkaline water (pH 9-10), 24 times faster in the distilled water (pH 5), and 28 times faster in the DI water (pH 5) than it did in the tap water (pH 8). Increased amalgam water-reaction rate correlates with water pH that is more acidic or basic, rather than neutral. This correlation between amalgam water-reactivity and water pH will be analyzed in relation to solubility characteristics of the $Al(OH)_3$ film that is on the Al in the amalgam.

### 3.7.1. Reactions of Al, and of its semi-passivating film, with $[OH]^{-}_{(aq)}$, $H^{+}_{(aq)}$, and $[H_3O]^{+}_{(aq)}$

In acidic pH conditions, there is excess $H^{+}/[H_3O]^{+}$ relative to $[OH]^{-}$, and vice-versa for basic pH conditions. For neutral or moderate pH conditions, the ratio of $[OH]^{-}$ to $H^{+}/[H_3O]^{+}$ is roughly one.

From the ΔG° of reactions given in Table B5, under standard conditions, the thermodynamic favorability of several reactions can be determined. It is favorable for each species of Al cation to react with $[OH]^{-}$ to form Al species with less positive charge states until they become $Al(OH)_3$, $AlO(OH)$, and/or

$Al_2O_3$. It is slightly favorable for $Al_2O_3$ to react with $[OH]^-$ but unfavorable for $Al(OH)_3$ and $AlO(OH)$ to react with $[OH]^-$. It is favorable for the species of Al cations to react with $H^+$ and $[H_3O]^+$ to form Al cations of more positive charge state. But it is unfavorable for $Al(OH)_3$, $AlO(OH)$, and $Al_2O_3$ to form Al cation species by reacting with $H^+$ or $[H_3O]^+$ (Except it is slightly favorable for $Al_2O_3$ to react with $[H_3O]^+$.). It is favorable for the Al anion species to react with $H^+$ and $[H_3O]^+$ to form $Al(OH)_3$, $AlO(OH)$, and $Al_2O_3$.

From this, it may be expected that, at least near standard conditions, the semi-passivating film that forms on Al underwater tends to not react with $H^+/[H_3O]^+$ or $[OH]^-$ in water, regardless of whether it is $Al(OH)_3$ or $AlO(OH)$, which are expected to be the dominant phases present (However, there is a drive for $Al_2O_3$ to react.). However, Table B5 shows ΔG° (standard-state Gibbs free energy change of formation) rather than ΔG (nonstandard-state Gibbs free energy change of formation), which is defined below in Eq. 3.3.

Eq. 3.3 $\Delta G = \Delta G° + RT\ln(Q)$

where $Q = ([C]^c \times [D]^d)/([A]^a \times [B]^b)$ for the equation $aA + bB \rightleftharpoons cC + dD$ [21]

When the Al film incipiently forms on the Al, the ΔG for the reactions given by the Table B5 equations in which $Al(OH)_3$ and $AlO(OH)$ are reactants may initially be negative despite ΔG° being positive, due to the initially large concentration of reactants relative to products. This results in a favorable reaction of the Al film with some amount of $[OH]^-$ and/or $H^+/[H_3O]^+$ due to Le Chatelier's principle, until ΔG increases to zero, at which point the forward and reverse reaction rates become equal and will continue to remain equal. The initially large concentration of reactants relative to products is due to zero products being initially present but can also be due to the water being initially very basic or acidic, in which there is a large initial concentration of, respectively, $[OH]^-$ or $H^+/[H_3O]^+$, making the ln(Q) term in Eq. 3.3 more negative, allowing ΔG to become negative if and when RTln(Q) is negative and $RT\ln(Q) > \Delta G°$. So, the Al film may be increasingly susceptible to reaction in water of increasing acidity or basicity, increasing film removal. This would align with the observed greater amalgam water-reactivity in DI, distilled, and alkaline waters vs in tap water. But the degree of film reaction may be expected to be low as $\Delta G°$ is positive, and perhaps also if pH values of the waters used in this chapter's experiments were too moderate. But the degree of film reaction is unknown without more in-depth investigation.

Table B2 includes an "Alternative Al reactions" section of reactions that may occur instead of or in parallel with reactions of Al with only water, Eqs. B2.1-B2.5. "Alternative Al reactions" are more energetically favorable under standard conditions than are those of Eqs. B2.1-B2.5, as they have more negative $\Delta G°$ values, but they rely on significant availability of $H^+$, $[H_3O]^+$, and/or $[OH]^-$. The alternative Al reactions produce $H_2$:Al in the same 3:2 molar ratio that was observed experimentally for each tested amalgam-water combination in this chapter, so they may have occurred. And if they occurred, it is energetically favorable, according to the equations in Table B5, for the ionic Al species that are produced to then convert into $Al(OH)_3$, $AlO(OH)$, and/or $Al_2O_3$, aligning with observations of white precipitate production (However, the white precipitate was not quantified, such as by collecting and weighing it, to obtain the stoichiometric ratio of how much of it was produced with respect to the amount of Al that was consumed.).

The alternative Al reactions may occur if $[OH]^-$, $H^+$, and/or $[H_3O]^+$ become significantly available to react with Al. This should more likely occur if pH becomes increasingly basic or acidic and/or if $[OH]^-$, $H^+$, and/or $[H_3O]^+$ diffuse readily through the semi-passivating Al film to react with the Al substrate. If such diffusion occurs more readily than does $H_2O$ diffusion through the film, this may align with the observed greater amalgam water-reactivity in DI, distilled, and alkaline waters vs in tap water.

### 3.7.2. Significance of the Al Pourbaix diagram

An Al Pourbaix diagram is in Figure 3.5 below, illustrating corrosion resistance at 25°C of Al vs pH. Water is stable in the region between diagonal dashed lines. The figure shows the formula $Al_2O_3 \cdot H_2O$. Some Pourbaix diagrams in the literature display $Al_2O_3 \cdot 3H_2O$. $Al_2O_3 \cdot H_2O$ corresponds to $AlO(OH)$ and $Al_2O_3 \cdot 3H_2O$ corresponds to $Al(OH)_3$, as these are given by the ratios of Al:O:H atoms in these formulas. $Al(OH)_3$ should be more stable below ~72°C and $AlO(OH)$ should be more stable above ~72°C (p.43 of [2]); in Table B3, this value was instead calculated as ~63°C. The Pourbaix diagram, as with phase diagrams, does not account for activation energy barriers or kinetic limitations, so reaction rates of Al vs pH cannot be determined from the diagram.

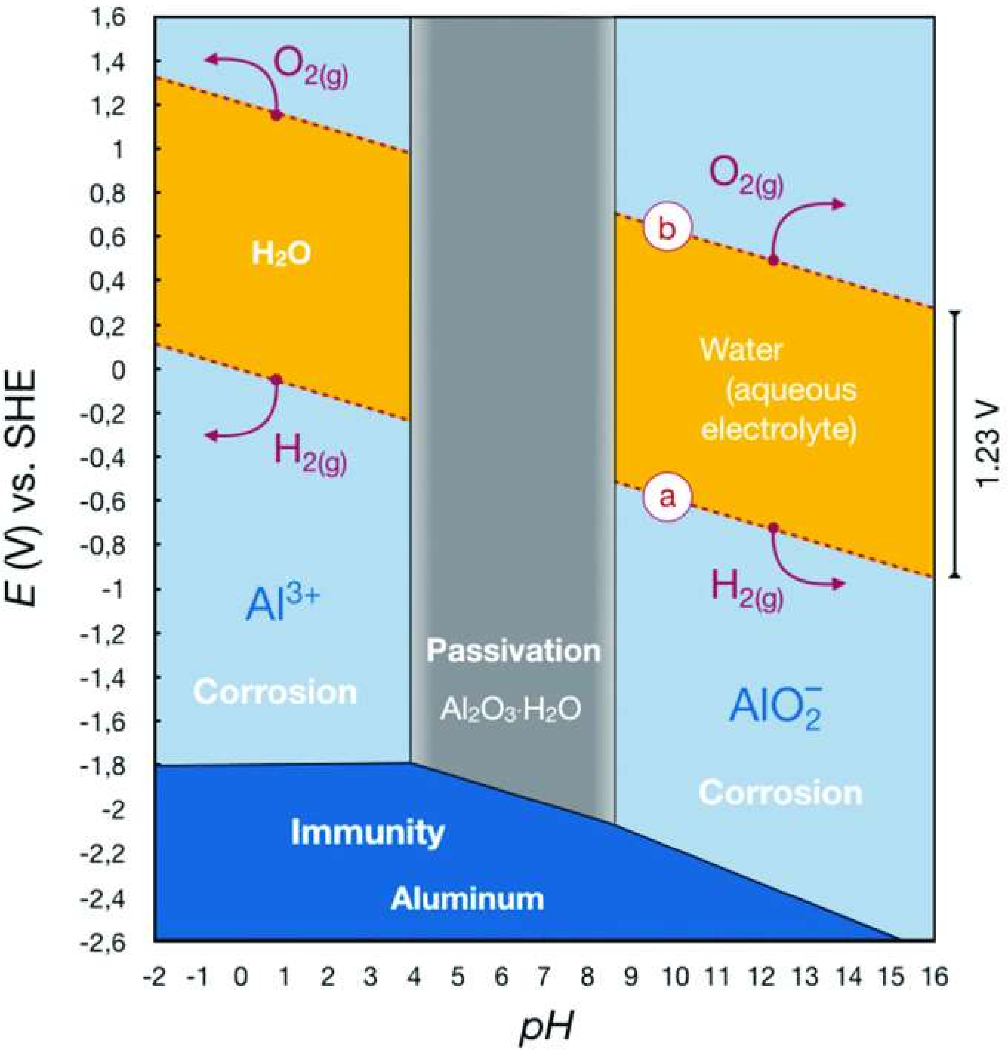

**Figure 3.5. Pourbaix diagram for Al at 25°C.** [22]

(Reprinted with permission from the Frontiers in Chemistry journal).

From the Pourbaix diagram, Al should not corrode in moderate-pH water, as it is passivated. But outside a moderate water pH range, Al may corrode and form other species that are more thermodynamically favored and stable. The region of Al immunity to corrosion is well below the region of water stability at all pH values, reflecting a “very large” [23] thermodynamic driving force for Al to corrode in water at all pH values. For example, the driving force for Al water-corrosion [23] is a potential difference of ~2.9V (as the standard oxidation potential of water is 1.23V and the standard reduction potential of Al is −1.7V) in the relatively moderate pH range from ~4 to 8.4. Despite this, the diagram shows that Al remains significantly protected from water-reaction at moderate pH, reflecting the imperviousness of its passivating film at moderate pH.

However, the diagram shows this film is not passivating outside of a moderate pH range—that is, in acidic or basic conditions. This is roughly consistent with the observed faster amalgam water-reaction rates in more acidic or basic conditions (distilled/DI/alkaline water) rather than at more moderate pH (tap water). But the Pourbaix diagram shows Al should be protected at ~pH 4, which is below ~pH 5 for the DI/distilled waters used experimentally. This may be partly because this diagram does not directly apply to the case of an Al-eGIS amalgam in contact with water.

The diagram assumes Al is solid-phase and can thus adhere well to its passivating film. However, the Al in an Al-eGIS amalgam that takes part in water-reaction is liquid-phase Al, so its film should comparatively be less-adherent and more weakly passivating. This goes for the initial film that was present on the liquid Al that spontaneously formed in air before water-reaction and also for the film that formed on the liquid Al during water-reaction. The native film on the liquid Al before the amalgam is placed underwater should quickly delaminate from the liquid Al when the amalgam is placed underwater, as seen by the lack of any measurable induction period in Figures 3.1-3.4. Then, the liquid Al quickly reacts to completion with water, whereas solid Al was shown to instantly re-passivate while underwater if its passivation film was removed and to show no further observable reaction [8]. All of this suggests the film on liquid Al during water-reaction is weakly passivating compared to the film on solid Al during water-reaction.

There does not appear to be an Al Pourbaix diagram in the literature for liquid Al, but such a diagram would likely not depict $Al(OH)_3$ as a passivating film, because liquid Al should not be passivated but should instead react with water. So, the displayed Al Pourbaix diagram does not apply directly for liquid Al but instead shows why solid Al in Al-eGIS may not be water-reactive in DI/distilled/tap water, as it tends to be well-passivated in a pH range of ~4 to 8.4. It also shows it is possible solid Al in Al-eGIS amalgams may be water-reactive in the alkaline water, as its pH is >8.4. This was untested but may be tested with experiments involving placing pure, solid-phase Al in the alkaline water.

### 3.7.3. Significance of the solid-phase, amorphous $Al(OH)_3$ solubility diagrams

From its solubility diagram (p.910 of [24]), solid-phase, amorphous $Al(OH)_3$ in water at 25°C is most stable in a pH range of ~5.8 to 8.6, as its solubility remains at a constant, minimum value. As the pH increases above ~8.6, the solid-phase, amorphous $Al(OH)_3$ dissolves further, due to greater availability of $[OH]^-$ in water to react with, and it primarily dissolves as $[Al(OH)_4]^-$. The more that pH decreases below ~5.8, solid-phase, amorphous $Al(OH)_3$ dissolves more, due to greater availability of $H^+/[H_3O]^+$ in water to react with, and it primarily dissolves as cations such as $[Al(OH)_2]^+$.

This solubility diagram (p.910 of [24]) is for $Al(OH)_3$ that is amorphous. It is hypothesized that the $Al(OH)_3$ that forms on the liquid Al in an Al-eGIS amalgam likely has much amorphous character. This is because it is quickly formed, so atoms may have little time to arrange into a well-ordered crystal structure, and because the Al is liquid, so it does not have a well-ordered crystal structure for $Al(OH)_3$ growth to map onto. XRD data (pp.17-20 of [2]) shows that $\alpha$-$Al(OH)_3$ is the main liquid Al water-reaction product, in both the 50wt%Al-50wt%eGIS alloy and in eutectic Al-Ga alloy. The $\alpha$-$Al(OH)_3$ may have high % crystallinity, compared to % amorphousness, as the α designates it is as a crystalline phase (specifically, bayerite). However, the experiments in [2] used a powder that was first dried (pp.17-19 of [2]) and would have also aged before XRD was performed, which may have increased its % crystallinity and decreased its % amorphousness. So, the structure of the $Al(OH)_3$ may have changed from when it was initially created to when it was analyzed.

For this chapter's 50°C water-reactions, it is expected that the pH range of constant, minimum solubility of amorphous $Al(OH)_3$ (shown on p.910 of [24]) for water of 25°C should widen, and solubility within this pH range should increase, as this trend is already observed when temperature increases from 4°C to 25°C (as shown on p.910 of [24]). If so, then all trials (DI/distilled/tap/alkaline) may be within this predicted pH range of constant, minimum solubility for amorphous $Al(OH)_3$ at 50°C, but there is uncertainty regarding the edges of the solubility boundary for the most acidic (DI/distilled) and basic (alkaline) waters. In this case, water pH may not affect solubility of amorphous $Al(OH)_3$ for the tested waters.

But it is possible this was not so for the 50°C tested waters of lowest pH (DI/distilled) and highest pH (alkaline), even if they appear to fall within the expected pH range of constant, minimum solubility. For example, the film on liquid Al in an Al-eGIS amalgam may have different solubility characteristics. To begin the argument, literature shows amorphous $Al(OH)_3$ is significantly more water-soluble than crystalline $Al(OH)_3$ (gibbsite) (Figure 16 of [25]). From this, it may be assumed that increasing the degree of amorphousness increases the solubility of $Al(OH)_3$. As the $Al(OH)_3$ degree of amorphousness (shown on p.910 of [24]) was unquantified, it is possible it is less amorphous than the $Al(OH)_3$ film on the liquid Al in an Al-eGIS amalgam. The $Al(OH)_3$ film may be very amorphous, as it likely formed rapidly (partly due to the moderately warm water of 50°C in the experiments), formed in a thin film, and formed by mapping onto the disordered arrangement (highly amorphous lattice) of atoms in liquid Al rather than onto a well-ordered, solid Al lattice. The $Al(OH)_3$ film may also be more amorphous because it experiences partial, continual dissolution while it grows, and vigorous production of $H_2$ bubbles locally may mechanically agitate it, causing defects. Also, multiple phases of varyingly amorphous Al oxide/hydrate(s) may form on the liquid Al (as multiple phases of Al oxide/hydrate(s) are closely thermodynamically favorable, as seen by their close ΔG° values in Eqs. B2.1-B2.5 in Table B2)—and may only later convert, via Eqs. B2.32 and B2.33 in Table B2, to the more stable $Al(OH)_3$ phase, which is favored below ~72°C (p.43 of [2]) or below ~63°C in Table B3. The presence of these multiple phases may increase $Al(OH)_3$ solubility by decreasing $Al(OH)_3$ stability, due to the likelihood of less coherency (weaker bonding) among multiple phases of Al oxide/hydrate(s), as they would have different crystal structures and/or lattice constants. This same scenario may also occur between the $Al(OH)_3$ film and adjacent GIS oxide(s)/hydrate(s) film(s).

So, possibly, for this chapter's experiments in 50°C waters, only the tap water had a pH that fell within the unknown but actual pH range of minimum solubility for the Al oxide/hydrate(s) film on liquid Al. If so, this film would be more soluble in the DI/distilled/alkaline waters than in the tap water. Increased film solubility/dissolution would decrease its thickness, allowing faster diffusion of $H_2O$, $[OH]^-$, $H^+$, and/or $[H_3O]^+$ through it, increasing amalgam hydrogen-generation rate. Increased dissolution may also occur at locations of adhesion and bonding that would otherwise enable the Al oxide/hydrate(s) film to remain in place to act as a semi-passivating film on the liquid Al, such as adhesion and bonding to Al (liquid and/or solid) and/or to GIS oxide(s)/hydrate(s). These explanations are consistent with the observation of significantly increased Al-eGIS amalgam water-reaction rate in DI/distilled/alkaline waters vs in tap water.

As shown in the diagram on p.910 of [24], at 25°C, dissolution of $Al(OH)_3$ increases more sharply as pH decreases below ~4.8, as compared to dissolution increasing less sharply for same-sized increases in pH on the basic-pH side of the diagram. If the amalgam's Al oxide/hydrate(s) film is less stable and more soluble than the amorphous $Al(OH)_3$ (that is shown on p.910 of [24]) and has a minimum-solubility pH region that is smaller than that predicted for the 25°C diagram that is shown on p.910 of [24], then this may be consistent with the faster amalgam water-reaction rates observed in the DI and distilled waters (~pH 5) than in the alkaline water (~pH 9-10).

The bulk water's pH changes during or after amalgam water-reaction, such as due to variation in the ratio of $[OH]^-$ to $H^+/[H_3O]^+$, were not measured. Further, local pH changes near reaction sites were not measured but may differ from bulk water measurements and would require specialized pH measurement techniques for small-scale areas/volumes.

## 3.8. Impact of water contaminants on the water-reaction rate of a 10wt%eGIS-90wt%Al amalgam

Contaminants present in the tested waters may also affect the passivity of the $Al(OH)_3$ film on liquid Al in the Al-eGIS amalgam via adsorption and/or precipitation on/in the $Al(OH)_3$ film. The contaminants may act as physical barriers on/in the film, hindering penetration of reactants into the film and hindering their mobility through the film, slowing the rate that they reach and react with liquid Al. Precipitate formation and/or adsorption on water-contacting surfaces of the $Al(OH)_3$ film may also slow the dissolution rate of the film into water by acting as physical barriers between the film and water. Both of these mechanisms may slow the amalgam water-reaction rate.

### 3.8.1. Precipitate formation on/in the $Al(OH)_3$ film

As shown in the diagram on p.910 of [24], at all pH values, amorphous $Al(OH)_3$ partially dissolves as per Eq. 3.4 below.

Eq. 3.4 $Al(OH)_{3,\,(s)} \rightleftharpoons Al^{3+}_{(aq)} + 3\,[OH]^-_{(aq)}$

$K_{sp} = 10^{-33.9}$ (gibbsite), and $K_{sp} = 10^{-31.2}$ (amorphous gibbsite) (Figure 16 of [25])

where $K_{sp}$ is the solubility product constant.

$Al(OH)_{3,\,(aq)}$ is a prevalent dissolution product in all tested waters and is the only one discussed, but analyses of other dissolution products would involve similar concepts. The dissolved $Al^{3+}$ and $[OH]^{-}$ ions may react with dissolved ionic contaminants in all tested waters in precipitation reactions to form insoluble compounds, potentially on/in the $Al(OH)_3$ film (as per the diagrams that are displayed in [26], p.C205 of [27], and p.5 of [28]) (These references are non-exhaustive but show some relevant, common compounds.).

When ionic water contaminants react with $Al^{3+}$ and $[OH]^{-}$ to form insoluble products, the products that are more likely to precipitate are those with the lowest solubility product constant ($K_{sp}$) values, compared to those of higher values under identical conditions (the same pH, temperature, etc.). The table on p.C205 of [27] lists $K_{sp}$ values for some relevant, common compounds. The large list of compounds is particularly relevant for tap water, which contains numerous contaminants.

According to the diagrams shown on p.5 of [28], most hydroxides dissolve at acidic pH values; however, at neutral and basic pH values, most have low solubility, and thus are more likely to precipitate. This trend is consistent with the fastest water-reactions of the amalgam occurring at more acidic pH (DI/distilled waters) and with the slower water-reactions occurring at slightly basic pH (tap water) and moderately basic pH (alkaline water).

The alkaline water was labeled to contain "less than 0.5% of: magnesium sulfate, calcium chloride, potassium bicarbonate." The solubility table in [26] shows that KOH is soluble so would not precipitate. The diagrams shown on p.5 of [28] show $Ca(OH)_2$ only precipitates above ~pH 12, and $Mg(OH)_2$ only precipitates at just over ~pH 9. So, $Mg(OH)_2$ may have precipitated as pH of the alkaline water was ~9-10, whereas it is unlikely $Ca(OH)_2$ precipitated. It is noted that the data for the diagrams shown on p.5 of [28] were measured at 25°C, but the experiments in this chapter were done at 50°C. The alkaline water underwent "multi-stage purification and filtration" [16], so, apart from its aforementioned added ingredients, it should have low levels of hydroxide-precipitating contaminants, similar to the distilled/DI waters and dissimilar to the tap water, which was not extensively purified/filtered and had four times higher TDS than did the alkaline water (320ppm vs 80ppm).

Of the tested waters, the tap water has by far the highest TDS; some dissolved solids are known and some are unknown. There are numerous metal cations in the tap water that can form insoluble hydroxides. But because the alkaline water may precipitate $Mg(OH)_2$, as its main added ingredient by mass (as it is listed first on the ingredient list) is magnesium sulfate, it may be incorrect to assume the tap water has a more significant degree of precipitation formation on/in the Al oxide/hydrate(s) film than does the alkaline water.

As shown in the solubility table in [26], in the tap water, $Al^{3+}$, originating from the dissolved Al oxide/hydrate(s) film, may precipitate in/on the film as aluminum phosphate. The phosphate concentration in the tap water was not measured [11], as not all substances in the tap water were required to be reported in the water safety report [12], but it is claimed to be present from 0.1 to 0.8ppm [12]; also, ortho-phosphate was stated to have been injected into the water (p.1 of [11]). $Al^{3+}$ may be unlikely to precipitate as aluminum arsenate, as only ~3.8ppb (p.7 of [11]) of As was measured in the tap water. The solubility table in [26] shows Mg, Ca, Fe, Cu, Ag, Zn, Pb, and Al may precipitate as metal hydroxides. Besides Ag and Zn, which were not measured but may have been present, all of these were found in the tap water [11], although Al concentration is not given as it was stated to be below the testing limit (p.5 and p.7 of [11]). As with the alkaline water, $Ca(OH)_2$ is unlikely to precipitate. However, hydroxides of Mg, Fe, and Cu may have.

The DI/distilled waters should have exceedingly low to no contaminants other than those in Eq. 3.2 (re-written below). So, the only significant precipitation reactions expected to occur would be those related to carbonic acid, such as between $Al^{3+}$ and $HCO_3^-$ and/or $CO_3^{2-}$ to form aluminum bicarbonate, $Al(HCO_3)_3$, and/or aluminum carbonate, $Al_2(CO_3)_3$.

Eq. 3.2 $CO_{2,(aq)} + H_2O_{(l)} \rightleftharpoons H_2CO_{3,(aq)} \rightleftharpoons HCO_3^-{}_{(aq)} + H^+{}_{(aq)} \rightleftharpoons CO_3^{2-}{}_{(aq)} + 2\,H^+{}_{(aq)}$ [19]

There is very scarce literature on $Al(HCO_3)_3$ and $Al_2(CO_3)_3$. The solubility table in [26] shows $Al_2(CO_3)_3$ reacts with water rather than dissolving, and its swift decomposition is briefly discussed in [29], which mentions it has little commercial value and is difficult to store and study (which may be why there is a dearth of literature on this topic). But it is unclear how fast the decomposition reaction with water occurs. If $Al_2(CO_3)_3$ decomposes slowly, it may act as a solid precipitate on a short timescale, such as during the growth and exfoliation of the $Al(OH)_3$ film of the liquid Al in the amalgam. However, even if the presence of carbonic acid results in $Al_2(CO_3)_3$ precipitation that slows amalgam water-reaction rate, the size of this effect is unclear compared to the pH effect of carbonic acid acidifying the DI/distilled waters to potentially increase amalgam water-reaction rate.

## 3.8.2. Adsorption of contaminants on the $Al(OH)_3$ film

Inorganic and organic contaminant species may adsorb on the $Al(OH)_3$ film to form additional film(s) [30]. Nonionic and ionic substances may adsorb through numerous adsorption mechanisms; some that may occur on $Al(OH)_3$ are electrostatic interaction, hydrophobic interaction, hydrogen bonding, van der Waals, and ligand exchange (as cited in [31], section: Introduction). Ligand exchange is the strongest of these (as cited in [31], section: Introduction). Primarily, ligand exchange and electrostatic adsorption of ions will be discussed.

Ligand exchange may occur in which $[OH]^-$ ligand groups on Al in Al hydrates are replaced by anionic water contaminants. Highly amorphous AlO(OH) (which is expected for the Al oxide/hydrate(s) film that forms on liquid Al-Ga/eGIS) has a larger surface area than more crystalline AlO(OH), giving it a larger adsorption capacity (as cited in [32], section: Aluminum adjuvants). Numerous anionic substances may adsorb via ligand exchange with Al hydrate(s), and there is a high affinity for ligand exchange adsorption on AlO(OH) with phosphate and fluoride, a moderate affinity with sulfate, and a low affinity with chloride and nitrate (as cited in [32], section: Aluminum adjuvants). These species were present in the tap water: ~0.1 to 0.8ppm phosphate [12], ~0.11ppm fluoride (p.7 of [11]), and ~32.2ppm sulfate (p.7 of [11]).

The isoelectric point (IEP) is the pH at which there is no net surface charge. Based on the surface charge of the $Al(OH)_3$ film (for example, a negative charge), counterions (in this case, cations) in the water may more strongly adsorb in the Stern (Helmholtz) film or layer, the layer directly on the $Al(OH)_3$, as opposite charges are attracted to each other in an attempt to neutralize the net surface charge on the $Al(OH)_3$. A mix of anions and cations may also adsorb in the diffuse (Gouy-Chapman) layer, the layer that envelops the Stern film, as the anions are attracted to the cations in the Stern film, and the cations in the diffuse layer are attracted to the negative surface charge of the $Al(OH)_3$. In this way, the surface of the $Al(OH)_3$ may become semi-passivated by adsorption of numerous charged species, which may continuously adsorb until the net surface charge on the $Al(OH)_3$ film is fully neutralized. [33]

For an amphoteric hydroxide, such as $Al(OH)_3$, the IEP corresponds with the point of minimum solubility (p.1271 of [34]). So, from the $Al(OH)_3$ solubility diagrams (p.910 of [24]), the minimum solubility is between ~pH 5.8 and 8.6, or, on average, ~7.2. The IEP appears to shift slightly from ~pH 7.5 to 7.2 going from 4°C to 25°C (p.910 of [24]). So, the IEP may be at a slightly lower pH than that at 25°C, for this chapter's experiments at 50°C.

By changing the water pH, the $Al(OH)_3$ surface charge also changes, affecting the adsorption affinity and adsorption capacity of each charged contaminant. At pH values above its IEP, $Al(OH)_3$ primarily forms $[Al(OH)_4]^-$ anions (as shown in the diagrams on p.910 of [24]). Some of these anions may remain adsorbed on the $Al(OH)_3$ film to make its surface negatively charged, and this negative surface charge increases as pH increases farther above the IEP, as more of these anions are present. At pH values below its IEP, $Al(OH)_3$ primarily forms cations, such as $[Al(OH)_2]^+$ (as shown in the diagrams on p.910 of [24]). Some of these cations may remain adsorbed on $Al(OH)_3$ to make its surface positively charged, and this positive surface charge increases as pH decreases farther below the IEP, as more of these cations are present. A plot of pH vs average charge of species of dissolved Al is shown in the illustration on p.4 of [35] (reproduced from [36]).

The pH values of the tap water (~8) and the alkaline water (~9-10) should be above the IEP, so primarily cations may adsorb onto the negatively charged $Al(OH)_3$ surface. The pH is higher above the IEP for the alkaline water than for the tap water. So, the net surface charge of the $Al(OH)_3$ is more unbalanced and more strongly attracts cations. This may result in greater passivity of the $Al(OH)_3$, thereby favoring slower amalgam water-reaction rate, in the alkaline water than in the tap water with all else equal. But faster amalgam water-reaction rate was seen. This may be partly because the types of adsorbed species are different, as the waters have different contaminants. Also, the tap water has a TDS that is four times higher than that of the alkaline water (320ppm vs 80ppm), so the tap water has more charged species that may adsorb. Also, there are other mechanisms affecting difference in passivity that are discussed in previous sections.

The pH of the DI/distilled waters (~5) is below the IEP, so primarily anions may adsorb onto the positively charged $Al(OH)_3$ surface. Bicarbonate and carbonate anions from dissolved $CO_2$ would have been present in all tested waters. In the tap and alkaline waters, the surfaces should be negatively charged, so they would largely repel these. However, in the DI/distilled waters, the $Al(OH)_3$ surface should be positively charged, so these anions may adsorb. This may slow amalgam water-reaction rate. But the degree of this effect may be difficult to experimentally determine, as removing $CO_2$ from water to compare amalgam water-reaction rate in $CO_2$-rich vs $CO_2$-free water would also vary pH. It is unclear if this adsorption effect is small compared to the effect of carbonic acid acidifying the DI/distilled waters, which may increase amalgam water-reaction rate.

It is assumed the displayed average net charge vs pH, shown in the illustration on p.4 of [35] (reproduced from [36]), correlates to the relative strength and sign of the surface charge of the $Al(OH)_3$ film. From the aforementioned illustration, at pHs of 5, 9, and 10, the net charge is, respectively, about +1.4, −0.9, and −1.1. So, the $Al(OH)_3$ film in the DI/distilled waters (~pH 5) may more strongly electrostatically attract counterions to adsorb than in the alkaline water (~pH 9-10), as the magnitude of the surface charge is greater. This may result in greater passivity of the $Al(OH)_3$ film in the DI/distilled waters than in the alkaline water. However, the amalgam water-reaction rate is much faster in the DI/distilled waters. Further, for the DI/distilled waters vs the tap water, the gap in amalgam water-reaction rate is even greater, despite the pH of the tap water being the closest to the IEP.

These discrepancies may be from several factors. Firstly, the types of adsorbed species are different, as the waters have different contaminants. To this point, in the tested waters, additional ionic contaminant adsorbates may form from complexation reactions. For example, tap water contains ~0.11ppm fluoride (p.7 of [11]), and Eq. 3.5 below shows the complex ion $[AlF_6]^{3-}{}_{(aq)}$ may form if six $F^{-}{}_{(aq)}$ react with one $Al^{3+}{}_{(aq)}$.

Eq. 3.5 $Al^{3+}{}_{(aq)} + 6\ F^{-}{}_{(aq)} \rightleftharpoons [AlF_6]^{3-}{}_{(aq)}$ $K_f = 6.9 \times 10^{19}$ ([37], as cited in [38])

Secondly, the tap and alkaline waters have TDS values of, respectively, >32 times and >8 times higher than those of the DI/distilled waters (320ppm and 80ppm, vs <10ppm), and they have specific resistivity values of, respectively, >266 times and >67 times lower than those of the DI/distilled waters (~0.0075 MΩ-cm and 0.00188 MΩ-cm, vs >0.5MΩ-cm). So, the tap and alkaline waters should have significantly larger quantities of charged contaminant species that may adsorb on the $Al(OH)_3$ film than for the DI/distilled waters. Also, there are other mechanisms affecting difference in passivity that are discussed in previous sections.

### 3.8.3. Correlation between total dissolved solids (TDS) and the water-reaction rate of a 10wt%eGIS-90wt%Al amalgam

The TDS may be used as an estimate of the overall quantity of contaminants in the tested waters that are involved in adsorption and/or precipitation on/in the $Al(OH)_3$ film. A comparison of TDS values and amalgam water-reaction rates is shown in Figure 3.6.

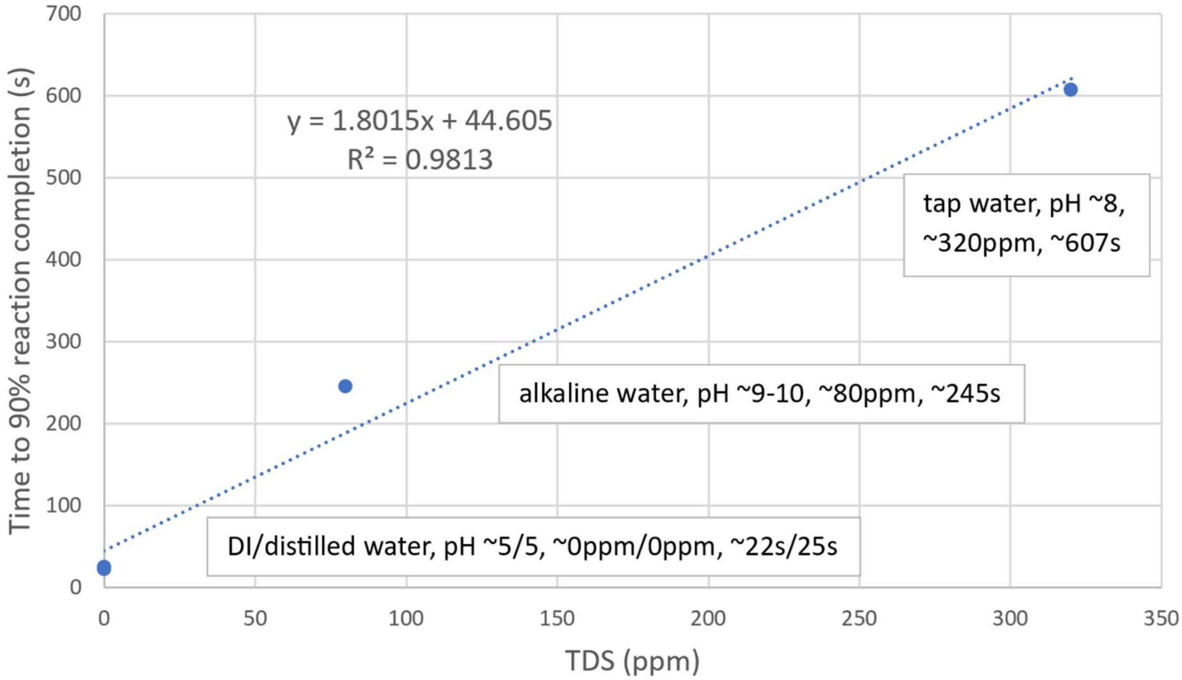

**Figure 3.6. TDS vs time to 90% water-reaction completion for 10wt%eGIS-90wt%Al amalgam in different tested waters, each at 50°C.** A linear-fit equation was made from the data in Table 3.1. DI/distilled waters were assumed to have ~0ppm TDS. pH and contaminant type are uncontrolled variables in the plot.

The DI/distilled waters are taken to be closely identical in type and concentration of contaminants, and thereby also closely identical regarding pH and TDS, so it makes sense that their amalgam water-reaction rates were closely identical. Waters with higher TDS correlate with slower amalgam water-reaction rates (longer times to 90% water-reaction completion), as shown in Figure 3.6. This correlation supports the hypotheses of increased adsorption and/or precipitation on/in the $Al(OH)_3$ film increasing $Al(OH)_3$ film passivity, which in turn decreases amalgam water-reaction rate. However, the correlation may also possibly be explained by pH differences and/or contaminant type differences of the tested waters, although their relative degrees of contribution are unclear.

## 3.9. Impact of galvanic corrosion reactions on the water-reaction rate of a 10wt%eGIS-90wt%Al amalgam

Galvanic corrosion will not occur if the amalgam is in a dry environment but may occur if moisture is present in air or if the amalgam is placed into water. Table B4 lists half-reactions that may occur in the amalgam-water system. If two half-reactions are selected from Table B4, the half-reaction with lower standard reduction potential, $E^\circ$, donates electrons to the half-reaction with higher $E^\circ$. Half-reactions with Al have lower $E^\circ$ values compared to those of other half-reactions in Table B4, and this dissimilarity creates an electromotive force or cell voltage that drives Al to, via the half-reactions listed in the Al section of Table B4, donate electrons to, for example, the left-hand-side of the half-reactions listed in the Ga, In, Sn, $O_2$, and $H_2$ sections of Table B4. This driving force, $E^\circ_{cell}$, is given by Eq. 3.6 below, and it increases the greater the difference is between $E^\circ_{cathode}$ and $E^\circ_{anode}$.

Eq. 3.6 $E^\circ_{cell} = E^\circ_{cathode} - E^\circ_{anode}$

From the equations in Table B4, most galvanic reactions appear to play a very limited role in Al consumption compared to Al water-reactions in Table B2 Eqs. B2.1-B2.5, at least on the timescale in which Al in the amalgam takes to fully react. This is because ~100% $H_2$ gas yield was observed for each amalgam water-reaction. Also, much white precipitate ($Al(OH)_3$ reaction product) was observed to be produced (However, it was not quantified, such as by collecting and weighing it, to obtain the stoichiometric ratio of how much of it was produced with respect to the amount of Al that was consumed.). However, many pairs of half-reactions in Table B4 do not align with these observations. For example, Al half-reactions paired with half-reactions in any section besides the $H_2$ section do not produce $H_2$, so they are inconsistent with the observed ~100% $H_2$ yields. Had they occurred, they would have consumed Al without producing $H_2$, resulting in <100% observed yield of $H_2$. This suggests galvanic reactions occur an insignificant amount between Al and GIS and between Al and dissolved $O_2$ gas.

However, it is possible that galvanic reactions between half-reactions in the $H_2$ and Al sections of Table B4 occur. Such reactions correspond to a 3:2 molar ratio of $H_2$:Al, aligning with the observed ~100% yield of $H_2$ gas. And if they occur, it is energetically favorable ($\Delta G° < 0$), according to the equations in Table B5, for the ionic Al species that are produced to then convert into $Al(OH)_3$, $AlO(OH)$, and/or $Al_2O_3$, aligning with qualitative observations of the generation of white precipitate reaction products. It is unclear to what extent these galvanic reactions occur, but they may be limited from occurring by lack of significant amounts of available $[OH]^-$ and/or $H^+$, which are necessary reactants in these galvanic reactions, according to the equations in Table B4. Galvanic reactions otherwise appear to be insignificant consumers of Al, regardless of water type, at least for the tested water types.

## 3.10. Conclusions

This chapter offered a framework for understanding how water type can impact amalgam water-reaction rate. But for deeper understanding, further experiments must be performed that isolate the effects of pH and of individual water contaminants.

It is also largely unclear which and how many precipitates form on/in the $Al(OH)_3$ film and which and how many species adsorb on the $Al(OH)_3$ film in the brief time intervals in which the film forms and exfoliates. Precipitation reaction products and adsorbed species, if they occurred, may remain post-reaction on/in $Al(OH)_3$, so future work may analyze the types and concentrations of impurities in post-reaction $Al(OH)_3$.

Future research may study how changing the concentrations of individual contaminants, such as by using water containing only one contaminant, affects amalgam water-reaction rate, working up to increasingly complex multi-contaminant systems.

# Chapter 4: The Impact of the Adhesion and Bonding, Between the Al Oxide/Hydrate(s) Film and the GIS Oxide(s)/Hydrate(s) Film That Are on Al-eGIS, on the Water-Reaction Rate of Al-eGIS

## 4.1. Introduction

The only Al in Al-eGIS that is significantly water-reactive is liquid Al, which is dissolved in liquid GIS. The liquid GIS is likely close to the eGIS composition of ~68.5wt%Ga, ~21.5wt%In, and ~10wt%Sn, or may possibly contain less Ga than this if some Ga diffused into Al grains. The maximum solubility of Al in liquid GIS is expected to be low in experiments involving Al-eGIS alloys or amalgams in this work and in literature, as such experiments are performed in waters with temperatures that do not exceed the boiling point of water, 100°C. The maximum solubility of Al in liquid Ga at 100°C is only ~2.5wt%, based on the Al-Ga phase diagram. Predictions based on the Al-In and Al-Sn phase diagrams are more complex since their eutectics occur well above 100°C and are at, respectively, 156°C and 228°C, as shown in Appendix C of [2] (reproduced from [1]). At the same time, it must be considered that In and Sn are fully liquid, even at far below RT, when they comprise eGIS. But even so, in the Al-In and Al-Sn phase diagrams, the liquidus boundary line on the Al-rich side of the eutectics rises very sharply as wt% of Al increases relative to that of In or Sn, so the minimum temperature required to maintain Al solubility in liquid In and liquid Sn increases rapidly with increased dissolved wt% of Al in liquid In and liquid Sn. So, it seems unlikely that more than a few wt% of Al can dissolve into the liquid GIS in Al-eGIS alloys or amalgams that are reacted in water, regardless of if the water is cold or boiling.

So, the vast majority of the surface of the fully liquid Al-GIS, the only location in which water-reaction can occur in Al-eGIS, should be GIS rather than Al. As solubility of liquid Al should be only up to a few wt% throughout the liquid GIS, and as the Al and GIS should be miscible liquids (There is no liquid miscibility gap in the Al-Ga and Al-Sn phase diagrams, although there is one in the Al-In phase diagram but only at over 3wt%Al.), dissolved Al atoms should be highly coordinated by liquid GIS atoms rather than by Al atoms. Given this, the $Al(OH)_3$ film that forms on the liquid Al may be well-coordinated by the GIS oxide(s)/hydrate(s) film that grows on directly adjacent GIS. The GIS film of oxide(s)/hydrate(s), as it is prevalent and in close proximity to the $Al(OH)_3$ film, may impact the exfoliation rate of the $Al(OH)_3$ film, impacting Al-eGIS water-reaction rate.

## 4.2. Goal

Throughout this work and throughout the literature of reacting Al-Ga/eGIS with water to generate $H_2$ gas, the waters that are used are relatively warm or hot in temperature; they are also exposed to ordinary air and thus are well-oxygenated. This experiment aims to determine if the use of such waters results in the formation of oxide(s)/hydrate(s) on liquid Ga and/or liquid eGIS.

## 4.3. Methods

In separate beakers that were on hot plates, 4N-purity liquid eGIS and 4N-purity liquid Ga were placed fully underwater in 80°C water that was exposed to ordinary air. These samples were observed after remaining under these conditions for 2 days and 4 days.

## 4.4. Data

Figures 4.1-4.4 below show observed growth of oxide(s)/hydrate(s) on liquid Ga and liquid eGIS under the experimental conditions.

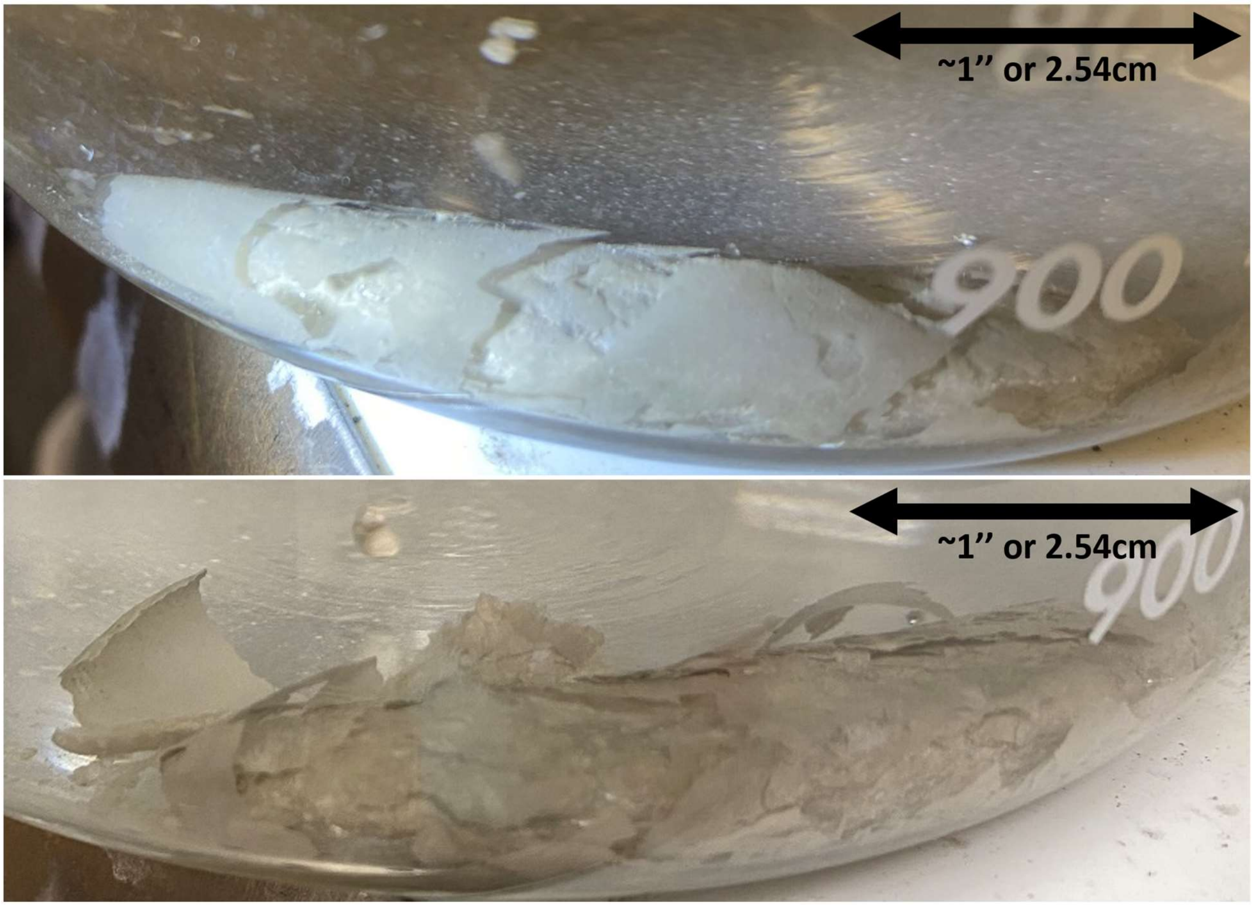

**Figure 4.1. Observations of eGIS pools in water.**

Top image: a large pool of high-purity liquid eGIS was placed in 80°C water and the image was taken after 2 days in the 80°C water. It grew a film(s) of GIS oxide(s)/hydrate(s), which appears to be partially delaminated.

Bottom image: after 4 days in 80°C water, the delaminated film(s) drifted farther away from the surface of the liquid GIS, but the sample does not appear to have much additional GIS oxide(s)/hydrate(s) formation.

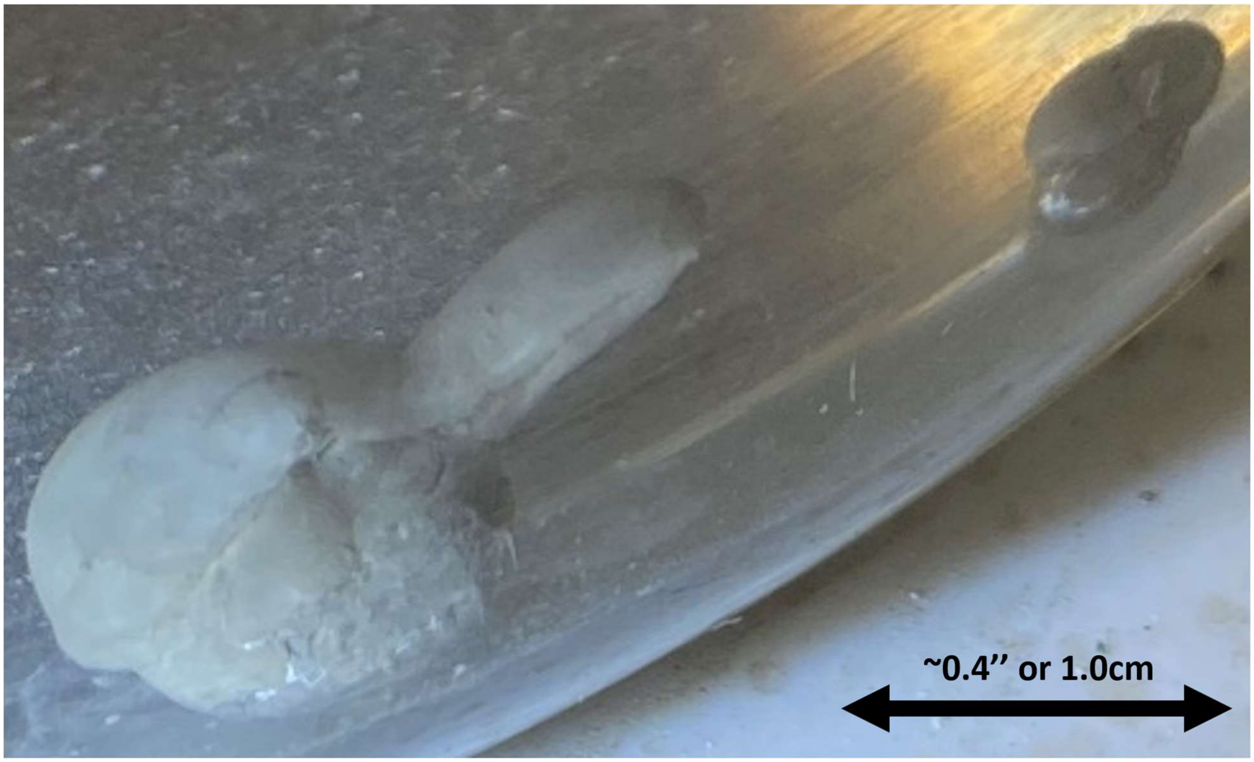

**Figure 4.2. Observations of eGIS droplets in water.**

Two small droplets of high-purity liquid eGIS were placed in 80°C water, and the image was taken after 2 days in the 80°C water. They grew a film(s) of GIS oxide(s)/hydrate(s).

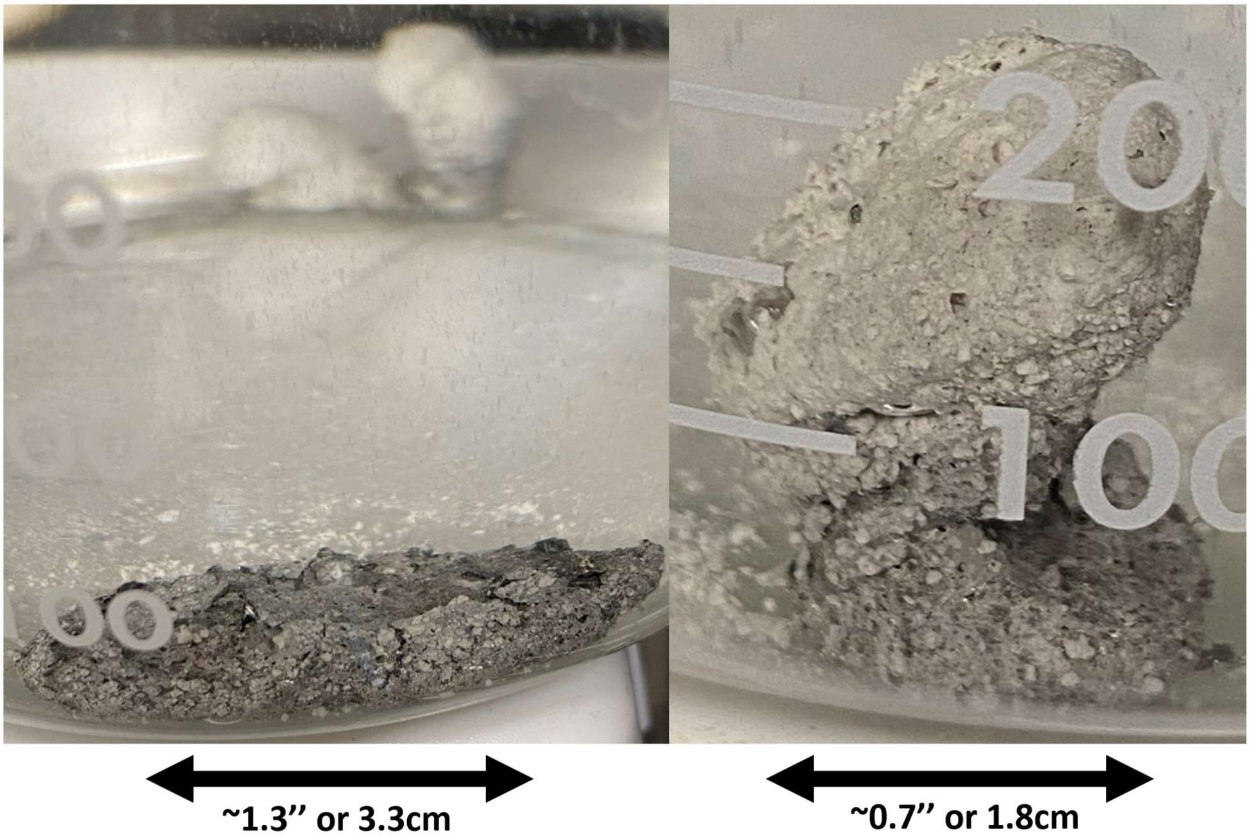

**Figure 4.3. Observations of Ga pools in water.**

Left image: a large pool (the area of the image in sharper focus) of high-purity liquid Ga was placed in 80°C water, and the image was taken after 2 days in the 80°C water. The Ga pool grew some white, particle-like Ga oxide/hydrate(s) on its surface.

Right image: after 4 days in 80°C water, the Ga pool curled up into a shape with less surface area, and Ga oxide/hydrate(s) growth increased.

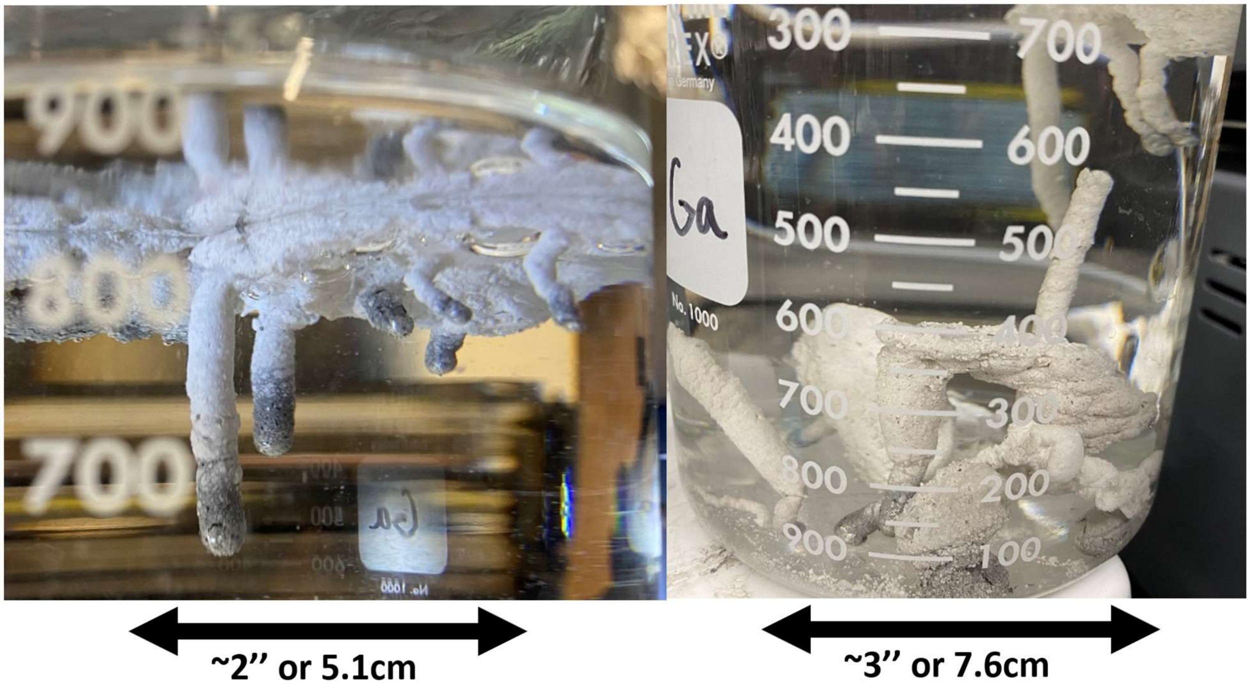

**Figure 4.4. Observations of Ga droplets in water.**

Left image: droplets of high-purity liquid Ga were placed in 80°C water, and the image was taken after 2 days in the 80°C water. The Ga droplets grew much Ga oxide/hydrate(s), and the Ga oxide/hydrate(s) formations floated to the top of the water in the beaker, towing with them what appear to be liquid Ga droplets that are fully coated with Ga oxide/hydrate(s).

Right image: after 4 days in 80°C water, more Ga oxide/hydrate(s) formed, and some of the Ga oxide/hydrate(s) formations sank.

## 4.5. Analyses of the image data (Figures 4.1-4.4)

Both eGIS and Ga produced large amounts of water-reaction products—observable by naked eye (Ga appeared to grow much more water-reaction product than did eGIS.). Prior literature observed similar Ga oxide/hydrate(s) growth formation on liquid Ga in hot water (p.59 of [5]). As GIS oxide(s)/hydrate(s) formation on liquid GIS was observed to occur under relatively similar conditions to those used in this chapter's amalgam water-reaction rate experiments (underwater in oxygenated, warm/hot water), a relatively similar GIS oxide(s)/hydrate(s) film, although much smaller in size, may be expected to form on the liquid GIS in an Al-eGIS amalgam.

In Figure 4.1, much GIS oxide(s)/hydrate(s) appears to be loosely bound to the GIS and easily delaminated from the GIS without outside influence. But it is possible there is a thin oxide(s)/hydrate(s) film on the surface of the liquid GIS that is more well-adhered but simply not visible to the naked eye, and that delamination may require significant growth time (significant compared to the water-reaction completion time of, for example, an Al-eGIS amalgam, which is usually only a few seconds or minutes).

In Figures 4.3-4.4, the Ga oxide/hydrate(s) did not appear to delaminate from the Ga. In Figure 4.3 (right-side image), liquid Ga appears to be forced into a shape with more minimal surface area during its film growth yet does not delaminate from its film. In Figure 4.4 (left-side image), it appears liquid Ga droplets are fully coated with Ga oxide/hydrate(s), yet, even though they are dangling mid-beaker, the liquid Ga does not break through or away from its semi-passivating film.

The composition of the GIS oxide(s)/hydrate(s) may contain oxide(s)/hydrate(s) of In and/or Sn, rather than only Ga oxide/hydrate(s), as suggested by the large differences in growth formations on the Ga vs eGIS and as eGIS contains In and Sn (~21.5wt%In and ~10wt%Sn) whereas the Ga sample did not. As no visibly large formations seem to occur on liquid eGIS/Ga left in air (not shown) instead of in water, it is expected that the very large and highly visible growth formations in the figures are primarily hydrate(s) rather than oxide(s).

## 4.6. Identifying the phases of Al oxide/hydrate(s) and GIS oxide(s)/hydrate(s) that are present on Al-eGIS

In the literature, SEM analysis of the Al oxide/hydrate(s) reaction product of a fully liquid Al-Ga alloy that was reacted with water shows Ga species are not only adhered to the Al oxide/hydrate(s) reaction product as large, spherical droplets of bulk, liquid Ga (likely via a film of Ga oxide/hydrate(s) on Ga) but are also homogeneously and finely intermixed with the Al oxide/hydrate(s) (pp.73-78 of [5]). These homogenously and finely intermixed species are likely Ga oxide/hydrate(s) (pp.76-78 of [5]). Further, in individual experiments, liquid Ga was mechanically stirred underwater with particles of α-Al2O3, α-Al(OH)3, and amorphous Al(OH)3, and "Ga" appeared to stick to each (pp.53-56 and p.61 of [5]). This suggests the Ga oxide/hydrate(s) film on Ga likely adheres and/or bonds with α-Al2O3, α-Al(OH)3, and amorphous Al(OH)3 (p.53 and p.62 of [5]).

As the aforementioned results occurred for fully liquid Ga in one case and for fully liquid Al-Ga in another case, there is a strong possibility similar results may be observed for fully liquid eGIS and for the fully liquid Al-GIS portion of an Al-eGIS alloy/amalgam, as eGIS is similar to Ga in that both are fully liquid phases and are primarily composed of liquid Ga. If similar results are observed, they would suggest GIS oxide(s)/hydrate(s) adhere and/or bond with the Al oxide/hydrate(s) film during growth of the Al oxide/hydrate(s) film on the liquid Al in Al-eGIS alloys/amalgams.

Before forms of adhesion and bonding of Al oxide/hydrate(s) and GIS oxide(s)/hydrate(s) are considered, the phases of Al oxide/hydrate(s) and GIS oxide(s)/hydrate(s) that may be present should be identified.

### 4.6.1. Identifying the phases of GIS oxide(s)/hydrate(s) that are present on Al-eGIS

It is reasoned that portions of the GIS film may be continuously removed via $Al(OH)_3$ film exfoliation from liquid Al adjacent to liquid GIS, over the course of Al-eGIS water-reaction, as the GIS film may adhere and/or bond to the $Al(OH)_3$ film. Continuous GIS film removal would allow for continuous production of new GIS film layers via GIS reactions with water and/or $O_2$ gas dissolved in water.

The composition of the film that cyclically forms underwater on liquid GIS in Al-eGIS was not determined with analytical equipment, so this section hypothesizes the composition.

Reactions of eGIS with water were calculated to have $\Delta G° < 0$ (pp.39-40 of [2]). To confirm this, this paper re-calculates $\Delta G°$ values in Table B2, showing $\Delta G° < 0$ for every listed reaction between eGIS and water in Eqs. B2.6-B2.12 (Eq. B2.12 in Table B2 obtains $\Delta G° = -17$ kJ for the reaction of Sn and $H_2O$ to produce $Sn(OH)_2$ and $H_2$, rather than $\Delta G° = +219.7$ kJ on p.40 of [2].). Additional calculations show $\Delta G° < 0$ for eGIS reactions with ambient $O_2$ gas (such as in air) and dissolved $O_2$ gas in water in Eqs. B2.14-B2.17 and Eqs. B2.19-B2.22. So, there is thermodynamic drive for these reactions to occur under standard conditions.

The unpassivated surface of eGIS rapidly oxidizes. Literature reports that eGIS may spontaneously form an oxide layer in <0.25s “in a mere 0.2% oxygen environment—100 times less than in ambient air” (p.445 of [39]). This causes eGIS to act as a “gel droplet” that is “easily distorted to an irreversible nonspherical shape” rather than “like mercury or other normal liquids” when its surface is unpassivated (p.445 of [39]). eGIS was only observed to be liquid-like/oxide-free when under ambient gas containing a very low level of oxygen of <1ppm (0.0001%) (p.445 of [39]). Such hypoxic conditions are never present in this present work. For Al-eGIS that is placed in oxygenated waters, when the GIS film is removed from GIS during and due to Al-eGIS water-reaction, GIS likely rapidly reacts with dissolved $O_2$ gas in the water to form GIS oxide(s), as per Table B2 Eqs. B2.19-B2.22, which have negative $\Delta G°$ values.

A recent study shows unpassivated, eutectic Ga-In reacted when exposed to high-purity $O_2$ gas and, separately, when exposed to high-purity $H_2O$ vapor, in all cases forming a $Ga_2O_3$ outer layer and a $Ga_2O$ interlayer [40]. Formation of Ga hydrate(s) was not observed when Ga reacted with the $H_2O$

vapor [40]. But this may be because the experiment used a low pressure, high temperature (550K) environment, which may have favored formation and stability of the oxide over the hydrate(s).

The present work measures ~100% yield of gas for reacted Al-eGIS amalgams; notably, there is neither excessive nor scant yield. Based on the expected 3:2 molar ratio of $H_2$:Al, it is expected that only Al reacted with water to produce $H_2$ gas and ~0wt% of the eGIS did, suggesting that there was 0% yield given by the reactions in Table B2 Eqs. B2.6-B2.12 (Such reasoning does not apply to Eqs. B2.19-B2.22 for reactions of eGIS with dissolved $O_2$ gas, as they do not produce any gas phase.). However, if one or more reactions in Eqs. B2.6-B2.12 occurred between, say, 0% and 1% (~0%), which may have been the case, this may be enough to contribute significantly to film formation of both oxide(s) and hydrate(s) on liquid GIS, as the film is likely very thin, requiring very little GIS to react for it to rapidly form and passivate GIS from further reaction.

It is expected GaO(OH) is the dominant film phase that forms on liquid Ga, as this phase is shown to be stable by the Pourbaix diagram for liquid Ga (p.286 of [41]). This diagram shows GaO(OH) should form on liquid Ga in water and act as a passivating layer in temperature and pH ranges that encapsulate the conditions that are present throughout this work's experiments. However, the Pourbaix diagram assumes equilibrium conditions are met, which may not be the case.

In one study, pure liquid Ga was left in oxygenated, 90°C water for ~2 weeks, and the film that grew on it was determined via XRD to be α-GaO(OH) (p.59 of [5]). This is consistent with Table B3, which predicts α-GaO(OH) is the most stable phase between −152°C and 195°C. However, it was not specified how the film was dried via heating and/or aging (pp.50-51 of [5]) before XRD was performed. These factors, in addition to the high-temperature, water-annealing conditions of the experiment, may have increased the percent crystallinity, and changed the quantities of phase(s) present, of the film material from when it incipiently formed on the liquid Ga.

In one recent study [42], the following reaction pathway was proposed to occur in oxygen-rich waters, such as those that are used in the present work and throughout the literature in which Al-Ga/eGIS is reacted with water. When liquid eGIS is placed in oxygen-rich water, the Ga in liquid eGIS quickly reacts primarily with dissolved $O_2$ gas in water to form $Ga_2O_3$. This $Ga_2O_3$ then converts to a reaction intermediate, $Ga(OH)_3$, and then converts over time into GaO(OH).

So, depending on the rates of conversions of Ga to the oxide, the oxide to the hydroxide, and the hydroxide to the oxyhydroxide, possibly all of these Ga oxide/hydrate(s) may be present on the liquid eGIS in an Al-eGIS alloy/amalgam during the same timeframe as the growth-and-exfoliation cycles of the Al oxide/hydrate(s).

Overall, for reactions of Al-Ga/eGIS with water, which are generally performed in water of at most 100°C, the GIS film is likely a mix of GIS oxide(s)/hydrate(s). As reasoned previously in Section 4.5., it likely contains Ga hydrate(s) and hydrate(s) of In and/or Sn. The Ga-containing film phases likely comprise the largest wt% of the overall GIS oxide(s)/hydrate(s) film, as eGIS is ~68.5wt% Ga and as liquid GIS would otherwise freeze, fully halting the water-reactivity of the amalgam, if its Ga content was not large. GaO(OH) is likely the dominant phase present, and $Ga(OH)_3$ and/or $Ga_2O_3$ may also be present to a lesser degree as film phases on the liquid GIS. In experimental setups such as that which is used in the present work, some wt% of oxides of Ga, In, and Sn may be present from several sources: native oxide formations already present on the purchased eGIS; >1ppm oxygen being present in the glovebox during amalgam fabrication; briefly opening the amalgam capsules just before placing them in water to initiate amalgam water-reaction; and, especially, liquid GIS reacting with water and with dissolved $O_2$ gas in water. All film phases may have more amorphous character than XRD results (such as on p.60 of [5]) suggest.

### 4.6.2. Identifying the phases of Al oxide/hydrate(s) that are present on Al-eGIS

The Al-containing water-reaction product of fully liquid Al-Ga was found via XRD to be α-$Al(OH)_3$ (bayerite) (p.114 of [5] and p.33 of [43]). Some γ-$Al(OH)_3$ (gibbsite) was also observed (p.33 of [43]). Water-reaction temperatures were not specified. Eutectic Al-Ga was reacted in water initially at 27°C and 50wt%eGIS-50wt%Al was reacted in water initially at 20°C; in both cases the Al-containing water-reaction product was observed via XRD as α-$Al(OH)_3$ (pp.17-20 of [2]). However, these studies dried out and aged the Al oxide/hydrate(s) reaction products before analyzing them with XRD (p.17 of [2] and p.51 of [5]). Drying was required so the samples were compatible with analysis equipment, and aging was a consequence of the drying process. These factors may have increased the percent crystallinity, and perhaps changed the phase(s) present, of the Al oxide/hydrate(s) reaction products from the timeframe during which they incipiently formed on and exfoliated from the liquid Al.

In one study [44], the reaction of Al-eGIS in water of up to 60°C was seen to produce $Al(OH)_{3,\ (s,\ bayerite)}$, and, in water of 50°C and 60°C, some $AlO(OH)_{(boehmite)}$ was observed. This is roughly consistent with the predicted phase stability regions for these, calculated in Table B3.

It is also possible $Al_2O_3$ forms when Al-Ga/eGIS is reacted in water, but this is unclear for several reasons. Table B2 shows there is relatively similar thermodynamic drive for its formation via Al water-reaction as for formation of $Al(OH)_3$ and $AlO(OH)$ (Eqs. B2.1-B2.5). Also, conversion of $Al_2O_3$ to $AlO(OH)$ in water is favorable under standard conditions (Eq. B2.32), and $AlO(OH)$ may also convert to $Al(OH)_3$ in water via Eq. B2.33, although this is slightly unfavorable under standard conditions. From Table B3, both conversions may be expected as $Al(OH)_3$ is predicted to be the most stable of these three phases below ~63°C. Also, having more dissolved $O_2$ gas in water may increase formation of the oxide, as per Eq. B2.18 in Table B2. However, if $Al_2O_3$ initially forms on the liquid Al before or during when

Al-Ga/eGIS is reacted underwater, it possibly may not be experimentally observed in post-reaction analyses if it subsequently converts into the hydrates. Such conversion behavior in water was also seen for their group 13 periodic table family members; in oxygen-rich water, $Ga_2O_3$ forms on Ga first, followed by its conversion to $Ga(OH)_3$ and then to GaO(OH) [42].

Overall, in the time intervals during which the Al oxide/hydrate(s) cyclically grows and exfoliates in oxygenated water, it is expected $Al(OH)_3$ is the dominant phase formed below ~63°C but possible some AlO(OH) and $Al_2O_3$ also form, and it is expected AlO(OH) is the dominant phase formed above ~63°C but possible some $Al(OH)_3$ and $Al_2O_3$ also form.

## 4.7. Identifying the types of adhesion and bonding that are between the Al oxide/hydrate(s) and the GIS oxide(s)/hydrate(s) that are present on Al-eGIS

Weak electrostatic forces of attraction may result in physisorption of GIS species onto the Al oxide/hydrate(s) film, but these forces are weak compared to ionic/covalent bonding (chemisorption) and hydrogen bonding (which has a strength in between physisorption and chemisorption) (pp.99-100 of [5]). Experiments suggest physisorption and chemisorption were present and caused adhesion and bonding between Ga-containing species—likely Ga oxide/hydrate(s)—and the Al oxide/hydrate(s) reaction product of an Al-Ga alloy reacted with water (p.100 of [5]). A similar result is suspected for Al-eGIS alloys/amalgams if similar experiments were to be conducted, for similar reasons as mentioned in Section 4.6.

α-$Al_2O_3$ (bayerite) and α-$Ga_2O_3$ are both group 13 oxides and are cited as being isostructural (p.16 of [45]). α-$Al_2O_3$ has lattice parameters of a = 4.8Å and c = 13.0Å (p.15 of [45]), and α-$Ga_2O_3$ has lattice parameters of a = 5.0Å and c = 13.4Å (p.16 of [45]). So, they may be likely to chemically combine coherently (p.56 of [2]). The intramolecular bonding within $Al_2O_3$ and $Ga_2O_3$ is more ionic on the ionic-covalent spectrum of bonding (p.131 of [46]). So, if $Al_2O_3$ and $Ga_2O_3$ chemically combine, bonds between these different films should be mostly ionic, with partial covalent bonding character. This is expected to be the strongest possible form of bonding between the two films (pp.99-100 of [5]).

α-AlO(OH) (diaspore) and α-GaO(OH) are both group 13 oxyhydroxides, and they are cited as being isostructural ([47], section: Introduction). α-AlO(OH) has lattice parameters of a = 4.4Å, b = 9.4Å, and c = 2.8Å [48], and α-GaO(OH) has lattice parameters of a = 4.5Å, b = 9.8Å , and c = 3.0Å ([47]). So, they may be likely to chemically combine coherently. It is cited that α-AlO(OH) and GaO(OH) contain "moderately stable hydrogen bonds," and the Al-O and Ga-O bonds are likely "largely covalent" bonds [49]. Based on these bond types, bonding between these two film materials should be strong. Bonding between these may be especially relevant as α-GaO(OH) (of varying % amorphousness) is, as aforementioned, assumed to be the main reaction product and main film material present on liquid Ga/eGIS in water.

As aforementioned, the main films on Al and Ga in water may be α-$Al(OH)_3$ (bayerite) and α-GaO(OH) (both of varying % amorphousness). But these may be unlikely to form strong ionic/covalent bonds with each other in a coherent lattice structure, as α-$Al(OH)_3$ crystallizes in a different crystal system than that of α-GaO(OH) (Bayerite has a monoclinic crystal system, with lattice parameters of a = 5.1Å, b = 8.7Å, c = 9.4Å, and β = 90.26°.) ([50], section: Structure of the aluminum (oxo)hydroxides). α-$Al(OH)_3$ and α-GaO(OH) may, however, form hydrogen bonds.

Hydrogen bonding may occur between Al hydrates and GIS hydrates, as these hydrates have intramolecular polar covalent bonding between O and H, resulting in a partial positive charge on H and a partial negative charge on O. This unbalanced electron distribution may electrostatically attract an H or O of one Al hydrate molecule, respectively, to an O or H of an adjacent Ga, In, or Sn hydrate molecule, forming a hydrogen bond. Perhaps hydrogen bonding may also occur between Al oxide with each GIS hydrate and between each GIS oxide with each Al hydrate, as, even though the oxides do not contain H, H in the hydrates may attract O in the oxides.

## 4.8. The impact of the adhesion and bonding, between the Al oxide/hydrate(s) and the GIS oxide(s)/hydrate(s), on the exfoliation rate of the Al oxide/hydrate(s) film on Al-eGIS

For an Al-eGIS amalgam, the exfoliation rate of the Al oxide/hydrate(s) film on the liquid Al in the liquid Al-GIS appears to be vastly faster than that of the GIS oxide(s)/hydrate(s) film on liquid eGIS (for the case in which the liquid eGIS is pure and does not contain Al). This is because complete water-reaction of liquid Al in liquid Al-GIS occurs very fast compared to complete water-reaction of pure liquid eGIS. Al oxide/hydrate(s) are observed to form much faster by liquid Al than GIS oxide(s)/hydrate(s) are formed by liquid GIS. For example, all of the Al in a bulk piece of 50wt%Al-50wt%eGIS alloy that reacts with water is liquid Al (All solid Al in the alloy must convert to liquid Al before reacting with water.), and all of this liquid Al was seen to fully react with 40°C water in ~150s (p.37 of [2]). However, as qualitatively shown in Figures 4.1-4.2, only a small fraction of liquid GIS reacts with water, even after 4 days at 80°C. The reaction of liquid eGIS with water is so slow that in one study it appeared to display "no reactivity" in 22°C water or 50°C water, even when mechanically agitated with a spoon (p.12 of [2]).

Regarding the surface of the liquid Al-GIS in an Al-eGIS amalgam, if exfoliation rate of the Al oxide/hydrate(s) film is faster than that of the GIS oxide(s)/hydrate(s) film (for the case in which the liquid eGIS is pure and does not contain Al), then adhesion and bonding between the two films should have an overall effect of slowing the exfoliation rate of the Al oxide/hydrate(s) film.

The ability of the GIS oxide(s)/hydrate(s) film to slow the exfoliation rate of the Al oxide/hydrate(s) film by tending to hold it in place at the surface of the liquid Al-GIS should depend on the strength of adhesion and bonding of the GIS oxide(s)/hydrate(s) film to liquid GIS. This adhesion and bonding should be present to a degree, but it may be weak. This is implied from qualitative observations of Figure 4.1, as the GIS oxide(s)/hydrate(s) film appears to readily delaminate from liquid GIS without external influence (However, as aforementioned, it is possible that there is a thin oxide(s)/hydrate(s) film on the surface of the liquid GIS that is more well-adhered but simply not visible to the naked eye.). Further, the interface between liquid GIS and its GIS oxide(s)/hydrate(s) film may have disrupted bonding due to the lack of a rigid, fixed crystal structure in the liquid, and also from increased disorder due to the liquid GIS containing three elements rather than one, resulting in the formation of an array of films of oxides and hydrates of Ga, In, and Sn with dissimilar lattice parameters and some dissimilar crystal structures with respect to each other.

However, if the strength of adhesion and bonding of the GIS oxide(s)/hydrate(s) film to the liquid GIS is not overcome, the $Al(OH)_3$ film may also exfoliate by exceeding cohesive forces within liquid Al-GIS, breaking off some liquid Al-GIS, perhaps as droplets, with it into the water. This phenomenon was potentially previously observed in SEM analysis of the Al oxide/hydrate(s) reaction product of a fully liquid Al-Ga alloy that was reacted with water, as bulk droplets of Ga were seen adhered to this Al oxide/hydrate(s) reaction product (pp.73-75 of [5]). A similar phenomenon may also occur in the fully liquid Al-GIS phase in an Al-eGIS amalgam, as this is similarly a fully liquid, low-Al phase that is primarily composed of liquid Ga.

By similar mechanisms discussed throughout this chapter for the Al oxide/hydrate(s) film, water type variation may also alter the nature of adhesion and bonding of the GIS oxide(s)/hydrate(s) film with the Al oxide/hydrate(s) film, as well as alter the rate at which the GIS oxide(s)/hydrate(s) film grows and exfoliates. These alterations to the GIS oxide(s)/hydrate(s) film may impact the exfoliation rate of the Al oxide/hydrate(s) film, if these two films are adhered and/or bonded. The same framework that was used to understand the exfoliation rate of the Al oxide/hydrate(s) film should apply to the potential future study of the exfoliation rate of the GIS film of oxide(s)/hydrate(s).

# Chapter 5: Investigating the Water-Reactivity of Al-In-Sn Alloys

## 5.1. Goals

An experiment was performed to quantify the water-reactivity of Al-In-Sn and to investigate the roles of In, Sn, and Ga in Al alloy/amalgam water-reactivity.

## 5.2. Methods

Mixtures of 99.5%-pure Al pellets, 4N-purity In pellets, and 4N-purity Sn pellets were placed in an inert aluminum oxide crucible in a box furnace filled with ordinary air. They were heated at 800°C to fully melt them and then stirred to homogenize them. They were quenched to form ingots, while still fully melted liquids, on a stainless-steel quench plate at RT, with RT water circulating through a built-in copper tube just below the quench plate's surface. The ingots appeared to solidify in several seconds. Large ingots were made (rather than a fine powder with a large surface-area-to-volume ratio), about a half-inch thick and one-inch in diameter, such that there were substantial amounts of bulk, unoxidized internal material underneath their oxidized outer surfaces to be utilized for water-reaction.

At RT, the ingots were cut into several pieces in ordinary air to help facilitate their water-reaction. This mechanical force was employed to disrupt regions of the outer oxide layer on the ingots and to expose fresh, less-oxidized surfaces than those that may have formed on outer surfaces of the ingots from the high furnace temperature. The cut pieces were then reacted with 50°C DI water and water-reaction yields were quantified.

Further experimental methods details are in Chapter 2.

# 5.3. Data

**Table 5.1. Al-In-Sn alloy water-reactivities in 50°C DI water.** When reacted with water, each alloy made a small amount of $H_2$ gas bubbles, as seen by naked-eye, for up to a few minutes until there was no further water-reaction. Each gave <1% water-reaction yield.

| Composition | | | Water-reaction yield |
|---|---|---|---|
| **Al (wt%)** | **In (wt%)** | **Sn (wt%)** | |
| 96.7 | 2.2 | 1.1 | <1% |
| 90 | 5 | 5 | <1% |
| 90 | 10 | 0 | <1% |
| 90 | 0 | 10 | <1% |
| 67 | 33 | 0 | <1% |
| 67 | 0 | 33 | <1% |
| 50 | 25 | 25 | <1% |

# 5.4. Analyses and conclusions

A broad range of Al-In-Sn alloy compositions were made but none displayed significant water-reactivity.

As mentioned in Section 1.2.3., from the Al-In and Al-Sn phase diagrams at 50°C (the water temperature of the experiment), it is expected that ~0wt% of In or Sn diffuse into Al as α-Al solid solution. Also, ~0wt% of Al diffuses into In or Sn to form β-In solid solution or β-Sn solid solution. So, In and Sn should not have combined as solids with Al in solid Al grains when the alloys were quenched but should instead have formed a different phase or phases, which may be solid and/or liquid, in Al GBs, and the In and Sn should not have migrated from this GB phase into Al grains. Al grains should dissolve into the In-Sn GB phase if the GB phase contains liquid, forming a liquid Al (liquid Al mixed with liquid In-Sn) phase, as there is nonzero solubility of Al in these liquids, according to the Al-In and Al-Sn phase diagrams.

Although the Al-In-Sn eutectic composition and eutectic temperature are unknown, as there does not appear to be an Al-In-Sn ternary phase diagram in the literature, it is very unlikely liquid phase(s) were present in any tested Al-In-Sn alloys. The lowest melting point (the eutectic) of In-Sn, according to its phase diagram, is 120°C. From the Al-In and Al-Sn phase diagrams, Al-In and Al-Sn eutectic temperatures are even higher (156°C and 228°C, respectively). As eutectic compositions of alloys frequently have lower melting points than those of their pure metals (For example, observe binary-alloy phase diagrams such as those for Al-Ga, Al-In, Al-Sn, In-Sn, etc.), it is expected that eutectic Al-In-Sn melts at a lower temperature than that of any combination of its binary elements. It is possible that eutectic Al-In-Sn forms under certain conditions as a liquid phase in Al GBs, enabling water-reactivity for Al-In-Sn alloys. However, it is very likely that the water bath temperature of 50°C was too low for a liquid phase to form and/or remain stable, as it is very unlikely that the melting temperature of eutectic Al-In-Sn would be significantly lower than 120°C, the aforementioned lowest melting point of all possible binary-alloy combinations of Al-In-Sn, especially considering Al has a much higher melting point (660°C) than those of In (157°C) and Sn (232°C).

Further, the non-water-reactivity of the Al-In-Sn alloys suggests that none contained liquid In and/or Sn. If they did, then there is, as aforementioned, a nonzero solubility of Al in these liquids, so Al from Al grains should dissolve into them, which should enable alloy water-reactivity via a similar water-reaction mechanism model as that of partially-liquid, partially-solid Al-Ga/eGIS discussed in Section 1.2.3.

This chapter's non-water-reactivity results suggest that, at least for water bath temperatures at or below 50°C, the addition of Ga is needed for Al-GIS alloys and amalgams to become activated (water-reactive). The results also suggest that in Al-GIS alloys and amalgams that are significantly water-reactive in water at or below 50°C (such as for several experiments in other chapters in this dissertation), a significant amount of Ga does not migrate from liquid GIS in Al GBs into Al grains; otherwise, only non-water-reactive solid phases should be present in Al GBs, resulting in non-water-reactivity similar to that observed in this chapter.

# Chapter 6: Effects of Long-Term Storage on the Water-Reactivity of a 10wt%eGIS-90wt%Al Amalgam

## 6.1. Goal

Shelf-life stability is a useful parameter of a potential commercial product. Optimally, there will be no loss in water-reactivity over time when a 10wt%eGIS-90wt%Al amalgam is stored for a long time at ~RT (similar to real-world temperature storage conditions, such as on a store shelf, in a warehouse, etc.) in an inert environment. However, it is hypothesized that the amalgam water-reactivity may decrease over a long enough storage period. This chapter quantifies water-reactivity loss over a 6-month storage period at 20°C.

## 6.2. Methods

A 10wt%eGIS-90wt%Al amalgam was made via the experimental methods in Chapter 2.

The amalgam was stored for 6 months in a glovebox. During the storage period, glovebox RH was consistently maintained at a measured 2%-10% via constantly flowing 4N-purity $N_2$ gas through the glovebox at a high enough rate to counteract leaks in the glovebox that allow in trace amounts of ordinary air containing moisture/$O_2$ gas. The amalgam is a powder with a high surface-area-to-volume ratio, so it is more impacted by exposure to moisture/$O_2$ gas in air than bulk alloys of low surface-area-to-volume ratio (e.g., furnace-made alloys) would be. So, the amalgam was stored in a threaded-lid glass jar in the glovebox to further reduce the trace amounts of air, containing moisture/$O_2$ gas, that would pass over it.

Portions of the amalgam at 6 months of storage and of a freshly made amalgam of same composition (made and reacted on the same day) were reacted in water baths to quantify water-reaction yields/times.

Details of these methods are in Chapter 2.

## 6.3. Data

**Table 6.1. Water-reactivities of 10wt%eGIS-90wt%Al amalgams under different storage times and water-reaction temperatures.**

| Storage time | Water temperature | Water-reaction yield | Time to 90% water-reaction completion |
|---|---|---|---|
| <1 day | 5°C | ~98% | 423s |
| 6 months | 5°C | ~99% | 369s |
| <1 day | 20°C | ~101% | 182s |
| 6 months | 20°C | ~101% | 186s |
| <1 day | 50°C | ~102% | 21s |
| 6 months | 50°C | ~102% | 19s |

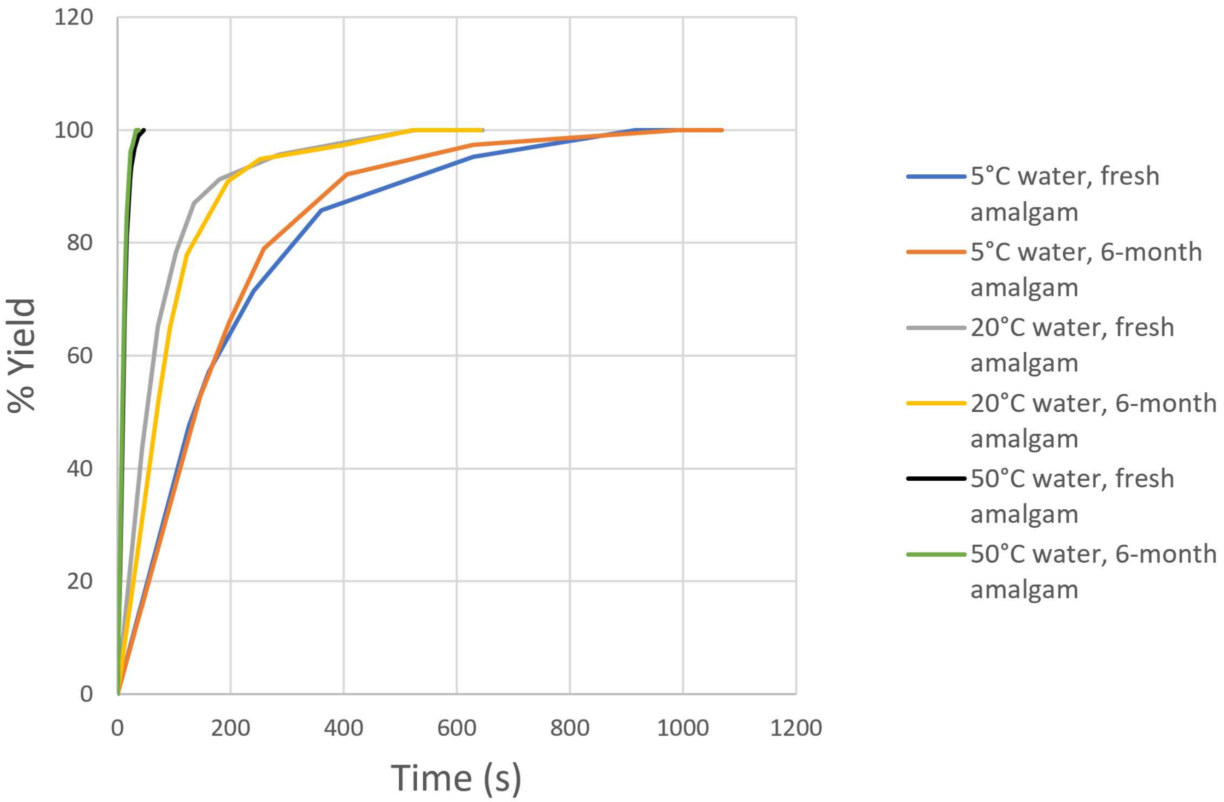

**Figure 6.1. Water-reaction rate curves of 10wt%eGIS-90wt%Al amalgams, freshly made vs stored for 6 months, vs water bath temperature.**

**Figure 6.2. Stored vs non-stored amalgam.** Image width: ~3in or ~7.6cm. Left: 10wt%eGIS-90wt%Al amalgam at 6 months of storage. Right: a different amalgam of same composition at less than one day of storage.

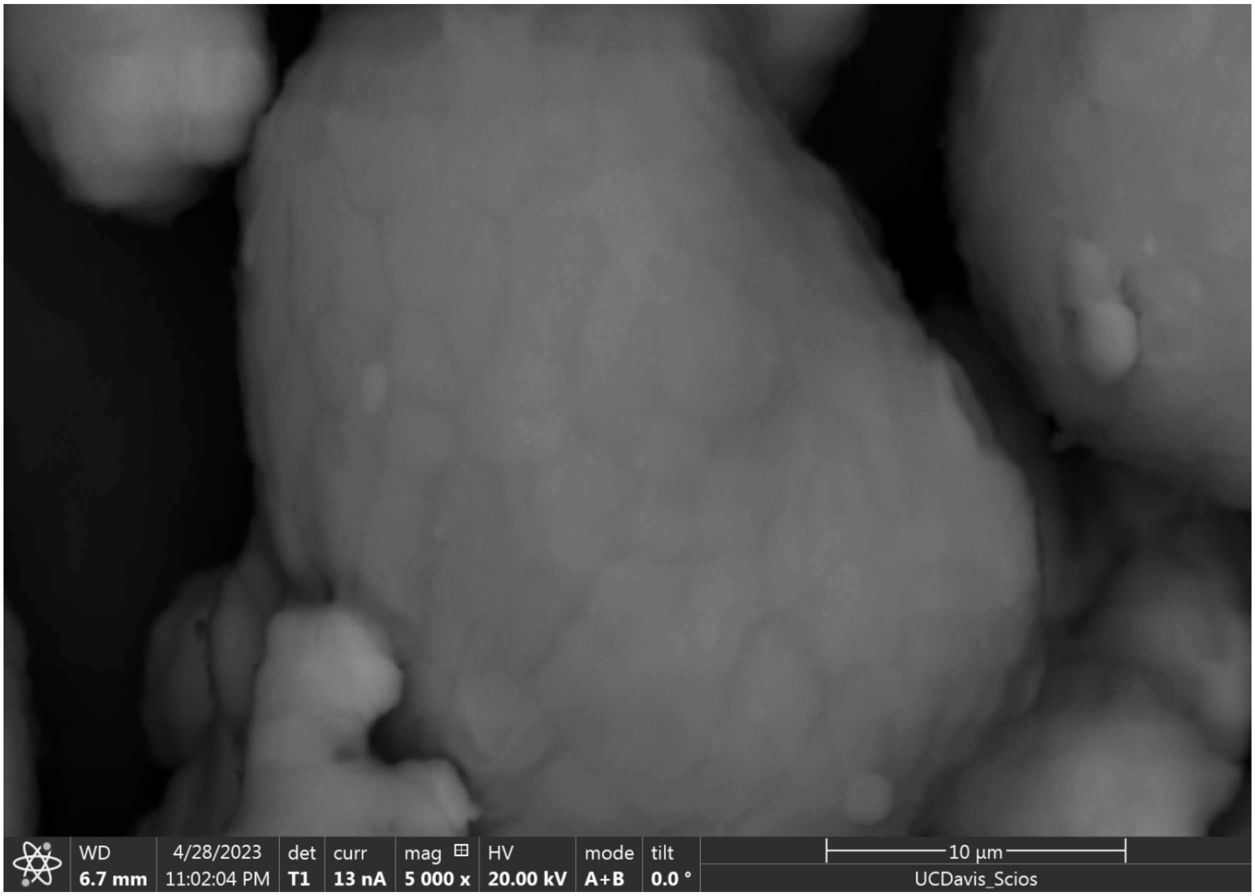

**Figure 6.3. SEM (BSE mode) image of 99.5%-purity, 30µm-average-diameter Al powder by Alpha Chemicals, without eGIS.** (No metallography treatment was used to reveal grains and GBs.).

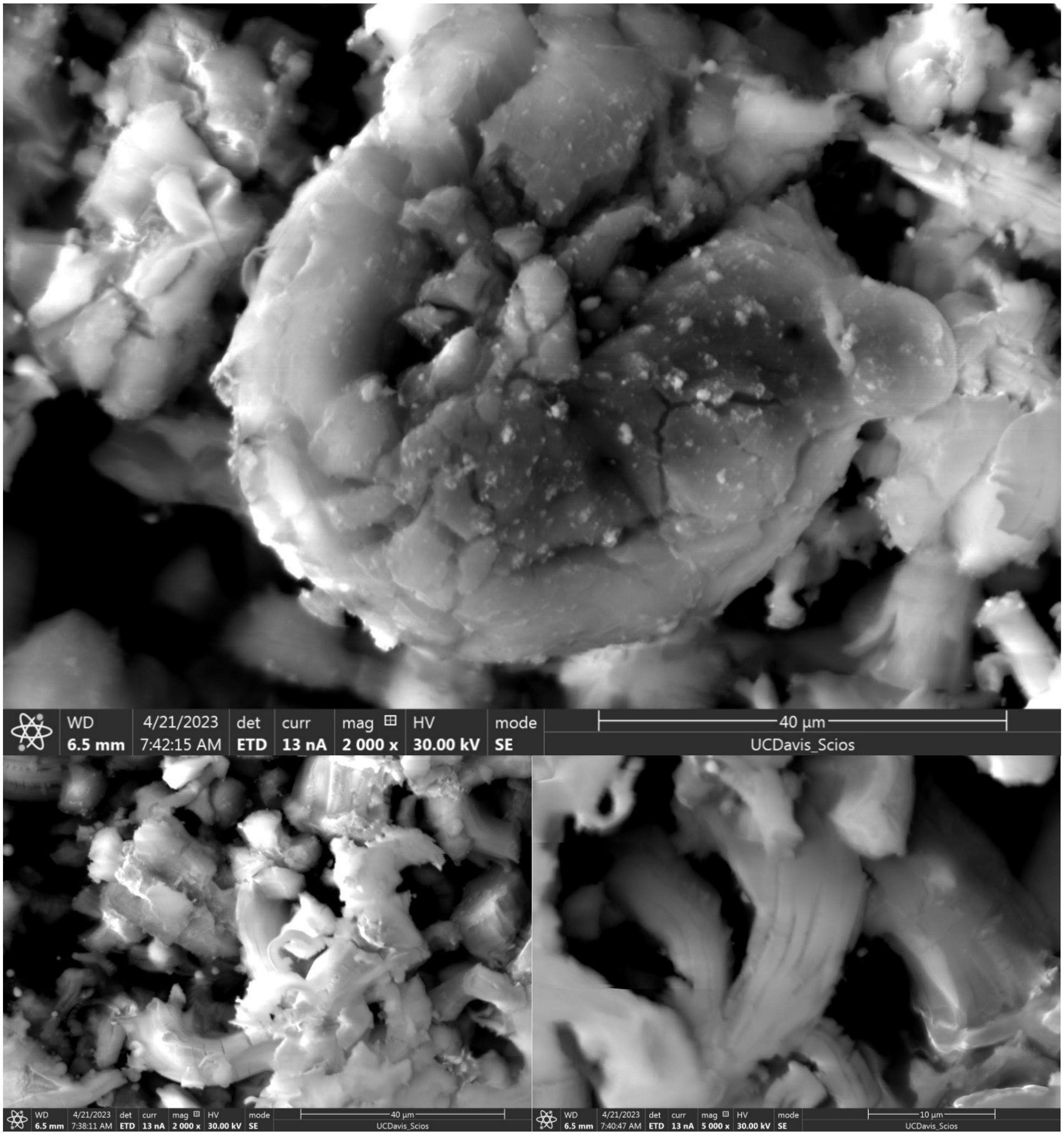

**Figure 6.4. SEM (SE mode) images of 10wt%eGIS-90wt%Al amalgam after continuous exposure to ordinary air of ~40%RH for 3 days.** Images show different regions of the same sample.

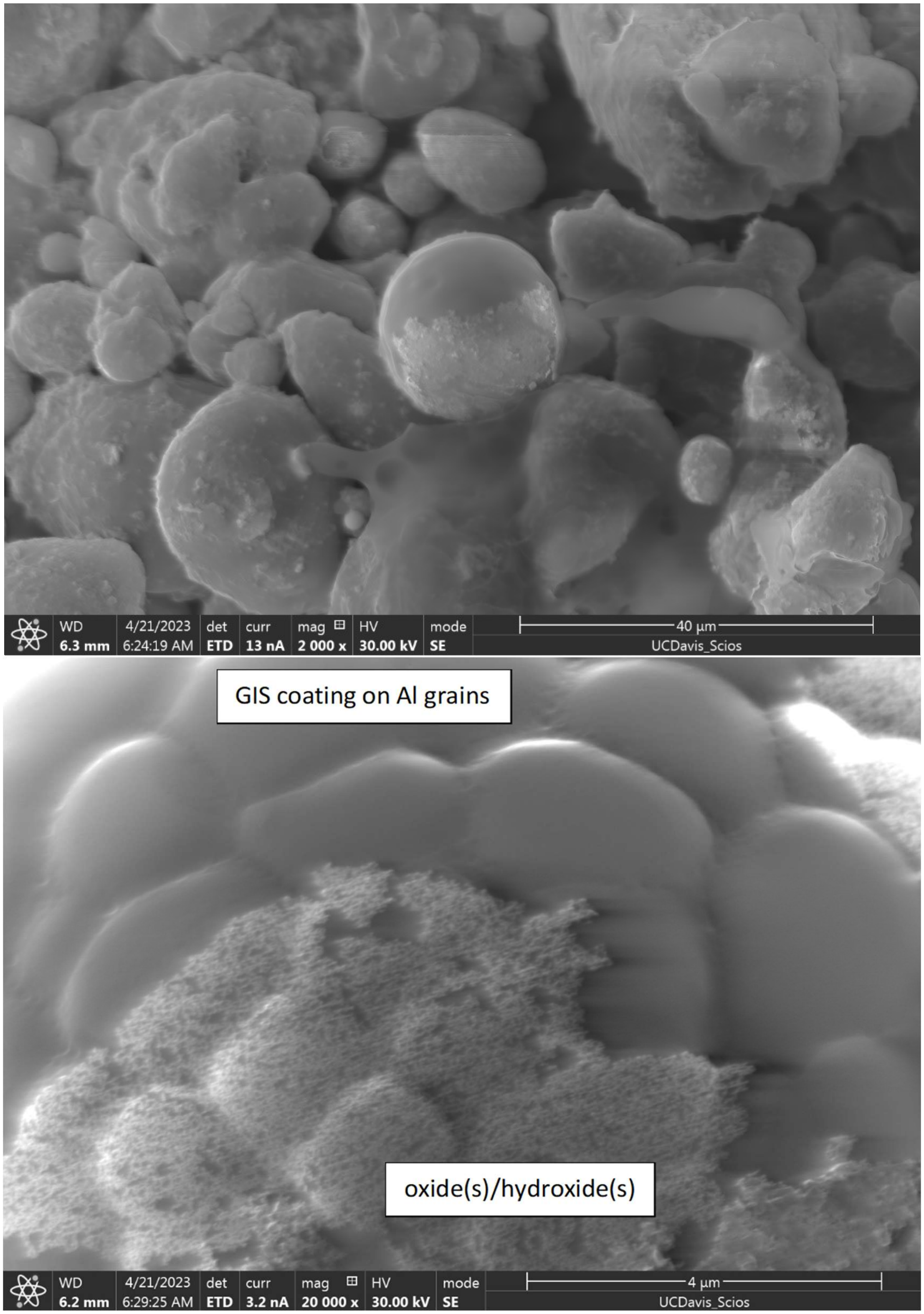

**Figure 6.5. SEM (SE mode) images of 10wt%eGIS-90wt%Al amalgam at 6 months of storage.** Bottom image is a zoomed-in view of the ~20µm-diameter round particle centered in the top image.

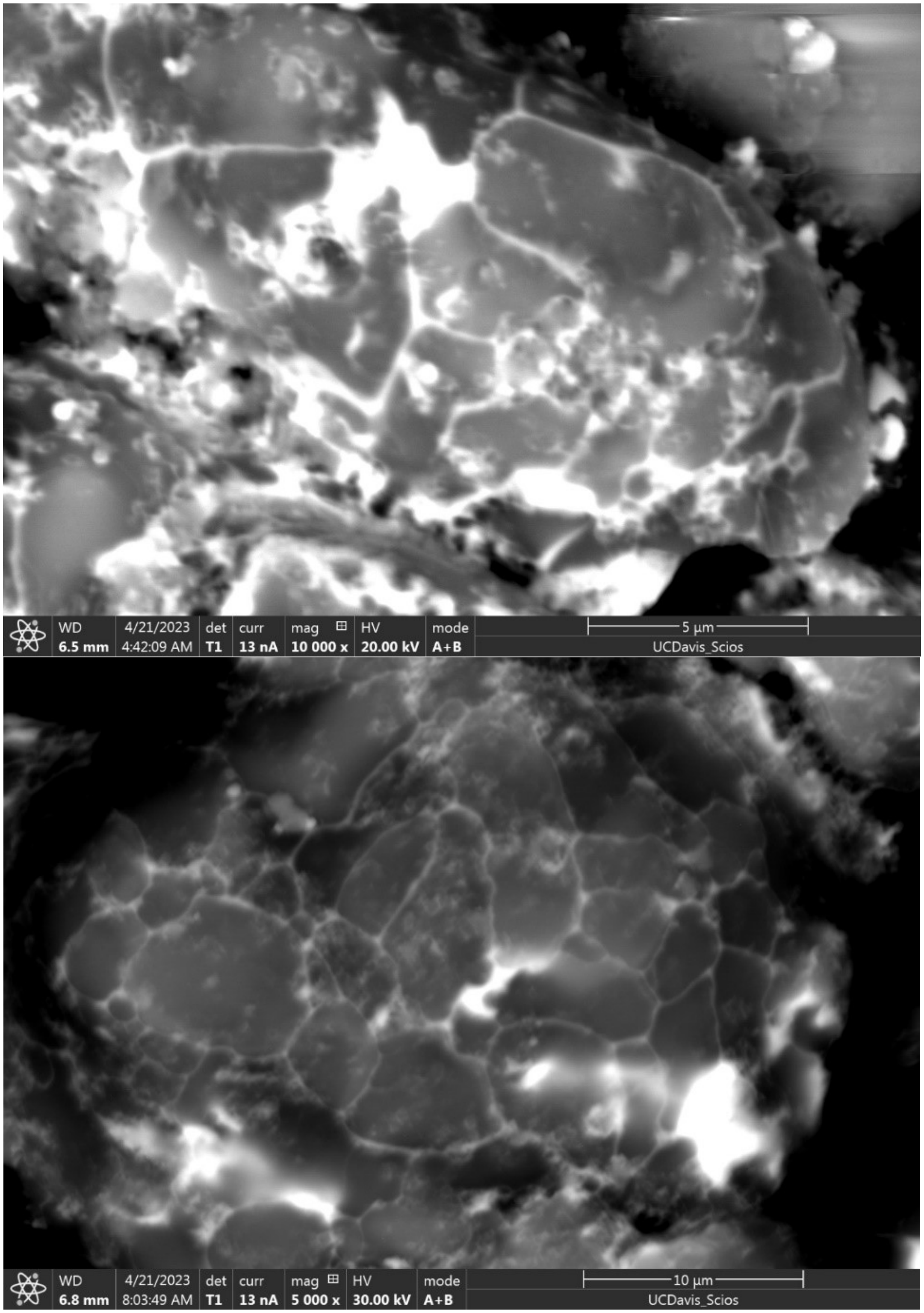

**Figure 6.6. SEM (BSE mode) images of Al-GIS particles in 10wt%eGIS-90wt%Al amalgam at 6 months of storage show Al grains, GIS surface pools, and GIS decorating Al GBs.** In BSE mode, GIS-rich areas are whitest and Al-rich areas are grey.

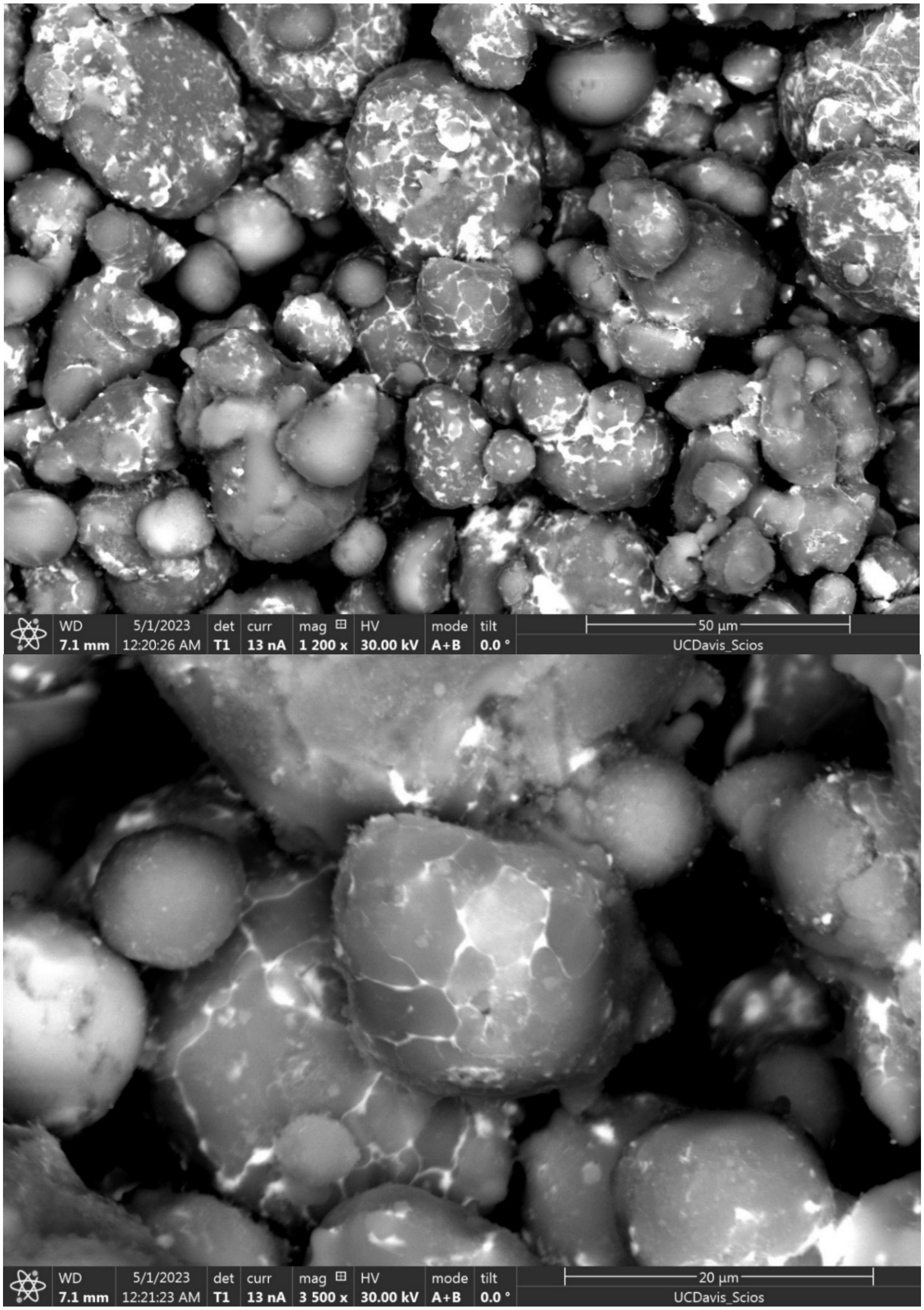

**Figure 6.7. SEM (BSE mode) images of Al-GIS particles in 10wt%eGIS-90wt%Al amalgam at <1 day of storage show Al grains, GIS surface pools, and GIS decorating Al GBs.** In BSE mode, GIS-rich areas are whitest and Al-rich areas are grey.

## 6.4. Analyses

The amalgam water-reactivity was tested at three different water temperatures (Table 6.1 and Figure 6.1). For all three, there was no change in water-reaction yield, and water-reaction time varied by 2-15% relative to the freshly made (<1 day) sample. As explained in Section 2.4, these minor variations in measured water-reaction rates are insignificant and within uncertainty. This suggests no significant physical/chemical changes of the amalgam occurred over the storage period. Specifically, this supports the hypothesis in Section 1.2.3. that suggests, over the storage period, Ga migration from liquid eGIS in Al GBs into Al grains did not significantly occur and liquid eGIS remained in significant, widespread physical contact with Al grains. Also, the minimal water-reactivity difference observed in water at the lowest temperature (5°C) further suggests that it is unlikely that any significant amount of Ga migrated from liquid eGIS in Al GBs into Al grains, as otherwise the liquid Al-eGIS phase should freeze (due to containing low Ga wt%), disabling water-reactivity.

The extent of oxide(s)/hydroxide(s) formation on the amalgam, whether after 1 day or after 6 months, was insignificant, as it did not delay water-reaction onsets, as seen in Figure 6.1, and did not impact water-reaction rate/yield. Figure 6.2 shows the amalgam pre/post-storage (The "pre-storage" sample was a different amalgam of same composition stored <1 day.). By eye, the post-storage amalgam is essentially identical in terms of overall appearance, including macroscopic particle morphology and color, although its grey color is slightly lighter (whiter). This may be due to a thin layer of oxide(s)/hydroxide(s) formation on Al-eGIS particles, as characteristic oxide(s)/hydroxide(s) of the sample's metals (Al, Ga, In, and Sn) are white in color and may have formed via amalgam reaction with trace levels of moisture/$O_2$ gas in the glovebox during storage.

The macrostructure and microstructure of the aluminum and amalgam particles change when reacted with ordinary air. Figure 6.3 is an SEM image of the high-purity Al powder used to make the amalgam. It shows the Al particles are globular and approximately of 30μm average diameter with visible grain boundaries and grains (5-10 microns in diameter). Figure 6.4 shows what happens to the amalgam if it is continuously exposed to ordinary air at RT (and of ~40%RH) for 3 days. Al reacts with moisture in air to form Al hydrate(s) and with $O_2$ gas in air to form Al oxide. Figure 6.4's top image shows an Al particle breaking apart (seemingly along its GBs) with deep, wide cracks. Figure 6.4's lower images show long, rectangular/columnar growth structures of Al oxide/hydrate(s) formations. The lower right image shows long, parallel growth structures that are narrowly spaced apart. Such an amalgam would be expected to have low water-reactivity after significant exposure to air as much of its Al was already consumed via reactions with moisture and $O_2$ gas.

For comparison, Figures 6.5 and 6.6 show SEM images of the amalgam after the 6-month storage in the glovebox. In contrast to Figure 6.4, these figures show no significant formation of Al oxide/hydrate(s) structures. Figure 6.5 shows some such structures are present, but they appear to be only thin surface layers. The small degree of oxide(s)/hydroxide(s) formation in the post-storage amalgam may be due to reaction with trace levels of moisture/$O_2$ gas in the glovebox during storage and/or due to the ~10-20s exposure to ordinary air (of ~35%RH) during transfer of the amalgam into the SEM chamber.

Figure 6.6 shows BSE-mode SEM images of the post-storage amalgam, and the amalgam's features appear similar to those in Figure 6.7's BSE-mode SEM images at <1 day of storage, consistent with the observations of no change in amalgam water-reactivity at 6 months of storage vs <1 day of storage. In both Figure 6.6 and 6.7, atomic number contrast in BSE mode shows a phase that is rich in Ga, In, and/or Sn (likely GIS) visibly decorates Al GBs and forms surface pools in some locations. This further supports the hypothesis that no significant migration of Ga from GIS into Al grains occurred. In both figures, the GIS-rich phase should be liquid and contain dissolved liquid Al, but these qualities cannot be determined to be or not be present from these images. In both figures, the images offer some evidence that a GIS-rich phase in Al GBs thoroughly surrounds Al grains and is in significant, widespread physical contact with Al grains, but this is not visibly clear for all Al-GIS particles. However, it may be visibly clear for all Al-GIS particles if they could be cross-sectioned and viewed without significantly altering the areas to be viewed on the sample. Performing such a procedure may prove difficult (or impossible) for this type of sample and was outside the scope of this project.

SEM was used to make other observations of the amalgam's microstructure. In Figure 6.5's top image, some areas are extremely smooth like a liquid, suggesting these areas are liquid, GIS-rich phase. It would be unsurprising if liquid GIS-rich phase is what is being observed, because the amalgam is fully water-reactive (as discussed in Section 1.2.3.) and because eGIS only freezes at very low temperatures; eGIS exhibits a series of very low-temperature freezing/solidification points (−0.4°C, −26.4°C, and −38.5°C [51]). Figure 6.5's bottom image is a zoomed-in view of the smooth, seemingly liquid, surface of the ~20µm-diameter round particle centered in Figure 6.5's top image. In fact, during the process of zooming in on this particle, electrons/heating from the SEM electron beam caused the particle's surface to oscillate as a liquid; when oscillations stopped, Figure 6.5's bottom image was captured. Figure 6.5's bottom image's Al grain size/shape match those of Figure 6.3, so they are Al grains. The Al grains are extremely smooth, as if liquid-coated. Observations suggest Figure 6.5's bottom image shows liquid GIS coating Al grains on an Al-GIS particle. However, it is possible the coating was solid-phase until liquified from heating via the SEM electron beam (It is unclear how much temperature may be increased by such heating.). Also, it was seen during SEM analysis that other Al-GIS particles, such as some in Figure 6.5's top image, do not appear smooth like liquid and do not oscillate as liquids via SEM electron beam heating. However, as ~100% water-reaction yields were achieved, then, by deductive reasoning, all Al particles must have contained a significant amount of liquid GIS-rich phase such that they were fully activated (water-reactive). So, despite such variations in Al-GIS particles, these variations do not significantly impact water-reactivity, as, by deductive reasoning, all Al-GIS particles are fully water-reactive, as, again by deductive reasoning, they contain over a minimum threshold value of liquid GIS-rich phase (This value is undetermined.). Aforementioned variations in Al-GIS particles are likely due to randomness in the mixing (amalgamation) process, which haphazardly distributes liquid eGIS to Al particles. The variations may also be due to differences in physical characteristics of Al particles (size/shape/texture/etc.) affecting how and how much liquid GIS coats them individually during amalgamation.

## 6.5. Conclusions and future work

In conclusion, exposing the amalgam to ordinary air quickly degrades it, but it displays no water-reactivity degradation when stored in an inert environment at ~RT for at least 6 months (Longer times were not tested.). Further study may focus on the following:

- Quantify the amalgam water-reactivity degradation due to exposure to different concentrations of moisture and $O_2$ gas.
- Quantify the amalgam water-reactivity degradation in different mediums that may be more economically/commercially practical (storage in vacuum-sealed bags/containers, storage in liquids of low water content, storage in different low-moisture gases, etc.).
- Test increased storage time and/or temperature.
- Test the storage of different amalgam compositions.

# Chapter 7: Annealing-Related Studies Pertaining to the Water-Reactivity of Al-Ga/eGIS Amalgams

## 7.1. Goals

Optimally, high-temperature annealing of a 10wt%eGIS-90wt%Al amalgam would not decrease its water-reactivity. In Section 1.2.3., it was hypothesized as a possibility that annealing and/or aging may cause significant amounts of Ga in liquid GIS in Al GBs to migrate into Al grains, decreasing amalgam water-reactivity. Chapter 7 quantifies the change in water-reactivity due to high-temperature annealing. This relates to commercially useful parameters: high-temperature operational stability and high-temperature shelf-life stability. Also, the roles of Ga and eGIS in Al-Ga/eGIS amalgam water-reactivity are investigated.

## 7.2. Methods

10wt%eGIS-90wt%Al and 10wt%Ga-90wt%Al amalgams were made in a glovebox via the experimental methods in Chapter 2.

After being made, the amalgams were annealed in the glovebox for 1 week by placing them directly on the surfaces of hot plates (with inert, ceramic surfaces) that were measured with a metal thermocouple to have surface temperatures of ~400°C. They were then returned to RT.

4N-purity eGIS and 4N-purity Ga were amalgamated, via the amalgamation procedure in Chapter 2, with separate portions of the post-anneal 10wt%Ga-90wt%Al amalgam to make 10wt%Ga-5wt%eGIS-85wt%Al, 15wt%Ga-85wt%Al, and 50wt%Ga-50wt%Al amalgams.

Portions of all amalgams were reacted in water baths to quantify water-reaction yields/times. Some water-reaction rates were very slow in 50°C water, so near-boiling water (95°C) was used instead to simplify measuring water-reaction rates/yields, as shown in Table 7.1 below.

Further experimental methods details are in Chapter 2.

## 7.3. Data

Note that water-reaction rate curves for the data in Table 7.1 are in Appendix A.

**Table 7.1. Amalgam water-reactivities.**

| Sample | Water temperature | Water-reaction yield | Time to 90% water-reaction completion |
|---|---|---|---|
| Pre-anneal 10wt%eGIS-90wt%Al amalgam | 50°C | ~100% | 21s |
| Post-anneal 10wt%eGIS-90wt%Al amalgam | 50°C | ~99% | 18s |
| Pre-anneal 10wt%Ga-90wt%Al amalgam | 50°C | <1% | N/A |
| Post-anneal 10wt%Ga-90wt%Al amalgam | 95°C | ~5% | 15min |
| 15wt%Ga-85wt%Al amalgam, made from post-anneal 10wt%Ga-90wt%Al amalgam | 95°C | ~9% | 85min |
| 10wt%Ga-5wt%eGIS-85wt%Al amalgam, made from post-anneal 10wt%Ga-90wt%Al amalgam | 50°C | ~100% | 22s |
| 50wt%Ga-50wt%Al amalgam, made from post-anneal 10wt%Ga-90wt%Al amalgam | 95°C | ~98% | 8hrs |

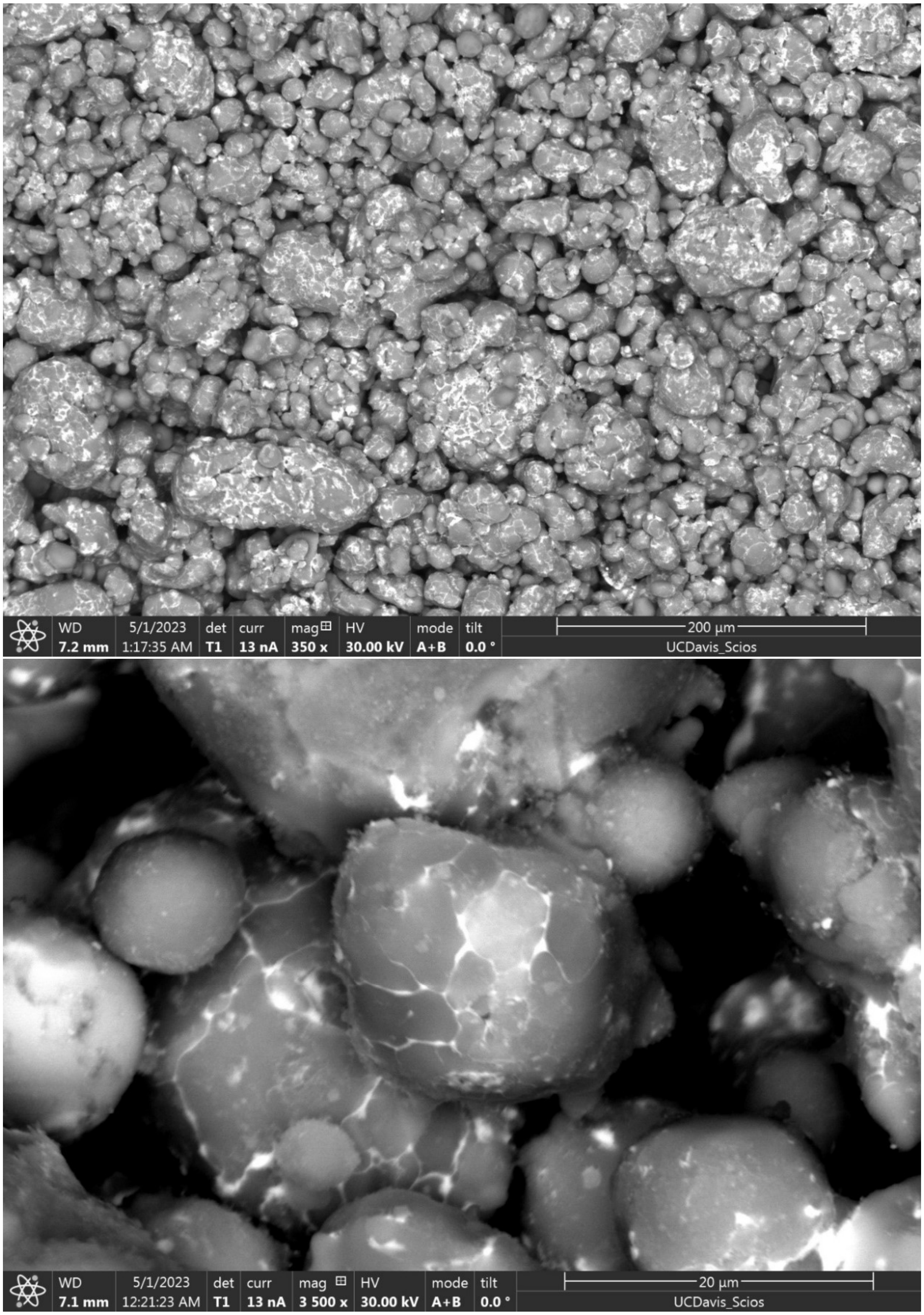

**Figure 7.1. BSE-mode SEM images of pre-anneal 10wt%eGIS-90wt%Al amalgam.** In BSE mode, areas rich in Ga, In, and/or Sn are whitest and Al-rich areas are grey.

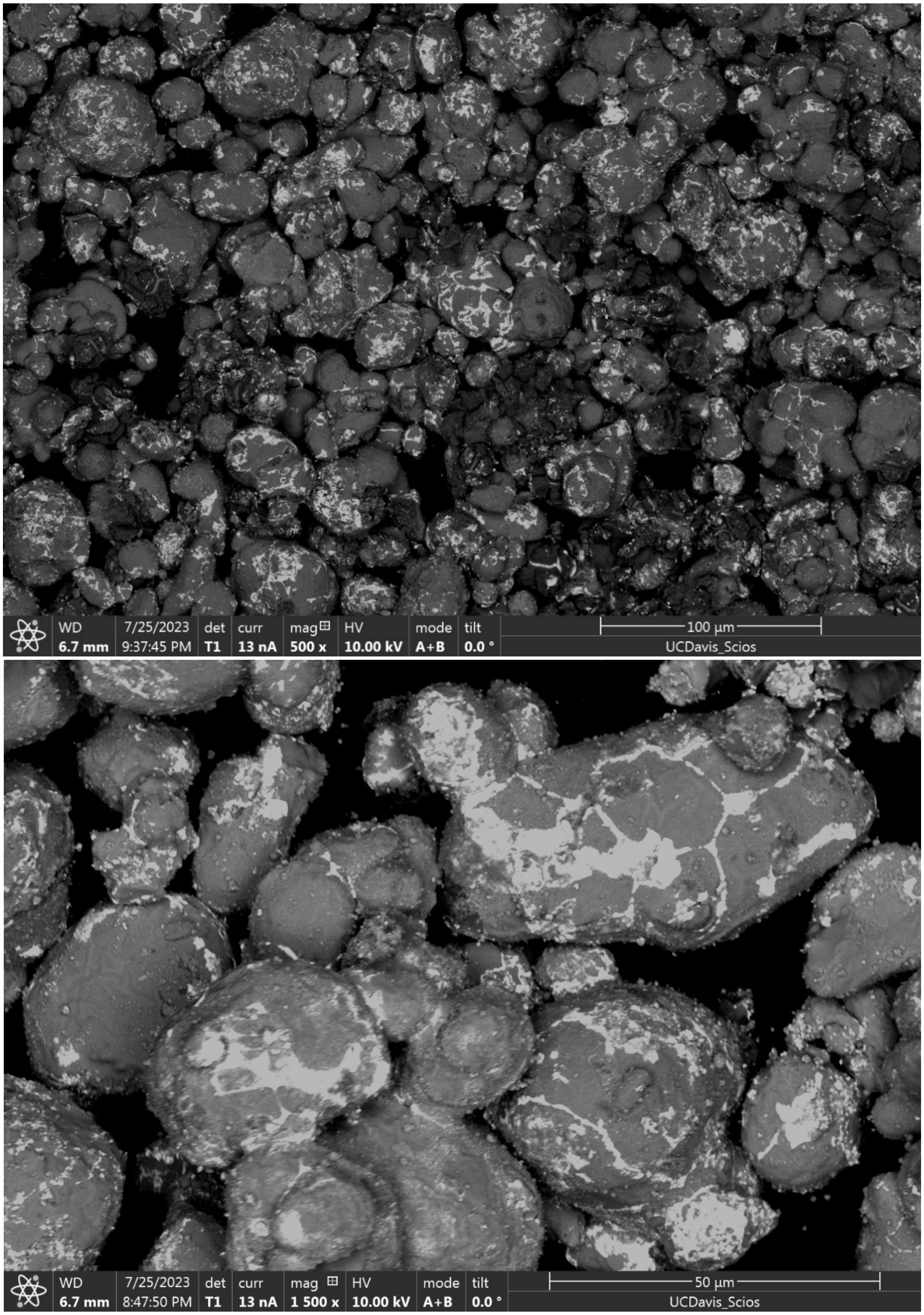

**Figure 7.2. BSE-mode SEM images of post-anneal 10wt%eGIS-90wt%Al amalgam.** In BSE mode, areas rich in Ga, In, and/or Sn are whitest and Al-rich areas are grey.

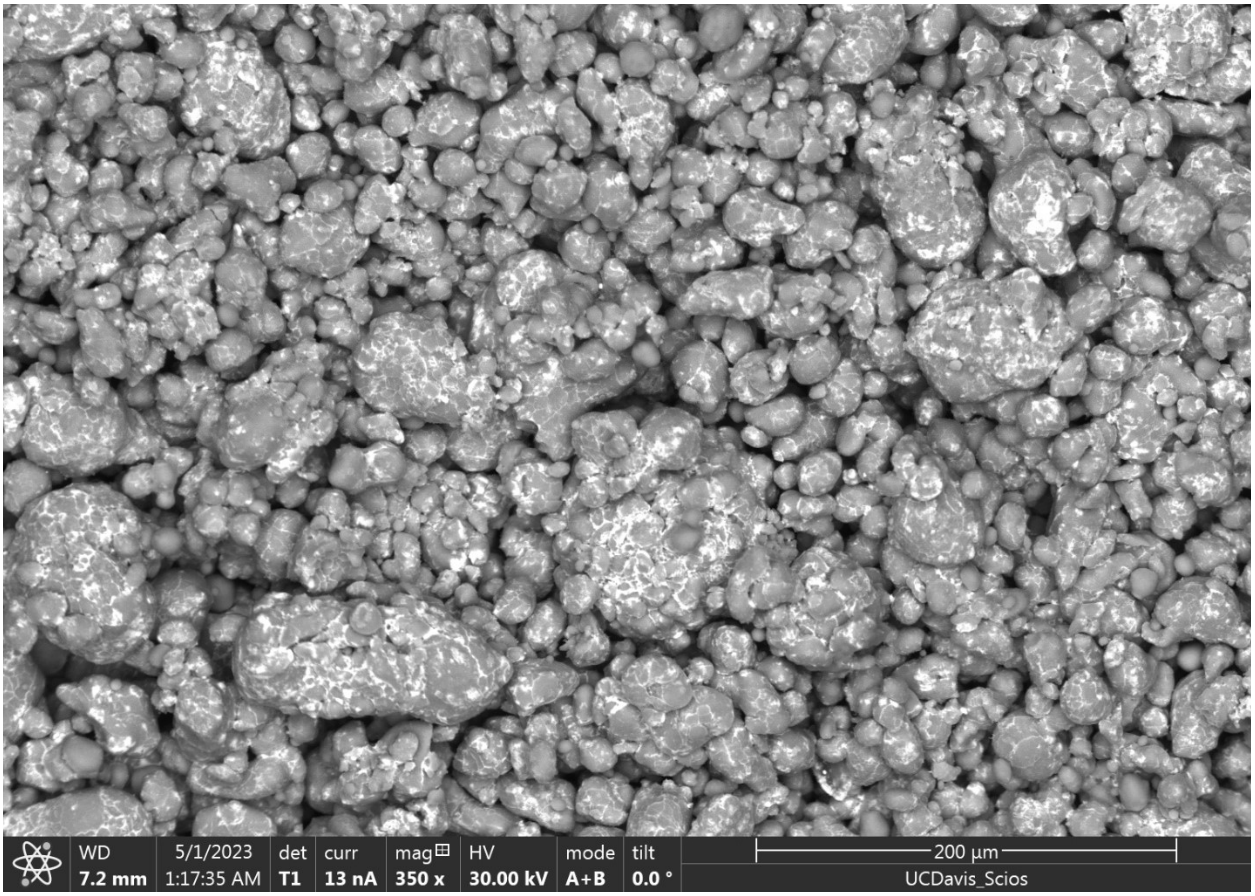

**Figure 7.3. BSE-mode SEM image of pre-anneal 10wt%Ga-90wt%Al amalgam.** In BSE mode, Ga-rich areas are whitest and Al-rich areas are grey.

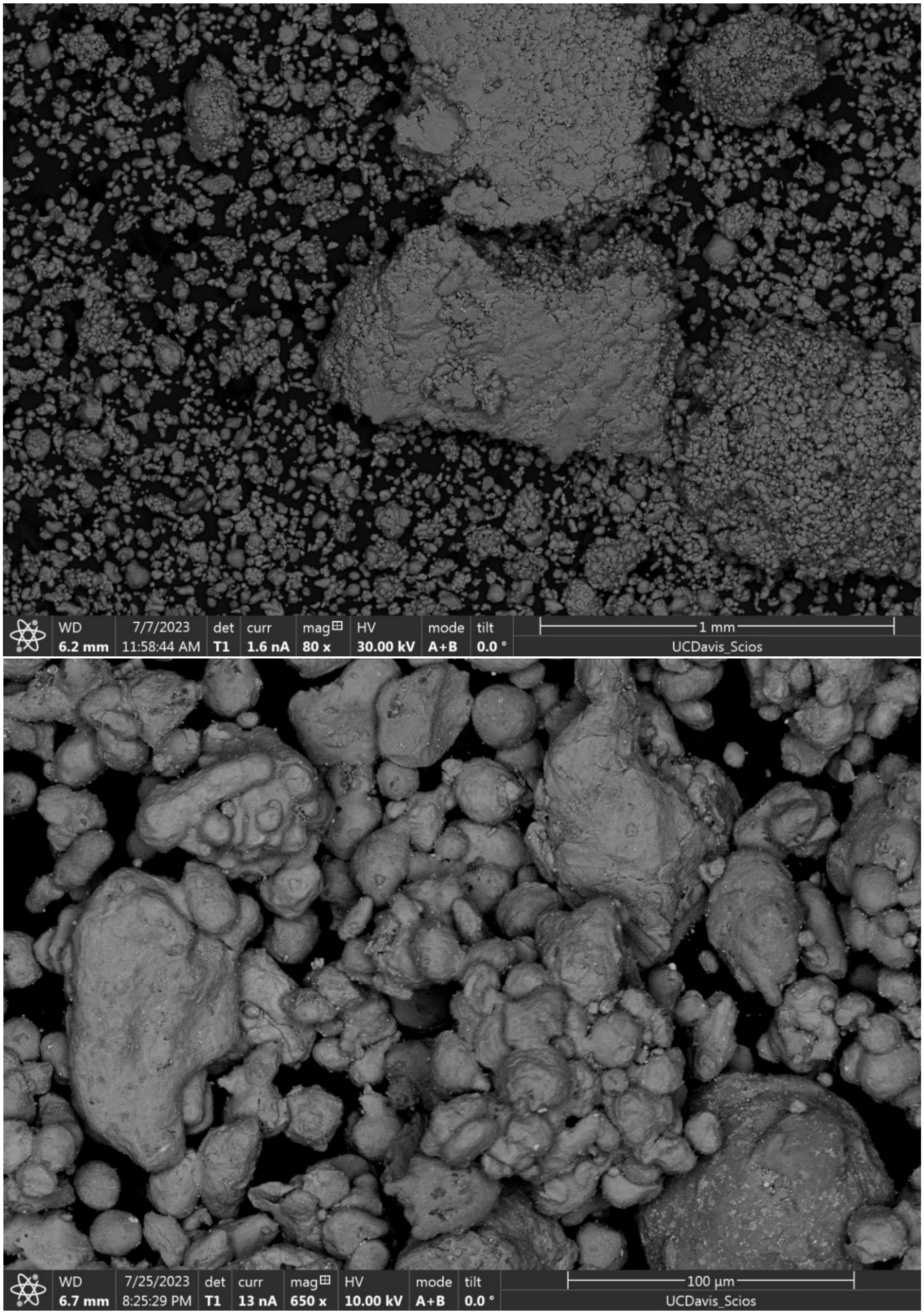

**Figure 7.4. BSE-mode SEM images of post-anneal 10wt%Ga-90wt%Al amalgam.** In BSE mode, Ga-rich areas are whitest (hardly present) and Al-rich areas are grey.

## 7.4. Introduction to analyses

The annealing temperature of ~400°C was selected as this temperature is above temperatures in most practical-use environments (The results should apply well to practical applications at temperatures at/below 400°C.) and is below the solidus curve for 10wt%Ga-90wt%Al on the Al-Ga phase diagram. As discussed in Section 1.2.3., it is expected that high-temperature annealing should accelerate Ga diffusion from Al GBs into Al grains in Al-Ga/eGIS amalgams that have a composition of phases that is partially liquid and partially solid.

Refer to SEM analyses discussions in Section 6.4 for improved understanding of statements regarding SEM analyses in this chapter, Chapter 7.

## 7.5. Effects of high-temperature annealing on the water-reactivity of a 10wt%eGIS-90wt%Al amalgam

The high-temperature annealing of the 10wt%eGIS-90wt%Al amalgam did not change its water-reaction rate or yield, according to the Table 7.1 data. These results are consistent with visual comparison of Figures 7.1 and 7.2; there do not appear to be obvious visual differences for pre-anneal vs post-anneal.

These results are consistent with, and may be explained by, the Section 1.2.3. hypothesis that Ga in eGIS/GIS in Al GBs tends to remain significantly bonded with In and/or Sn rather than migrate into Al grains. These results and this hypothesis are consistent with Chapter 5's discussion that Ga must be added to Al-In-Sn to form a liquid Al phase (at least at/below 50°C, but possibly also at somewhat higher temperatures) to enable Al water-reactivity. Further evidence that Ga in eGIS/GIS in Al GBs remained significantly bonded with In and/or Sn, post-anneal, is that Figure 7.2 uses BSE-mode SEM to show (at least in some areas) that a heavy-element phase (that is very likely eGIS-rich/GIS-rich) is in Al GBs, post-anneal, although using BSE mode does not clarify if this phase is Ga, In, and/or Sn. As discussed in

Section 6.4, SEM analyses of such amalgams has difficulties and only some areas may appear to show a heavy-element phase in Al GBs even if most/all Al GBs may contain such a heavy-element phase; unfortunately, it is difficult to successfully cross-section and view such samples.

## 7.6. Comparing the roles of Ga and eGIS in the water-reactivity of Al-Ga/eGIS amalgams

### 7.6.1. Comparing pre/post-anneal 10wt%Ga-90wt%Al amalgams

The observed very low water-reactivities of pre/post-anneal amalgams are consistent with prior work (p.19 of [6]) in which a 20wt%Ga-80wt%Al amalgam was found to be nonreactive in water at 80°C. In all cases, as discussed in Section 1.2.3., it is expected that very little to no liquid Al phase was present.

Comparing pre/post-anneal microstructures using atomic number contrast in BSE mode (Figures 7.3 and 7.4), the pre-anneal sample shows Ga in Al GBs, but the post-anneal sample shows Ga does not appear to be in Al GBs. This suggests annealing caused nearly all Ga to diffuse into Al grains. This was expected, as Al-Ga grains of α-Al solid solution is the only phase that is predicted to be present by the Al-Ga phase diagram for 10wt%Ga-90wt%Al. The result of the final yield of the post-anneal amalgam being very low suggests, as discussed in Section 1.2.3., that the post-anneal amalgam consisted almost entirely of nonreactive α-Al and there was little available liquid Ga for Al to dissolve into to form the water-reactive liquid Al phase.

Figure 7.3 shows that the pre-anneal amalgam has Ga in Al GBs. In general, the amalgamation process distributes Ga to Al particles and heats up the amalgam during the amalgamation process, because the rapid shaking of the capsule and its contents during mixing creates frictional heating. But this heating during amalgamation may have limited ability to cause Ga to diffuse into Al grains, which may instead require more significant time and/or temperature. But if liquid Ga is in Al GBs, why do Al grains not dissolve into it to enable amalgam water-reactivity? This may be because the Al-Ga phase diagram predicts that α-Al is the only phase that should be present, suggesting Ga diffuses into Al grains rather than Al grains dissolving into Ga. Also, to this point, when the amalgam was placed in 50°C water for water-reaction, Al grains should not dissolve into Ga, but instead, heat from the water may have only increased the rate of Ga diffusion into Al grains.

### 7.6.2. Effects of adding small amounts of Ga and eGIS to the post-anneal 10wt%Ga-90wt%Al amalgam

The post-anneal 10wt%Ga-90wt%Al amalgam discussed above was also used as an ingredient in two amalgams that were compared: 15wt%Ga-85wt%Al and 10wt%Ga-5wt%eGIS-85wt%Al. These amalgams with added Ga/eGIS were intentionally made with a total Ga wt% of <20wt%Ga with the aim of keeping them in the fully solid α-Al region of the Al-Ga phase diagram to avoid forming liquid Al, which is known to be water-reactive, as discussed in Section 1.2.3.

The two amalgams had very different water-reactivities. The 15wt%Ga-85wt%Al amalgam had very low water-reactivity, which is consistent with the discussion in the previous section. In contrast, the 10wt%Ga-5wt%eGIS-85wt%Al amalgam was fully water-reactive. This is consistent with the Section 1.2.3. hypothesis that Ga in eGIS/GIS in Al GBs remains significantly bonded with In and/or Sn rather than migrating into Al grains, allowing Al grains to dissolve as liquid Al into eGIS/GIS in Al GBs to enable amalgam water-reactivity.

### 7.6.3. Effects of adding a large amount of Ga to the post-anneal 10wt%Ga-90wt%Al amalgam

The 50wt%Ga-50wt%Al amalgam manufactured with the post-anneal 10wt%Ga-90wt%Al amalgam was fully water-reactive. The 50wt%Ga-50wt%Al amalgam is in the solid and liquid two-phase region of the

Al-Ga phase diagram. Its slow, continuous water-reaction rate in Figure A6 is consistent with the Section 1.2.3. model of Al grains and particles continuously diffusing into surrounding liquid Ga until all Al is consumed. This is because Al grains may only contain up to ~20wt%Ga (based on the Al-Ga phase diagram), so the excess Ga in the amalgam remains as a separate liquid phase that cannot enter Al grains, allowing Al grains to dissolve into it over time to enable ~100% water-reaction yield of the amalgam.

## 7.7. Conclusions

Results for the samples in which Ga and eGIS were added suggest α-Al solid solution (Al grains containing Ga that diffused into them) can fully react with water if placed in contact with liquid eGIS or significantly excess liquid Ga. This finding is consistent with the mechanistic model for the water-reactivity of partially-solid, partially-liquid bulk Al-Ga/eGIS alloys/amalgams that was proposed in prior work (p.57 of [2]).

The water-reaction yield results in this chapter are consistent with the expectation from the Al-Ga phase diagram that Al-Ga amalgams of <20wt%Ga are poorly water-reactive and Al-Ga amalgams of >20wt%Ga are fully water-reactive (at least above the eutectic temperature).

The water-reaction yield results for Al-eGIS amalgams are consistent with the hypothesis in Section 1.2.3. that high-temperature annealing does not cause significant Ga migration from eGIS/GIS in Al GBs into Al grains to occur.

# Chapter 8: Conclusions

A new finding was that α-Al solid solution (Al grains containing Ga that diffused into them) can fully react with water if placed in contact with liquid eGIS or significantly excess liquid Ga. This finding is consistent with the mechanistic model for the water-reactivity of partially-solid, partially-liquid bulk Al-Ga/eGIS alloys/amalgams that was proposed in prior work (p.57 of [2]).

Al-In-Sn without Ga displayed <1% water-reaction yield in water of ≤50°C. This suggests that, at least in water of ≤50°C, Ga is needed for Al-GIS alloys/amalgams to become activated/water-reactive. This also suggests that, in Al-GIS alloys/amalgams that are significantly water-reactive in water of ≤50°C, a significant amount of Ga does not migrate from liquid GIS in Al GBs into Al grains.

The 10wt%Ga-90wt%Al and 15wt%Ga-85wt%Al amalgams had very low water-reaction yields, but the 50wt%Ga-50wt%Al amalgam gave ~100% water-reaction yield. These results are consistent with the expectation, based on the Al-Ga phase diagram, that Al-Ga should display no water-reactivity if Ga wt% is <20wt% (at relatively "ordinary" temperatures—that is, below the solidus curve of the Al-Ga phase diagram) but should be fully water-reactive if Ga wt% is >20wt% (and if above the eutectic temperature). These results suggest Al-Ga amalgams can only be viable in real-world applications to produce hydrogen energy if Ga wt% is >20wt%.

The 10wt%eGIS-90wt%Al amalgam fully reacted in 50°C deionized/distilled waters and reacted very quickly, reaching 90% amalgam water-reaction yield in as fast as 18s. This fast water-reaction rate suggests that the 10wt%eGIS-90wt%Al amalgam is a promising candidate for applications that are centered on the rapid production of hydrogen energy. The 10wt%eGIS-90wt%Al amalgam reacted slower in alkaline and tap waters but nevertheless fully reacted. This is a promising result, as it shows the 10wt%eGIS-90wt%Al amalgam can produce a full yield of $H_2$ gas, even if it is reacted in inexpensive and/or “dirty” waters. Further, the $H_2$ gas that was produced was of high purity, regardless of if DI, distilled, alkaline, or tap water was used.

Exposing a 10wt%eGIS-90wt%Al amalgam to ordinary air quickly degrades it. However, it was found that a 10wt%eGIS-90wt%Al amalgam displays no water-reactivity degradation when stored in an inert environment at ~RT, at least for 6 months (longer times were not tested). Further, the high-temperature annealing (at 400°C for 1 week) of a 10wt%eGIS-90wt%Al amalgam did not cause any water-reactivity degradation. These results are consistent with, and may be explained by, the hypothesis that Ga in eGIS/GIS in Al GBs tends to remain significantly bonded with In and/or Sn rather than migrate into Al grains, even if exposed to significantly elevated temperature or even if there is prolonged physical contact between the liquid eGIS/GIS and Al grains. Also, these results suggest that the 10wt%eGIS-90wt%Al amalgam can be practical in real-world/commercial applications, because it appears to be very shelf-stable, relative to time and temperature, if care is taken to protect it from exposure to moisture (and to, perhaps of lesser significance, $O_2$ gas).

In closing, amalgamation-genre technology provides a simple, single-step process for the fast and successful production of energy-storage devices—amalgam batteries. These batteries, when simply placed in contact with water, rapidly generate on-demand hydrogen energy. This hydrogen energy may be utilized to power innumerable niche and commonplace applications.

# Appendices

## Appendix A. Water-reaction rate curves for Chapter 7

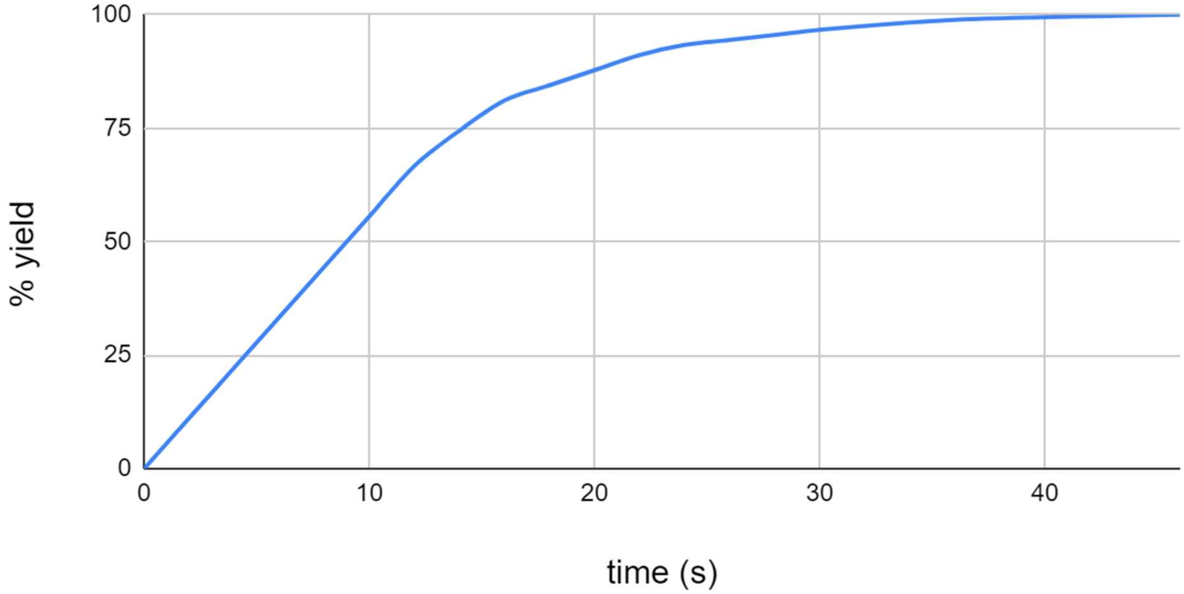

**Figure A1. Water-reaction rate curve for pre-anneal 10wt%eGIS-90wt%Al amalgam in 50°C DI water.**

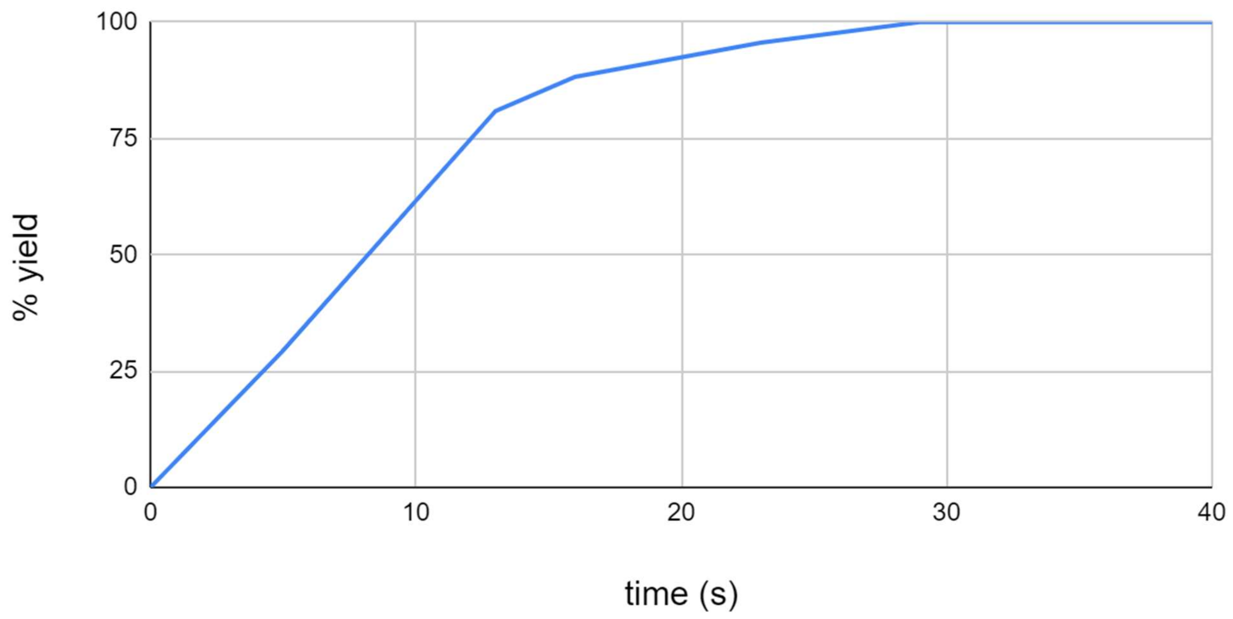

**Figure A2. Water-reaction rate curve for post-anneal 10wt%eGIS-90wt%Al amalgam in 50°C DI water.**

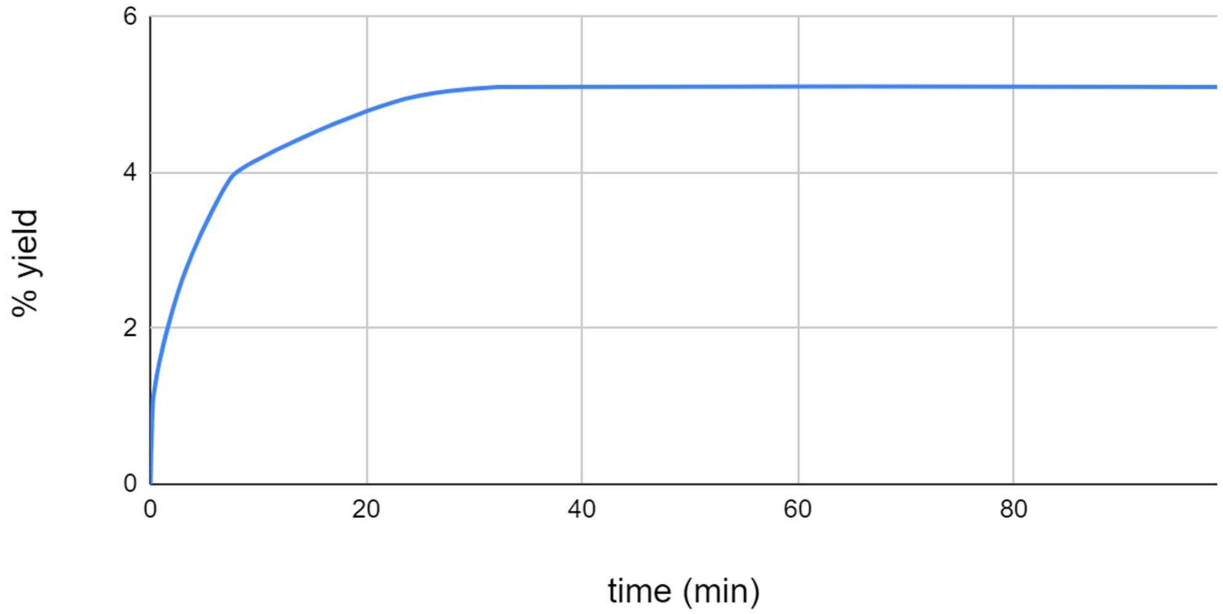

**Figure A3. Water-reaction rate curve for post-anneal 10wt%Ga-90wt%Al amalgam in 95°C DI water.**

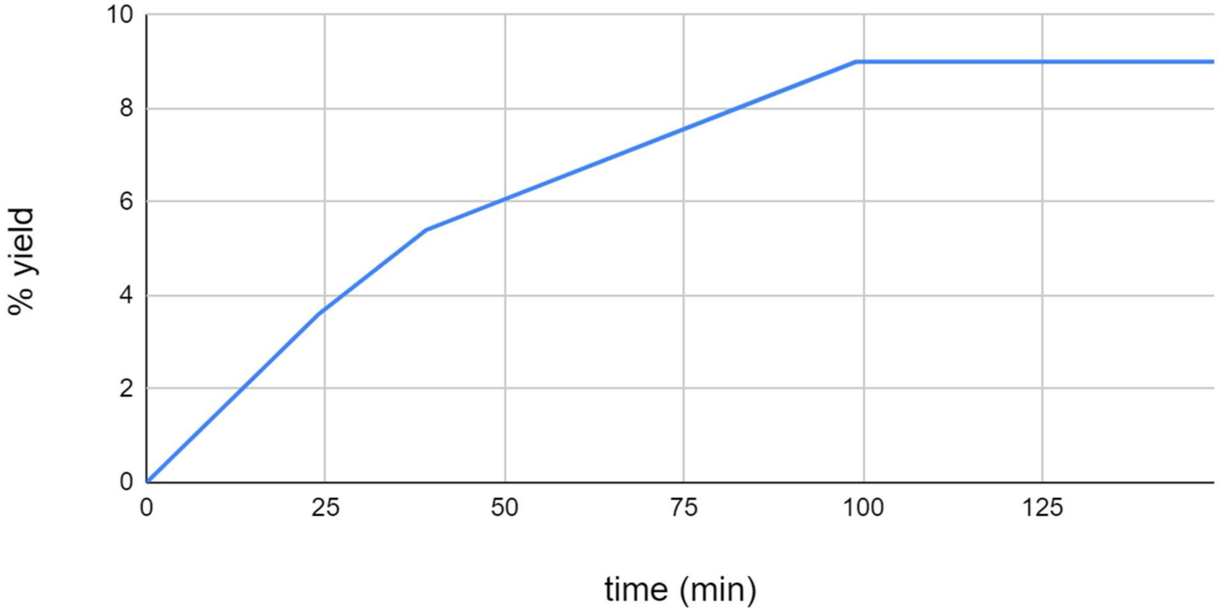

**Figure A4. Water-reaction rate curve for 15wt%Ga-85wt%Al amalgam, made from post-anneal 10wt%Ga-90wt%Al amalgam, in 95°C DI water.**

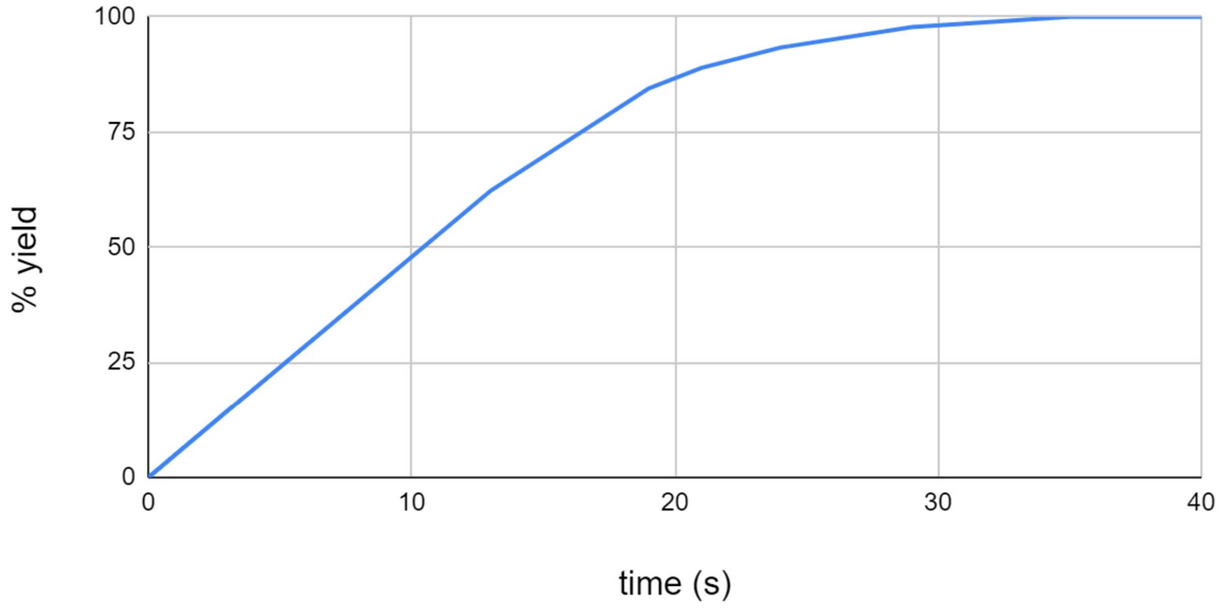

**Figure A5. Water-reaction rate curve for 10wt%Ga-5wt%eGIS-85wt%Al amalgam, made from post-anneal 10wt%Ga-90wt%Al amalgam, in 50°C DI water.**

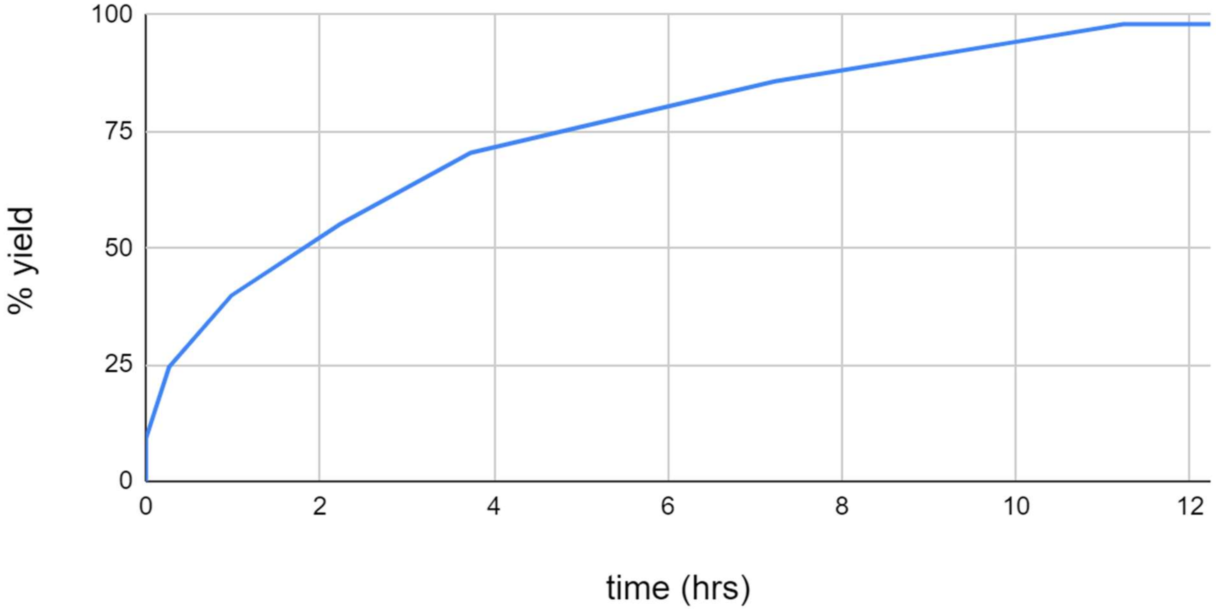

**Figure A6. Water-reaction rate curve for 50wt%Ga-50wt%Al amalgam, made from post-anneal 10wt%Ga-90wt%Al amalgam, in 95°C DI water.**

# Appendix B. Tables

**Table B1. Relevant ΔG° and ΔH° values of substances at STP.**

| Substance | ΔG° (kJ/mol) | ΔH° (kJ/mol) |
|---|---|---|
| $Al_{(cr)}$ | 0 (p.60 of [52]) | |
| $Al_{(l)}$ | +7.201 (p.61 of [52]) | +10.562 (p.61 of [52]) |
| $Al^{3+}_{(aq)}$ | −489.4 [53] | |
| $[Al(OH)]^{2+}_{(aq)}$ | −693.7 (p.308 of [54]) | |
| $[Al(OH)_2]^{+}_{(aq)}$ | −901.4 (p.308 of [54]) | |
| $Al(OH)_{3,\,(aq)}$ | −1100.7 (p.308 of [54]) | |
| $[Al(OH)_4\,]^{-}_{(aq)}$ | −1304.9 [55] | |
| $\alpha\text{-}Al_2O_{3,\,(s,\,corundum)}$ | −1582.2 ± 1.3 [56] | −1675.7 ± 1.3 [56] |
| $\gamma\text{-}Al_2O_{3,\,(s)}$ | −1563.850 (p.156 of [52]) | |
| $\delta\text{-}Al_2O_{3,\,(s)}$ | −1572.974 (p.155 of [52]) | |
| $\kappa\text{-}Al_2O_{3,\,(s)}$ | −1569.663 (p.157 of [52]) | |
| $Al(OH)_{3,\,(s,\,bayerite)}$ | −1153.0 ± 2 [56] | −1288.25 (p.2-127 of [57]) |
| $Al(OH)_{3,\,(s,\,gibbsite)}$ | −1154.9 ± 1.2 [56] | |
| $AlO(OH)_{(s,\,boehmite)}$ | −918.4 ± 2.1 [56] | −993.1 ± 2.2 [56] |
| $AlO(OH)_{(s,\,diaspore)}$ | −922.0 ± 5.0 [56] | |
| $Ga_{(cr)}$ | 0 (p.1256 of [52]) | |
| $Ga_{(l)}$ | +0.088 (p.1255 of [52]) | |
| $\beta\text{-}Ga_2O_{3,\,(s,\,rhombic)}$ | −998.3 (p.2-131 of [57]) | −1089.1 (p.2-131 of [57]) |
| $Ga(OH)_{3,\,(cr)}$ | −831.3 (p.2-131 of [57]) | −964.4 (p.2-131 of [57]) |
| $\alpha\text{-}GaO(OH)_{(s)}$ | −627.9 ± 2.0 [58] | −705.3 ± 2.5 [58] |
| $H_{(g)}$ | +203.247 (p.2-38 of [57]) | |
| $H^{+}_{(aq)}$ | 0 (p.2-38 of [57]) | |
| $H_{2,\,(g)}$ | 0 (p.2-38 of [57]) | 0 (p.2-38 of [57]) |
| $H_2O_{(l)}$ | −237.129 (p.2-38 of [57]) | −285.830 (p.2-38 of [57]) |
| $H_2O_{(g)}$ | −228.572 (p.2-38 of [57]) | −241.818 (p.2-38 of [57]) |
| $H_3O^{+}_{(aq)}$ | −228.6 [59] | |
| $In_{(cr)}$ | 0 (p.2-133 of [57]) | |
| $In_2O_{3,\,(cr)}$ | −830.68 (p.2-133 of [57]) | |
| $O_{2,\,(aq)}$ | +16.4 (p.2-37 of [57]) | |
| $O_{2,\,(g)}$ | 0 (p.2-37 of [57]) | |
| $OH^{-}_{(aq)}$ | −157.244 (p.2-38 of [57]) | |
| $Sn_{(cr1,\,white)}$ | 0 (p.2-116 of [57]) | |
| $Sn_{(cr2,\,gray)}$ | +0.13 (p.2-116 of [57]) | |
| $Sn(OH)_{2,\,(cr)}$ | −491.6 (p.2-116 of [57]) | |
| $SnO_{(cr)}$ | −256.9 (p.2-116 of [57]) | |
| $SnO_{2,\,(cr)}$ | −519.6 (p.2-116 of [57]) | |

**Table B2. ΔG° for Al-eGIS reactions (non-exhaustive).** Calculated from Table B1 data.

| **Eq. #** | **Al-eGIS reacting with $H_2O$ to form oxides and hydrates** | |
|---|---|---|
| B2.1 | $\Delta G^\circ = -455$ kJ/mol $Al_{(l)}$ | $2\,Al_{(l)} + 4\,H_2O_{(l)} \rightarrow 2\,AlO(OH),_{(s,\ diaspore)} + 3\,H_{2,\ (g)}$ |
| B2.2 | $\Delta G^\circ = -451$ kJ/mol $Al_{(l)}$ | $2\,Al_{(l)} + 6\,H_2O_{(l)} \rightarrow 2\,Al(OH)_{3,\ (s,\ gibbsite)} + 3\,H_{2,\ (g)}$ |
| B2.3 | $\Delta G^\circ = -451$ kJ/mol $Al_{(l)}$ | $2\,Al_{(l)} + 4\,H_2O_{(l)} \rightarrow 2\,AlO(OH),_{(s\ boehmite)} + 3\,H_{2,\ (g)}$ |
| B2.4 | $\Delta G^\circ = -449$ kJ/mol $Al_{(l)}$ | $2\,Al_{(l)} + 6\,H_2O_{(l)} \rightarrow 2\,Al(OH)_{3,\ (s,\ bayerite)} + 3\,H_{2,\ (g)}$ |
| B2.5 | $\Delta G^\circ = -443$ kJ/mol $Al_{(l)}$ | $2\,Al_{(l)} + 3\,H_2O_{(l)} \rightarrow Al_2O_{3,\ (s,\ corundum)} + 3\,H_{2,\ (g)}$ |
| B2.6 | $\Delta G^\circ = -154$ kJ/mol $Ga_{(l)}$ | $2\,Ga_{(l)} + 4\,H_2O_{(l)} \rightarrow 2\,\alpha\text{-}GaO(OH)_{(s)} + 3\,H_{2,\ (g)}$ |
| B2.7 | $\Delta G^\circ = -144$ kJ/mol $Ga_{(l)}$ | $2\,Ga_{(l)} + 3\,H_2O_{(l)} \rightarrow \beta\text{-}Ga_2O_{3,\ (s,\ rhombic)} + 3\,H_{2,\ (g)}$ |
| B2.8 | $\Delta G^\circ = -120$ kJ/mol $Ga_{(l)}$ | $2\,Ga_{(l)} + 6\,H_2O_{(l)} \rightarrow 2\,Ga(OH)_{3},_{\ (cr)} + 3\,H_{2,\ (g)}$ |
| B2.9 | $\Delta G^\circ = -60$ kJ/mol $In_{(cr)}$ | $2\,In_{(cr)} + 3\,H_2O_{(l)} \rightarrow In_2O_{3,\ (cr)} + 3\,H_{2,\ (g)}$ |
| B2.10 | $\Delta G^\circ = -45$ kJ/mol $Sn_{(cr,\ white)}$ | $Sn_{(cr,\ white)} + 2\,H_2O_{(l)} \rightarrow SnO_{2,\ (cr)} + 2\,H_{2,\ (g)}$ |
| B2.11 | $\Delta G^\circ = -20$ kJ/mol $Sn_{(cr,\ white)}$ | $Sn_{(cr,\ white)} + H_2O_{(l)} \rightarrow SnO_{(cr)} + H_{2,\ (g)}$ |
| B2.12 | $\Delta G^\circ = -17$ kJ/mol $Sn_{(cr,\ white)}$ | $Sn_{(cr,\ white)} + 2\,H_2O_{(l)} \rightarrow Sn(OH)_{2,\ (cr)} + H_{2,\ (g)}$ |
| **Eq. #** | **Al-eGIS reacting with $O_2$ gas in air to form oxides** | |
| B2.13 | $\Delta G^\circ = -798$ kJ/mol $Al_{(l)}$ | $4\,Al_{(l)} + 3\,O_{2,\ (g)} \rightarrow 2\,Al_2O_{3,\ (s,\ corundum)}$ |
| B2.14 | $\Delta G^\circ = -520$ kJ/mol $Sn_{(cr,\ white)}$ | $Sn_{(cr,\ white)} + O_{2,\ (g)} \rightarrow SnO_{2,\ (cr)}$ |
| B2.15 | $\Delta G^\circ = -499$ kJ/mol $Ga_{(l)}$ | $4\,Ga_{(l)} + 3\,O_{2,\ (g)} \rightarrow 2\,\beta\text{-}Ga_2O_{3,\ (s,\ rhombic)}$ |
| B2.16 | $\Delta G^\circ = -415$ kJ/mol $In_{(cr)}$ | $4\,In_{(cr)} + 3\,O_{2,\ (g)} \rightarrow 2\,In_2O_{3,\ (cr)}$ |
| B2.17 | $\Delta G^\circ = -257$ kJ/mol $Sn_{(cr,\ white)}$ | $2\,Sn_{(cr,\ white)} + O_{2,\ (g)} \rightarrow 2\,SnO_{(cr)}$ |
| **Eq. #** | **Al-eGIS reacting with dissolved $O_2$ gas in water to form oxides** | |
| B2.18 | $\Delta G^\circ = -811$ kJ/mol $Al_{(l)}$ | $4\,Al_{(l)} + 3\,O_{2,\ (aq)} \rightarrow 2\,Al_2O_{3,\ (s,\ corundum)}$ |
| B2.19 | $\Delta G^\circ = -536$ kJ/mol $Sn_{(cr,\ white)}$ | $Sn_{(cr,\ white)} + O_{2,\ (aq)} \rightarrow SnO_{2,\ (cr)}$ |
| B2.20 | $\Delta G^\circ = -512$ kJ/mol $Ga_{(l)}$ | $4\,Ga_{(l)} + 3\,O_{2,\ (aq)} \rightarrow 2\,\beta\text{-}Ga_2O_{3,\ (s,\ rhombic)}$ |
| B2.21 | $\Delta G^\circ = -428$ kJ/mol $In_{(cr)}$ | $4\,In_{(cr)} + 3\,O_{2,\ (aq)} \rightarrow 2\,In_2O_{3,\ (cr)}$ |
| B2.22 | $\Delta G^\circ = -265$ kJ/mol $Sn_{(cr,\ white)}$ | $2\,Sn_{(cr,\ white)} + O_{2,\ (aq)} \rightarrow 2\,SnO_{(cr)}$ |
| **Eq. #** | **Alternative Al reactions (*Notes are on the following page.)** | |
| B2.23 | $\Delta G^\circ = -443$ kJ/mol $Al_{(l)}$ | $2\,Al_{(l)} + 2\,[OH]^{-}_{(aq)} + 6\,H_2O_{(l)} \rightarrow 2\,[Al(OH)_4\,]^{-}_{(aq)} + 3\,H_{2,\ (g)}$ |
| B2.24 | $\Delta G^\circ = -483$ kJ/mol $Al_{(l)}$ | $2\,Al_{(l)} + 3\,[OH]^{-}_{(aq)} + H^{+}_{(aq)} + 5\,H_2O_{(l)} \rightarrow 2\,[Al(OH)_4\,]^{-}_{(aq)} + 3\,H_{2,\ (g)}$ |
| B2.25 | $\Delta G^\circ = -448$ kJ/mol $Al_{(l)}$ | $2\,Al_{(l)} + 2\,[OH]^{-}_{(aq)} + [H_3O]^{+}_{(aq)} + 5\,H_2O_{(l)} \rightarrow$ $2\,[Al(OH)_4\,]^{-}_{(aq)} + H^{+}_{(aq)} + 3\,H_{2,\ (g)}$ |
| B2.26 | $\Delta G^\circ = -495$ kJ/mol $Al_{(l)}$ | $2\,Al_{(l)} + [OH]^{-}_{(aq)} + H^{+}_{(aq)} + 3\,H_2O_{(l)} \rightarrow 2\,AlO(OH)_{(s,\ diaspore)} + 3\,H_{2,\ (g)}$ |
| B2.27 | $\Delta G^\circ = -491$ kJ/mol $Al_{(l)}$ | $2\,Al_{(l)} + [OH]^{-}_{(aq)} + H^{+}_{(aq)} + 5\,H_2O_{(l)} \rightarrow 2\,Al(OH)_{3,\ (s,\ gibbsite)} + 3\,H_{2,\ (g)}$ |
| B2.28 | $\Delta G^\circ = -483$ kJ/mol $Al_{(l)}$ | $2\,Al_{(l)} + [OH]^{-}_{(aq)} + H^{+}_{(aq)} + 2\,H_2O_{(l)} \rightarrow Al_2O_{3,\ (s,\ corundum)} + 3\,H_{2,\ (g)}$ |
| B2.29 | $\Delta G^\circ = -434$ kJ/mol $Al_{(l)}$ | $2\,Al_{(l)} + 2\,H^{+}_{(aq)} + 4\,H_2O_{(l)} \rightarrow 2\,[Al(OH)_2]^{+}_{(aq)} + 3\,H_{2,\ (g)}$ |
| B2.30 | $\Delta G^\circ = -464$ kJ/mol $Al_{(l)}$ | $2\,Al_{(l)} + 4\,H^{+}_{(aq)} + 2\,H_2O_{(l)} \rightarrow 2\,[Al(OH)]^{2+}_{(aq)} + 3\,H_{2,\ (g)}$ |
| B2.31 | $\Delta G^\circ = -497$ kJ/mol $Al_{(l)}$ | $2\,Al_{(l)} + 6\,H^{+}_{(aq)} \rightarrow 2\,Al^{3+}_{(aq)} + 3\,H_{2,\ (g)}$ |
| **Eq. #** | **Al/Ga oxides/hydrates reacting with $H_2O$** | |
| B2.32 | $\Delta G^\circ = -17$ kJ | $Al_2O_{3,\ (s,\ corundum)} + H_2O_{(l)} \rightarrow 2\,AlO(OH)_{(s,\ boehmite)}$ |
| B2.33 | $\Delta G^\circ = +3$ kJ | $AlO(OH)_{(s,\ boehmite)} + H_2O_{(l)} \rightarrow Al(OH)_{3,\ (s,\ bayerite)}$ |
| B2.34 | $\Delta G^\circ = -3$ kJ | $Al(OH)_{3,\ (s,\ bayerite)} \rightarrow AlO(OH)_{(s,\ boehmite)} + H_2O_{(l)}$ |
| B2.35 | $\Delta G^\circ = -20$ kJ | $\beta\text{-}Ga_2O_{3,\ (s,\ rhombic)} + H_2O_{(l)} \rightarrow 2\,\alpha\text{-}GaO(OH)_{(s)}$ |
| B2.36 | $\Delta G^\circ = +34$ kJ | $\alpha\text{-}GaO(OH)_{,\ (s)} + H_2O_{(l)} \rightarrow Ga(OH)_{3,\ (cr)}$ |
| B2.37 | $\Delta G^\circ = -34$ kJ | $Ga(OH)_{3,\ (cr)} \rightarrow \alpha\text{-}GaO(OH)_{(s)} + H_2O_{(l)}$ |

*****In the “Alternative Al reactions” section of Table B2, equations are only written with minimal amounts of $[OH]^-$, $H^+$, and/or $[H_3O]^+$ as reactants relative to $H_2O$ as a reactant. For example, in addition to Eq. B2.23, the additional Eqs. B2.24 and B2.25 may also be written; these equations are nearly identical, except Eq. B2.24 replaces one $H_2O$ with one $[OH]^-$ and one $H^+$ on the reactant side of Eq. B2.23, and Eq. B2.25 replaces one $H_2O$ with one $[H_3O]^+$ on the reactant side of the equation and adds one $H^+$ on the product side. Such replacements lead to equations with more negative ΔG° values (that are increasingly negative the more that the reactant $H_2O$ is replaced), so they are more energetically favorable. However, such equations are not included, as they may simply add unnecessary complexity to the work presented and as abundance/availability of $[OH]^-$, $H^+$, and/or $[H_3O]^+$ relative to $H_2O$ is assumed to be limited in most cases, increasing the unlikeliness of their real-world occurrences in the reactions.

**Table B3. Temperature ranges over which Al film phases and Ga film phases are predicted as stable.** ******Notes are below.

| **Al film phases** | **Temperature range of stability** |
|---|---|
| $Al(OH)_{3,\ (s,\ bayerite)}$ | <63°C |
| $AlO(OH)_{(s,\ boehmite)}$ | 63°C to 207°C |
| $\alpha\text{-}Al_2O_{3,\ (s,\ corundum)}$ | >207°C |
| **Ga film phases** | **Temperature range of stability** |
| $Ga(OH)_{3,\ (cr)}$ | <−152°C |
| $\alpha\text{-}GaO(OH)_{(s)}$ | −152°C to 195°C |
| $\beta\text{-}Ga_2O_{3,\ (s,\ rhombic)}$ | >195°C |

******Using the average values in Table B1 and the calculation procedure described in pp.40-43 of [2], which is partially shown here by written Eqs. B3.1-B3.4 below, the temperature ranges for the stability of β-$Ga_2O_{3,\ (s,\ rhombic)}$, $Ga(OH)_{3,\ (cr)}$, and α-$GaO(OH)_{(s)}$ were calculated. The results are shown in Table B3 (The phases in Table B3 may be different from other polymorphic and/or amorphous phases that may form simultaneously in practice, for which there is limited thermodynamic data.). Further, the temperature ranges for the stability of α-$Al_2O_{3,\ (s,\ corundum)}$, $Al(OH)_{3,\ (s,\ bayerite)}$, and $AlO(OH)_{(s,\ boehmite)}$ were previously calculated on p.43 of [2], but they are re-calculated here using the average values in Table B1 to confirm the prior work. Similar temperature ranges are obtained as on p.43 of [2], although they are slightly different, simply due to slight differences in the literature values that were used for calculations.

Eq. B3.1 $Ga(OH)_{3,\ (cr)} \rightarrow \alpha\text{-}GaO(OH)_{(s)} + H_2O_{(g)}$ $\Delta G° = -25$ kJ $\Delta H° = +17$ kJ

Eq. B3.2 $2\ \alpha\text{-}GaO(OH)_{(s)} \rightarrow \beta\text{-}Ga_2O_{3,\ (s,\ rhombic)} + H_2O_{(g)}$ $\Delta G° = +29$ kJ $\Delta H° = +80$ kJ

Eq. B3.3 $Al(OH)_{3,\ (s,\ bayerite)} \rightarrow AlO(OH)_{(s,\ boehmite)} + H_2O_{(g)}$ $\Delta G° = +6$ kJ $\Delta H° = +53$ kJ

Eq. B3.4 $2\ AlO(OH)_{(s,\ boehmite)} \rightarrow \alpha\text{-}Al_2O_{3,\ (s,\ corundum)} + H_2O_{(g)}$ $\Delta G° = +26$ kJ $\Delta H° = +69$ kJ

**Table B4. Al-eGIS electrochemical series (non-exhaustive).**
The data are from [60].

| **Eq. #** | **Al** | |
|---|---|---|
| B4.1 | $E° = -2.33\ V$ | $[H_2AlO_3]^{-}_{(aq)} + H_2O_{(l)} + 3\ e^{-} \rightleftharpoons Al_{(s)} + 4\ [OH]^{-}_{(aq)}$ |
| B4.2 | $E° = -2.328\ V$ | $[Al(OH)_4]^{-}_{(aq)} + 3\ e^{-} \rightleftharpoons Al_{(s)} + 4\ [OH]^{-}_{(aq)}$ |
| B4.3 | $E° = -2.31\ V$ | $Al(OH)_{3,\ (aq)} + 3\ e^{-} \rightleftharpoons Al_{(s)} + 3\ [OH]^{-}_{(aq)}$ |
| B4.4 | $E° = -2.069\ V$ | $[AlF_6]^{3-}_{(aq)} + 3\ e^{-} \rightleftharpoons Al_{(s)} + 6\ F^{-}_{(aq)}$ |
| B4.5 | $E° = ?$ | $[Al(OH)_2]^{+}_{(aq)} + 3\ e^{-} \rightleftharpoons Al_{(s)} + 2\ [OH]^{-}_{(aq)}$ |
| B4.6 | $E° = ?$ | $[Al(OH)]^{2+}_{(aq)} + 3\ e^{-} \rightleftharpoons Al_{(s)} + [OH]^{-}_{(aq)}$ |
| B4.7 | $E° = -1.662\ V$ | $Al^{3+}_{(aq)} + 3\ e^{-} \rightleftharpoons Al_{(s)}$ |
| **Eq. #** | **Ga** | |
| B4.8 | $E° = -1.219\ V$ | $[H_2GaO_3]^{-}_{(aq)} + H_2O_{(l)} + 3\ e^{-} \rightleftharpoons Ga_{(s)} + 4\ [OH]^{-}_{(aq)}$ |
| B4.9 | $E° = -0.549\ V$ | $Ga^{3+}_{(aq)} + 3\ e^{-} \rightleftharpoons Ga_{(s)}$ |
| B4.10 | $E° = -0.498\ V$ | $[Ga(OH)]^{2+}_{(aq)} + H^{+}_{(aq)} + 3\ e^{-} \rightleftharpoons Ga_{(s)} + H_2O_{(l)}$ |
| B4.11 | $E° = -0.2\ V$ | $Ga^{+}_{(aq)} + e^{-} \rightleftharpoons Ga_{(s)}$ |
| **Eq. #** | **In** | |
| B4.12 | $E° = -1.034\ V$ | $In_2O_{3,\ (s)} + 3\ H_2O_{(l)} + 6\ e^{-} \rightleftharpoons 2\ In_{(s)} + 6\ [OH]^{-}_{(aq)}$ |
| B4.13 | $E° = -1.007\ V$ | $[In(OH)_4]^{-}_{(aq)} + 3\ e^{-} \rightleftharpoons In_{(s)} + 4\ [OH]^{-}_{(aq)}$ |
| B4.14 | $E° = -0.99\ V$ | $In(OH)_{3,\ (aq)} + 3\ e^{-} \rightleftharpoons In_{(s)} + 3\ [OH]^{-}_{(aq)}$ |
| B4.15 | $E° = -0.34\ V$ | $In^{3+}_{(aq)} + 3\ e^{-} \rightleftharpoons In_{(s)}$ |
| B4.16 | $E° = -0.14\ V$ | $In^{+}_{(aq)} + e^{-} \rightleftharpoons In_{(s)}$ |
| **Eq. #** | **Sn** | |
| B4.17 | $E° = -0.945\ V$ | $SnO_{2,\ (s)} + 2\ H_2O_{(l)} + 4\ e^{-} \rightleftharpoons Sn_{(s)} + 4\ [OH]^{-}_{(aq)}$ |
| B4.18 | $E° = -0.909\ V$ | $[HSnO_2]^{-}_{(aq)} + H_2O_{(l)} + 2\ e^{-} \rightleftharpoons Sn_{(s)} + 3\ [OH]^{-}_{(aq)}$ |
| B4.19 | $E° = -0.1375\ V$ | $Sn^{2+}_{(aq)} + 2\ e^{-} \rightleftharpoons Sn_{(s)}$ |
| B4.20 | $E° = -0.117\ V$ | $SnO_{2,\ (s)} + 2\ H^{+}_{(aq)} + 4\ e^{-} \rightleftharpoons Sn_{(s)} + 2\ H_2O_{(l)}$ |
| **Eq. #** | **$O_2$** | |
| B4.21 | $E° = +1.27\ V$ | $O_{2,\ (aq)} + 4\ H^{+}_{(aq)} + 4\ e^{-} \rightleftharpoons 2\ H_2O_{(l)}$ (p.450 of [61]) |
| B4.22 | $E° = +1.23\ V$ | $O_{2,\ (g)} + 4\ H^{+}_{(aq)} + 4\ e^{-} \rightleftharpoons 2\ H_2O_{(l)}$ |
| B4.23 | $E° = +0.695\ V$ | $O_2 + 2\ H^{+}_{(aq)} + 2\ e^{-} \rightleftharpoons H_2O_{2,\ (l)}$ |
| B4.24 | $E° = +0.401\ V$ | $O_2 + 2\ H_2O_{(l)} + 4\ e^{-} \rightleftharpoons 4\ [OH]^{-}_{(aq)}$ |
| B4.25 | $E° = -0.076\ V$ | $O_2 + H_2O_{(l)} + 2\ e^{-} \rightleftharpoons [HO_2]^{-}_{(aq)} + [OH]^{-}_{(aq)}$ |
| B4.26 | $E° = -0.146\ V$ | $O_2 + 2\ H_2O_{(l)} + 2\ e^{-} \rightleftharpoons H_2O_{2,\ (l)} + 2\ [OH]^{-}_{(aq)}$ |
| **Eq. #** | **$H_2$** | |
| B4.27 | $E° = 0\ V$ | $2\ H^{+} + 2\ e^{-} \rightleftharpoons H_{2,\ (g)}$ |

**Table B5. Al species reacting with $[OH]^-$, $H^+$, and $[H_3O]^+$ (ordered by charge state of reactant Al species).** This table uses the average values from Table B1 to calculate ΔG°.

| Eq. # | Al species reacting with $[OH]^-$ | |
|---|---|---|
| B5.1 | $\Delta G^\circ = -47$ kJ/mol $Al^{3+}_{(aq)}$ | $Al^{3+}_{(aq)} + [OH]^-_{(aq)} \rightarrow [Al(OH)]^{2+}_{(aq)}$ |
| B5.2 | $\Delta G^\circ = -50$ kJ/mol $[Al(OH)]^{2+}_{(aq)}$ | $[Al(OH)]^{2+}_{(aq)} + [OH]^-_{(aq)} \rightarrow [Al(OH)_2]^+_{(aq)}$ |
| B5.3 | $\Delta G^\circ = -88$ kJ/mol $[Al(OH)_2]^+_{(aq)}$ | $2\ [Al(OH)_2]^+_{(aq)} + 2\ [OH]^-_{(aq)} \rightarrow Al_2O_{3,\ (s,\ corundum)} + 3\ H_2O_{(l)}$ |
| B5.4 | $\Delta G^\circ = -96$ kJ/mol $[Al(OH)_2]^+_{(aq)}$ | $[Al(OH)_2]^+_{(aq)} + [OH]^-_{(aq)} \rightarrow Al(OH)_{3,\ (s,\ gibbsite)}$ |
| B5.5 | $\Delta G^\circ = -100$ kJ/mol $[Al(OH)_2]^+_{(aq)}$ | $[Al(OH)_2]^+_{(aq)} + [OH]^-_{(aq)} \rightarrow AlO(OH)_{(s,\ diaspore)} + H_2O_{(l)}$ |
| B5.6 | $\Delta G^\circ = -2$ kJ/mol $Al_2O_{3,\ (s,\ corundum)}$ | $Al_2O_{3,\ (s,\ corundum)} + 2\ [OH]^-_{(aq)} + 3\ H_2O_{(l)} \rightarrow 2\ [Al(OH)_4]^-_{(aq)}$ |
| B5.7 | $\Delta G^\circ = +7$ kJ/mol $Al(OH)_{3,\ (s,\ gibbsite)}$ | $Al(OH)_{3,\ (s,\ gibbsite)} + [OH]^-_{(aq)} \rightarrow [Al(OH)_4]^-_{(aq)}$ |
| B5.8 | $\Delta G^\circ = +11$ kJ/mol $AlO(OH)_{(s,\ diaspore)}$ | $AlO(OH)_{(s,\ diaspore)} + [OH]^-_{(aq)} + H_2O_{(l)} \rightarrow [Al(OH)_4]^-_{(aq)}$ |
| **Eq. #** | **Al species reacting with $H^+$** | |
| B5.9 | $\Delta G^\circ = -91$ kJ/mol $[Al(OH)_4\ ]^-_{(aq)}$ | $[Al(OH)_4\ ]^-_{(aq)} + H^+_{(aq)} \rightarrow AlO(OH)_{(s,\ diaspore)} + 2\ H_2O_{(l)}$ |
| B5.10 | $\Delta G^\circ = -87$ kJ/mol $[Al(OH)_4\ ]^-_{(aq)}$ | $[Al(OH)_4\ ]^-_{(aq)} + H^+_{(aq)} \rightarrow Al(OH)_{3,\ (s,\ gibbsite)} + H_2O_{(l)}$ |
| B5.11 | $\Delta G^\circ = -79$ kJ/mol $[Al(OH)_4\ ]^-_{(aq)}$ | $2\ [Al(OH)_4]^-_{(aq)} + 2\ H^+_{(aq)} \rightarrow Al_2O_{3,\ (s,\ corundum)} + 5\ H_2O_{(l)}$ |
| B5.12 | $\Delta G^\circ = +16$ kJ/mol $Al(OH)_{3,\ (s,\ gibbsite)}$ | $Al(OH)_{3,\ (s,\ gibbsite)} + H^+_{(aq)} \rightarrow [Al(OH)_2]^+_{(aq)} + H_2O_{(l)}$ |
| B5.13 | $\Delta G^\circ = +17$ kJ/mol $Al_2O_{3,\ (s,\ corundum)}$ | $Al_2O_{3,\ (s,\ corundum)} + 2\ H^+_{(aq)} + H_2O_{(l)} \rightarrow 2\ [Al(OH)_2]^+_{(aq)}$ |
| B5.14 | $\Delta G^\circ = +21$ kJ/mol $AlO(OH)_{(s,\ diaspore)}$ | $AlO(OH)_{(s,\ diaspore)} + H^+_{(aq)} \rightarrow [Al(OH)_2]^+_{(aq)}$ |
| B5.15 | $\Delta G^\circ = -29$ kJ/mol $[Al(OH)_2]^+_{(aq)}$ | $[Al(OH)_2]^+_{(aq)} + H^+_{(aq)} \rightarrow [Al(OH)]^{2+}_{(aq)} + H_2O_{(l)}$ |
| B5.16 | $\Delta G^\circ = -33$ kJ/mol $[Al(OH)]^{2+}_{(aq)}$ | $[Al(OH)]^{2+}_{(aq)} + H^+_{(aq)} \rightarrow Al^{3+}_{(aq)} + H_2O_{(l)}$ |
| **Eq. #** | **Al species reacting with $[H_3O]^+$** | |
| B5.17 | $\Delta G^\circ = -100$ kJ/mol $[Al(OH)_4\ ]^-_{(aq)}$ | $[Al(OH)_4]^-_{(aq)} + [H_3O]^+_{(aq)} \rightarrow AlO(OH)_{(s,\ diaspore)} + 3\ H_2O_{(l)}$ |
| B5.18 | $\Delta G^\circ = -96$ kJ/mol $[Al(OH)_4\ ]^-_{(aq)}$ | $[Al(OH)_4]^-_{(aq)} + [H_3O]^+_{(aq)} \rightarrow Al(OH)_{3,\ (s,\ gibbsite)} + 2\ H_2O_{(l)}$ |
| B5.19 | $\Delta G^\circ = -88$ kJ/mol $[Al(OH)_4\ ]^-_{(aq)}$ | $2\ [Al(OH)_4]^-_{(aq)} + 2\ [H_3O]^+_{(aq)} \rightarrow Al_2O_{3,\ (s,\ corundum)} + 7\ H_2O_{(l)}$ |
| B5.20 | $\Delta G^\circ = -1$ kJ/mol $Al_2O_{3,\ (s,\ corundum)}$ | $Al_2O_{3,\ (s,\ corundum)} + 2\ [H_3O]^+_{(aq)} \rightarrow 2\ [Al(OH)_2]^+_{(aq)} + H_2O_{(l)}$ |
| B5.21 | $\Delta G^\circ = +8$ kJ/mol $Al(OH)_{3,\ (s,\ gibbsite)}$ | $Al(OH)_{3,\ (s,\ gibbsite)} + [H_3O]^+_{(aq)} \rightarrow [Al(OH)_2]^+_{(aq)} + 2\ H_2O_{(l)}$ |
| B5.22 | $\Delta G^\circ = +12$ kJ/mol $AlO(OH)_{(s,\ diaspore)}$ | $AlO(OH)_{(s,\ diaspore)} + [H_3O]^+_{(aq)} \rightarrow [Al(OH)_2]^+_{(aq)} + H_2O_{(l)}$ |
| B5.23 | $\Delta G^\circ = -38$ kJ/mol $[Al(OH)_2]^+_{(aq)}$ | $[Al(OH)_2]^+_{(aq)} + [H_3O]^+_{(aq)} \rightarrow [Al(OH)]^{2+}_{(aq)} + 2\ H_2O_{(l)}$ |
| B5.24 | $\Delta G^\circ = -41$ kJ/mol $[Al(OH)]^{2+}_{(aq)}$ | $[Al(OH)]^{2+}_{(aq)} + [H_3O]^+_{(aq)} \rightarrow Al^{3+}_{(aq)} + 2\ H_2O_{(l)}$ |

# References

1 Baker, ASM Handbook, Volume 3: Alloy Phase Diagrams. ASM International, USA, 1992.

2 Ziebarth, Use of the Al-Ga-In-Sn System for Energy Storage and Conversion. Purdue University ProQuest Dissertations Publishing, 2010. Available: https://www.proquest.com/docview/750350087.

3 Pulsone et al., Aluminum-Water Energy System for Autonomous Undersea Vehicles. Lincoln Laboratory Journal 22, no. 2, pp.79-90, 2017. Available: https://api.semanticscholar.org/CorpusID:26541029.3.

4 Planete-Energies.com, The Many Uses of Hydrogen. 2015. Available: https://www.planete-energies.com/en/media/article/many-uses-hydrogen.

5 Shah, A Parametric Study of Gallium Adhesion to Gibbsite. UC Davis Electronic Theses and Dissertations, 2021. Available: https://escholarship.org/uc/item/1w85292r.

6 Choi, Aluminum Rich Alloys for Energy Storage and Conversion. Purdue University ProQuest Dissertations Publishing, 2012. Available: https://www.proquest.com/openview/cd0741b6c8fb6541d3c4aedbe624454a.

7 Pourbaix, Atlas of Electrochemical Equilibria in Aqueous Solutions. National Association of Corrosion Engineers, Second English Edition, 1974. Available: http://sunlight.caltech.edu/aic/pourbaix.pdf.

8 Uehara et al., Hydrogen Gas Generation in the Wet Cutting of Aluminum and its Alloys. Journal of Materials Processing Technology, Volume 127, Issue 2, pp.174-177, 2002. Available: https://www.sciencedirect.com/science/article/pii/S0924013602001218.

9 Deng et al., Physicochemical Mechanism for the Continuous Reaction of γ-$Al_2O_3$-Modified Aluminum Powder with Water. Journal of the American Ceramic Society, Volume 90, Issue 5, pp.1521–1526, 2007. Available: https://ceramics.onlinelibrary.wiley.com/doi/10.1111/j.1551-2916.2007.01546.x.

10 Bunker et al., Hydration of Passive Oxide Films on Aluminum. The Journal of Physical Chemistry B, Volume 106, No. 18, pp.4705-4713, 2002. Available: https://pubs.acs.org/doi/pdf/10.1021/jp013246e.

11 University of California, Davis, Facilities Management, 2022 Drinking Water Quality Report for University of California, Davis. facilities.ucdavis.edu, accessed: 2023-2024. Available: https://facilities.ucdavis.edu/utilities-services/water-quality.

12 McCoy, Joel (Facilities Management of University of California, Davis.). Subject: Water Quality. Email correspondence, received by Schmierer, Joel, 2023.

13 Millipore Sigma, Millipore Sigma Products. emdmillipore.com, accessed: 2023-2024. Available: https://www.emdmillipore.com/US/en.

14 Atekwana et al., The Relationship of Total Dissolved Solids Measurements to Bulk Electrical Conductivity in an Aquifer Contaminated with Hydrocarbon. Journal of Applied Geophysics, Volume 56, Issue 4, pp.281-294, 2004. Available: https://www.sciencedirect.com/science/article/pii/S0926985104000576.

15 Niagara Bottling, Water Quality Report 2023. niagarawater.com, accessed: 2023-2024. Available: https://www.niagarawater.com/quality/water-quality/.

16 BlueTriton Brands, Action Alkaline Water. bluetriton.com, accessed: 2023-2024. Available: https://www.bluetriton.com/action.

17 Test Aqua, Action Purified Alkaline Water Test. testaqua.com, 2023. Available: https://testaqua.com/usa-water/action-purified-alkaline-water-test/.

18 Sartorius Stedim Biotech GmbH, Resistivity/Conductivity Measurement of Purified Water. labmanager.com/author/sartorius, 2010. Available: https://www.labmanager.com/resistivity-conductivity-measurement-of-purified-water-19691.

19 Knoche, Chemical Reactions of $CO_2$ in Water. Proceedings in Life Sciences: Biophysics and Physiology of Carbon Dioxide, 1980. Available: https://doi.org/10.1007/978-3-642-67572-0_1.

20 Zimmermann et al., Plastic Products Leach Chemicals That Induce In Vitro Toxicity under Realistic Use Conditions. Environmental Science & Technology, Volume 55, Issue 17, pp.11814-11823, 2021. Available: https://pubs.acs.org/doi/10.1021/acs.est.1c01103.

21 Blaber et al., Gibbs Energy Changers (sic) for Non-Standard States. chem.libretexts.org, accessed: 2023-2024. Available: https://chem.libretexts.org/Bookshelves/General_Chemistry/Map%3A_A_Molecular_Approach_(Tro)/18%3A_Gibbs_Energy_and_Thermodynamics/18.09%3A_Gibbs_Energy_Changers_for_Non-Standard_States?readerView.

22 Leisegang et al., The Aluminum-Ion Battery: A Sustainable and Seminal Concept? Frontiers in Chemistry, Volume 7, Article 268, 2019. Available: https://www.frontiersin.org/articles/10.3389/fchem.2019.00268/full.

23 Ashby et al., Chapter 26- Wet Corrosion of Metals. Engineering Materials 1, Fourth Edition, pp.385-400, 2012. Available: https://www.sciencedirect.com/topics/chemistry/pourbaix-diagram.

24 Xiao et al., Effects of Low Temperature on Aluminum(III) Hydrolysis: Theoretical and Experimental Studies. Journal of Environmental Sciences, Volume 20, Issue 8, pp.907-914, 2008. Available: https://www.sciencedirect.com/science/article/pii/S1001074208621853?via%3Dihub.

25 Langmuir et al., Issue Paper on the Environmental Chemistry of Metals. U.S. Environmental Protection Agency, 2004. Available: https://www.epa.gov/sites/default/files/2014-11/documents/enviro_checmical.pdf.

26 Millipore Sigma, Solubility Rules | Solubility of Common Ionic Compounds. sigmaaldrich.com, accessed: 2023-2024. Available: https://www.sigmaaldrich.com/US/en/technical-documents/technical-article/materials-science-and-engineering/solid-state-synthesis/solubility-rules-solubility-of-common-ionic-compounds.

27 Monhemius, Precipitation Diagrams for Metal Hydroxides, Sulphides, Arsenates and Phosphates. Transactions Institution of Mining & Metallurgy, Volume 86, pp.C202-C206, 1977. Available: https://www.researchgate.net/publication/266137129_Precipitation_diagrams_for_metal_hydroxides_sulphides_arsenates_and_phosphates.

28 Dyer et al., A Practical Guide for Determining the Solubility of Metal Hydroxides and Oxides in Water. Environmental Progress & Sustainable Energy, Volume 17, Issue 1, pp.1-8, 1998. Available: https://onlinelibrary.wiley.com/doi/epdf/10.1002/ep.670170112.

29 Aluminum Manufacturers, Aluminum Carbonate. aluminummanufacturers.org, accessed: 2023-2024. Available: https://www.aluminummanufacturers.org/aluminum-sulfate/aluminum-carbonate/.

30 Pommerenk, Adsorption of Inorganic and Organic Ligands Onto Aluminum Hydroxide and Its Effect in Water Treatment. Old Dominion University Digital Commons, Civil & Environmental Engineering Theses & Dissertations, 2001. Available: https://digitalcommons.odu.edu/cee_etds/100/.

31 Jully et al., Mechanisms of Antigen Adsorption Onto an Aluminum-Hydroxide Adjuvant Evaluated by High-Throughput Screening. Journal of Pharmaceutical Sciences, Volume 105, Issue 6, pp.1829-1836, 2016. Available: https://www.sciencedirect.com/science/article/pii/S0022354916413353#bib4.

32 HogenEsch et al., Optimizing the Utilization of Aluminum Adjuvants in Vaccines: You Might Just Get What You Want. Nature Partner Journals: Vaccines, Volume 3, Article number 51, pp.1-11, 2018. Available: https://www.nature.com/articles/s41541-018-0089-x.

33 Wikipedia, Double Layer (Surface Science). wikipedia.org, accessed: 2023-2024. Available: https://en.wikipedia.org/wiki/Double_layer_(surface_science).

34 Gayer et al., The Solubility of Aluminum Hydroxide in Acidic and Basic Media at 25°C. Canadian Journal of Chemistry, Volume 36, No. 9, pp.1268-1271, 1958. Available: https://doi.org/10.1139/v58-184.

35 Johan et al., Phosphorus Transformation in Soils Following Co-Application of Charcoal and Wood Ash. Agronomy, Volume 11, Article number 10: 2010, 2021. Available: https://doi.org/10.3390/agronomy11102010.

36 Sparks, Environmental Soil Chemistry. Elsevier Science, Amsterdam, the Netherlands, 2003.

37 Dean et al., Lange's Handbook of Chemistry. Colombia, McGraw-Hill, 1999.

38 Chemistry LibreTexts, The Formation of Complex Ions. chem.libretexts.org, accessed: 2023-2024. Available: https://chem.libretexts.org/Bookshelves/General_Chemistry/Book%3A_General_Chemistry%3A_Principles_Patterns_and_Applications_(Averill)/17%3A_Solubility_and_Complexation_Equilibria/17.04%3A_The_Formation_of_Complex_Ions.

39 Liu et al., Characterization of Nontoxic Liquid-Metal Alloy Galinstan for Applications in Microdevices. Journal of Microelectromechanical Systems, Volume 21, No. 2, pp. 443-450, 2012. Available: https://ieeexplore.ieee.org/document/6097006.

40 Jia et al., Liquid–Gas Interfacial Chemistry of Gallium–Indium Eutectic in the Presence of Oxygen and Water Vapor. The Journal of Physical Chemistry C, Volume 123, No. 47, pp.28688-28694, 2019. Available: https://pubs.acs.org/doi/full/10.1021/acs.jpcc.9b07731.

41 Swain et al., Recycling of GaN, a Refractory eWaste Material: Understanding the Chemical Thermodynamics. International Journal of Applied Ceramic Technology, Volume 13, Issue 2, pp.280-288, 2016. Available: https://doi.org/10.1111/ijac.12473.

42 Gan et al., GaOOH Crystallite Growth on Liquid Metal Microdroplets in Water: Influence of the Local Environment. Langmuir, Volume 38, Issue 47, pp.14475-14484, 2022. Available: https://pubs.acs.org/doi/full/10.1021/acs.langmuir.2c02539.

43 Thomas, Continuous Generation of Hydrogen and Aluminum Hydroxide from Hydrolysis Using an Active Aluminum-Gallium Molten Alloy. University of California, Davis ProQuest Dissertations Publishing, 2016. Available: https://www.proquest.com/openview/d50ed74975fa1aba9c27c2802ab5aeea/.

44 Huang, Preparation of Al-Ga-In-Sn-Bi Quinary Alloy and Its Hydrogen Production via Water Splitting. International Journal of Hydrogen Energy, Volume 40, Issue 5, pp.2354-2362, 2015. Available: https://doi.org/10.1016/j.ijhydene.2014.12.034.

45 Okeke, Computational Study of Oxynitride Based Strong Materials. University of the Witwatersrand, Johannesburg e-Wits Catalogue, 2010. Available: https://wiredspace.wits.ac.za/server/api/core/bitstreams/788c9c15-3b82-4279-9dc3-3c364a7039e0/content.

46 Jemmis et al., Ionic to Covalent Bonding: a Density Functional Theory Study of Linear and Bent $X_2Y_3$ Monomers (X = B, Al, Ga, In; Y = O, S, SE). Electronic Journal of Theoretical Chemistry, Volume 2, Issue 1, pp.130-138, 1997. Available: https://doi.org/10.1002/ejtc.37.

47 Zhao et al., Anomalous Behavior and Phase Transformation of α-GaOOH Nanocrystals Under Static Compression. Chinese Physics B, Volume 26, No. 10, 2017. Available: https://doi.org/10.1088/1674-1056/26/10/106402.

48 Hill, Crystal Structure Refinement and Electron Density Distribution in Diaspore. Physics and Chemistry of Minerals, Volume 5, pp.179-200, 1979. Available: https://doi.org/10.1007/BF00307552.

49 Kolesova et al., Infrared Absorption Spectra of Diaspore α-AlOOH, Boehmite γ-AlOOH and GaOOH. Journal of Structural Chemistry: Zhurnal Strukturnoĭ Khimii, Volume 3, No. 6, pp.680-684, 1962. Available: https://apps.dtic.mil/sti/citations/AD0401011.

50 Kloprogge et al., XPS Study of the Major Minerals in Bauxite: Gibbsite, Bayerite and (Pseudo-)Boehmite. Journal of Colloid and Interface Science, Volume 296, Issue 2, pp.572-576, 2006. Available: https://doi.org/10.1016/j.jcis.2005.09.054.

51 Handschuh-Wang, The Subtle Difference Between Galinstan (R) and Eutectic GaInSn. Materialia, Volume 26, 101642, 2022. Available: https://doi.org/10.1016/j.mtla.2022.101642.

52 Chase, Journal of Physical and Chemical Reference Data, NIST-JANAF Thermochemical Tables, Fourth Edition. American Institute of Physics and American Chemical Society, 1998. Available: https://doi.org/10.18434/T42S31.

53 Hemingway et al., The Entropy and Gibbs Free Energy of Formation of the Aluminum Ion. Geochimica et Cosmochimica Acta, Volume 41, Issue 9, pp.1402-1404, 1977. Available: https://doi.org/10.1016/0016-7037(77)90085-0.

54 Anderson, Thermodynamics of Natural Systems. Wiley, 1996.

55 Chang, The Gibbs Free Energy of the Formation of the Al(OH)4⁻ Ion at Elevated Temperatures. Bulletin of the Chemical Society of Japan, Volume 55, Issue 6, 1982, pp.1949–1950. Available: https://doi.org/10.1246/bcsj.55.1949.

56 Hemingway et al., Revised Values for the Gibbs Free Energy of Formation of $[Al(OH)_4]^-_{(aq)}$; Diaspore, Boehmite and Bayerite at 298.15K and 1Bar, the Thermodynamic Properties of Kaolinite to 800K and 1Bar, and the Heats of Solution of Several Gibbsite Samples. Geochimica et Cosmochimica Acta, Volume 42, Issue 10, 1978, pp.1533-1543. Available: https://doi.org/10.1016/0016-7037(78)90024-8.

57 Wagman et al., The NBS Tables of Chemical Thermodynamic Properties: Selected Values for Inorganic and $C_1$ and $C_2$ Organic Substances in SI Units. American Chemical Society and American Institute of Physics, Journal of Physical and Chemical Reference Data, Volume 11, 1982. Available: https://srd.nist.gov/JPCRD/jpcrdS2Vol11.pdf.

58 Pokrovski et al., Thermodynamic Properties of Gallium Hydroxide Oxide (α-GaOOH) at Temperatures to 700K. European Journal of Mineralogy, Volume 9, No. 5, pp.941-952, 1997. Available: https://doi.org/10.1127/ejm/9/5/0941.

59 Bazhin et al., Thermodynamics of Hydronium, Zundel and Eigen Ions. OSF Preprints, 2021. Available: https://doi.org/10.31219/osf.io/b6v24.

60 Vanýsek, CRC Handbook of Chemistry and Physics, 91st Edition: Electrochemical Series. Taylor & Francis Group, 2010.

61 Snoeyink and Jenkins, Water Chemistry. Wiley, USA, 1980.

# End

* * *

**Author Contact Information for Joel Craig Schmierer:**
**joelschmierer@gmail.com and Facebook**

**Major Professor: Jerry M. Woodall**
**(jwoodall@ucdavis.edu)**